DETERMINATION OF DISPERSION CURVES FOR ACOUSTOELASTIC LAMB WAVE PROPAGATION

A Thesis
Presented to
The Academic Faculty

by

Navneet Gandhi

In Partial Fulfillment
of the Requirements for the Degree
Masters of Science in the
School of Electrical and Computer Engineering

Georgia Institute of Technology
December 2010

DETERMINATION OF DISPERSION CURVES FOR ACOUSTOELASTIC LAMB WAVE PROPAGATION

Approved by:

Professor Jennifer E. Michaels, Advisor
School of Electrical and Computer Engineering
Georgia Institute of Technology

Professor Thomas E. Michaels
School of Electrical and Computer Engineering
Georgia Institute of Technology

Professor Gregory D. Durgin
School of Electrical and Computer Engineering
Georgia Institute of Technology

Date Approved: 20 Aug 2010

To Friends and Family

ACKNOWLEDGEMENTS

First and foremost, I'd like to thank my advisor Prof. Jennifer E. Michaels for the rich and rewarding experience at the QUEST Lab. Her leadership and advice on all things academic and non-academic have allowed me to come this far and I owe to her some of the best things I take away from Georgia Tech. I would also like to thank the other members of my committee, Prof. Thomas E. Michaels and Prof. Gregory D. Durgin. Thanks to all my colleagues at QUEST lab: Dr. Sang Jun Lee, Dr. Dave Muir, Ler Gullayanon, Leo Lu, Phillip Marks, Ross Levine, Xin Chen and Shiv Chawla. You've taught me more things than you'll ever know! Special thanks to James S. Hall for sharing his experience and immense knowledge with the rest of us at QUEST lab, humbly disguised as peer review of course! Thanks to the knowledgeable faculty at Georgia Tech. It was always very difficult to pick between the courses knowing there were so many good ones out there. Thanks also to the ECE academic department and the rest of the staff at Georgia Tech.

The support of the Air Force Research Lab (AFRL) under Contract No. FA8650-09-C-52064 is gratefully acknowledged.

TABLE OF CONTENTS

LIST OF TABLES

LIST OF FIGURES

SUMMARY

The physics of wave propagation in stress-free isotropic and anisotropic bulk media is well understood and can be adequately described using theory based on linear stress-strain relationships. However, this formulation is inadequate to describe wave propagation in pre-stressed or loaded bulk media because the small non-linearities in the stress-strain relationships become significant. Acoustoelasticity refers to the stress dependence of acoustic wave velocities in bulk elastic media and its theory is well developed. The acoustoelastic effect is a result of the nonlinearity in the stress strain constitutive relation and the variation of density under elastic deformation. In this thesis the theory of acoustoelasticity is reviewed and relations for the specific case of a biaxially stressed, hyperelastic, isotropic material with assumptions of small predeformation and small incremental wave motion are derived. These relations allow the prediction of changes in wave speeds of bulk waves under the influence of stresses.

Introducing boundary conditions to construct a medium such as a plate gives rise to guided waves called Lamb waves. Existing theory for materials of monoclinic symmetry view Lamb waves as a composition of bulk waves reflecting between the boundaries of the plate. Using knowledge of effects of acoustoelasticity on bulk waves, theory is developed herein to understand the characteristics of Lamb waves in the presence of initial stresses. An approximate method using effective elastic constants (EECs) is also presented. A numerical method to generate dispersion curves is developed, which allows comparison between theory and EECs. In addition, the theory has been verified using experimental data obtained from an aluminum plate under uniaxial stress. Finally, a ray tracing model is used to compare the change in pulse shape under the effects of applied stress using the two methods as this is key

to applications in structural health monitoring and nondestructive evaluation.

The specific contributions of this thesis are:

1. Computation of acoustoelastic constants and the incremental stress-stain relationship for a biaxially stressed, hyperelastic, isotropic material with assumptions of small homogeneous pre-deformation and small incremental wave motion.

2. Development of theory for acoustoelastic Lamb waves using these acoustoelastic constants and the incremental stress-stain relationship.

3. Approximate characterization of acoustoelastic Lamb wave propagation using EECs for the case of uniaxial loads.

4. Validation of theory using previously acquired experimental data (experimental work was not a part of this thesis).

5. Numerical methods that enable comparison of dispersion curves and predicted pulse shapes between theory and EECs.

CHAPTER I

INTRODUCTION AND LITERATURE REVIEW

The theory of wave propagation in stress-free solids is well developed and dates back to the early 1800s with the discovery of dynamical equations and waves in solids by Cauchy and Poisson [1]. The linear theory of elasticity is based upon a linear approximation of the relation between stress and strain along with the assumption of small deformations. Although this theory does not give an exact description of dynamics, it does provide a very useful solution that is applicable as long as the assumptions are valid. This linear theory is the subject of many classic texts on wave propagation in solids [2, 3, 4, 1].

Presented in the following sections is a brief review of wave propagation in isotropic and anisotropic stress-free materials. This theory is essential to the development of the theory of wave propagation in stressed plates developed in later sections.

1.1 Physics of Wave Propagation in Isotropic Materials

The equations that govern dynamics for an isotropic material with Lamé constants λ and μ are the stress equation of motion [2, 5]

$$\sigma_{ij,j} + \rho f_i = \rho \ddot{u}_i, \tag{1}$$

Hooke's law

$$\sigma_{ij} = \lambda \epsilon_{kk} \delta_{ij} + 2\mu \epsilon_{ij}, \tag{2}$$

and the strain-displacement relation

$$\epsilon_{ij} = \frac{1}{2}(u_{i,j} + u_{j,i}), \tag{3}$$

where $\boldsymbol{\sigma}$ is the Cauchy stress tensor, $\boldsymbol{\epsilon}$ is the strain tensor, ρ is the material density, δ_{ij} is the Kronecker delta function, and $\boldsymbol{u}$ can represent the displacement in either

the material or spatial descriptions of the system. These descriptions are equivalent under the assumptions used for linearization of the equations of elastodynamics [2]. The external forces on the material particles are represented by $\boldsymbol{f}$ and are assumed to be zero. We use the standard Einstein's indical notation in this and all equations that follow. The second order derivative of $\boldsymbol{u}$ with respect to time is represented by $\ddot{\boldsymbol{u}}$.

Combining these equations in terms of the displacement $\boldsymbol{u}$ yields the equation of elastodynamics for isotropic materials,

$$\mu u_{i,jj} + (\lambda + \mu) u_{j,ji} + \rho f_i = \rho \ddot{u}_i. \tag{4}$$

1.1.1 Bulk Waves in Unbounded Isotropic Media

It can be shown using Helmholtz decomposition that the displacement field $\boldsymbol{u}$ decomposes into two independent vector fields for the simple case of isotropic symmetry and 2-dimensional wave propagation (plane-wave assumption) [5]. These two fields represent two different kinds of waves and are solutions to

$$\bar{u}_{,ij}\delta_{ij} = \frac{1}{{c_L}^2}\ddot{\bar{u}} \tag{5}$$

for the longitudinal wave, where $\bar{u}$ is the displacement in the direction of propagation, and

$$\tilde{u}_{,ij}\delta_{ij} = \frac{1}{{c_T}^2}\ddot{\tilde{u}} \tag{6}$$

for the shear wave, where $\tilde{u}$ is the displacement along a direction perpendicular to the direction of propagation. The equations above describe two different types of waves that can travel in the bulk medium (in any given direction) with velocities that are a function of material properties. Longitudinal waves travel with a velocity given by $c_L = \sqrt{\frac{\lambda+2\mu}{\rho}}$ and shear waves with velocity $c_T = \sqrt{\frac{\mu}{\rho}}$. These velocities are independent of direction of propagation.

1.1.2 Waves in Isotropic Plates

The theory for guided waves in plates was developed by Rayleigh and Lamb in 1888. The set of differential equations that govern waves in bulk media with additional boundary conditions can describe waves propagating in half-spaces, plates, cylindrical shells and other bounded media. Depending on the specific boundary conditions, different wave types may dominate in the system. A single free boundary gives rise to Rayleigh waves, while Love waves may propagate in a layer on a elastic half space. A plate like structure with two free boundaries gives rise to Lamb waves, which are also known as Rayleigh-Lamb waves or generalized Rayleigh waves. Only Lamb waves will be discussed in this dissertation.

1.1.2.1 Rayleigh-Lamb Waves

In the literature, there are two methods used to characterize waves that propagate in plates [2][5]:

1. **The method of potentials** where the displacement field is decomposed via Helmholtz decomposition into divergence-free and curl-free vector fields that are uncoupled for simple materials. "The usefulness of this method is restricted to isotropic plates" [5].

2. **The partial wave technique** where wave propagation in plates is considered as a combination of bulk waves that are reflecting between the boundaries of the plate. This method provides insight into the physical nature of the Lamb waves.

1.1.2.2 Dispersion Relations Using the Partial Wave Technique

A derivation of dispersion relations using the method of potentials is available in Ref. [1]. Presented in this section is a derivation using the partial wave technique, which will be useful for generalization to anisotropic and stressed plates presented in the

following sections. Consider an infinite plate of thickness d with its normal vectors aligned with the x_3 axis of a reference Cartesian coordinate system (x_1, x_2, x_3). The plate is also centered with respect to the x_3 axis. Then, assume plane wave solutions of the form

$$u_j = U_j e^{i\xi(x_1+\alpha x_3-ct)}, \tag{7}$$

where $\boldsymbol{u}$ is the particle displacement vector, $\boldsymbol{U}$ is the amplitude of displacement, ξ is the wave-number along the x_1 direction, α is the ratio of the wave-numbers in the x_3 direction to that along x_1, and c is the velocity of the wave along x_1. This general form represents plane waves traveling in the $x_1 - x_3$ plane with a x_1 velocity component of c. Only bulk waves whose velocity component along x_1 is c can participate to satisfy the boundary conditions [5].

If we can show that these are valid solutions to the equation of elastodynamics (Eq. (4)) and satisfy the free boundary conditions, the uniqueness theorem then guarantees that this is the only solution [2]. This approach will also allow us to find relations between the frequency and velocity of the guided wave.

Substituting the general form from Eq. (7) into the equation of elastodynamics (Eq. (4)) yields the following set of equations:

$$\begin{bmatrix} -\lambda - (2+\alpha^2)\,\mu + c^2\rho & 0 & -\alpha(\lambda+\mu) \\ 0 & -(1+\alpha^2)\,\mu + c^2\rho & 0 \\ -\alpha(\lambda+\mu) & 0 & -\mu - \alpha^2(\lambda+2\mu) + c^2\rho \end{bmatrix} \begin{bmatrix} U_1 \\ U_2 \\ U_3 \end{bmatrix} = 0. \tag{8}$$

The relation above shows that the displacements in the x_2 direction are independent of the displacements in the x_1 and x_3 directions. This is a result of the fact that the reflection of SV and L waves at a free boundary in isotropic media produce only SV and L waves. On the other hand SH waves produce only other SH waves at a free boundary. Guided wave modes created by the superposition of SV and L will be independent of the SH modes as depicted in Figure 1.

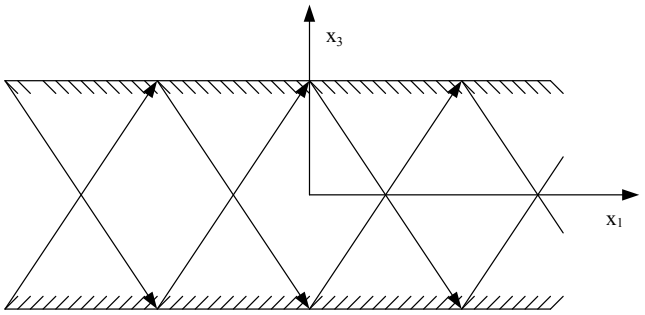

(a) SH waves.

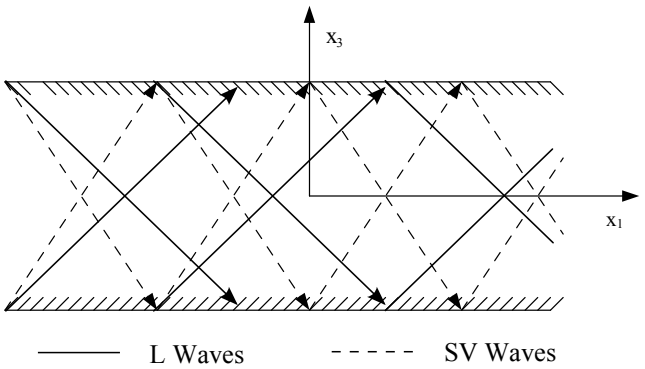

(b) L and SV waves.

Figure 1: Partial waves and coordinate system [5].

For non-zero displacement amplitudes, the determinant of the 3×3 matrix in Eq. (8) has to be zero, resulting in two independent equations,

$$\left(1 + \alpha^2\right) \mu - c^2 \rho = 0 \tag{9}$$

corresponding to the SH waves (with solutions α_1, α_2), and

$$((1 + \alpha^2)\mu - c^2\rho)((1 + \alpha^2)(\lambda + 2\mu) - c^2\rho) = 0 \tag{10}$$

corresponding to the possible L and SV waves (with solutions $\alpha_3, \alpha_4, \alpha_5$ and α_6).

Equations (9) and (10) show that there are six possible solutions (α_i) of plane-bulk waves that can participate in creating a guided wave that travels with a velocity c along the x_1 direction. Writing the total displacement due to these six solutions and

calculating the stresses using Eqs. (2) and (3) yields

$$\{u_1, u_2, u_3\} = \sum_{q=1}^{2} \{0, 1, 0\} U_{2q} e^{i\xi(x_1 + \alpha_q x_3 - ct)}, \tag{11}$$

$$\{\sigma_{13}, \sigma_{23}, \sigma_{33}\} = \sum_{q=1}^{2} i\xi \{0, \mu\alpha_q, 0\} U_{2q} e^{i\xi(x_1 + \alpha_q x_3 - ct)} \tag{12}$$

for the SH waves, and

$$\{u_1, u_2, u_3\} = \sum_{q=3}^{6} \{1, 0, R(\alpha_q)\} U_{1q} e^{i\xi(x_1 + \alpha_q x_3 - ct)}, \tag{13}$$

$$\{\sigma_{33}, \sigma_{13}, \sigma_{23}\} = \sum_{q=3}^{6} i\xi \{D_{1q}, D_{2q}, D_{3q}\} U_{1q} e^{i\xi(x_1 + \alpha_q x_3 - ct)} \tag{14}$$

for SV and L waves. The solutions corresponding to the SH waves are α_1 and α_2 while α_3 through α_6 are solutions corresponding to the SV and L waves. $R(\alpha_q)$ represents the ratio of displacements U_{3q}/U_{1q} and D_{nq} are the amplitudes of stresses corresponding to these displacements and are given by the following relations:

$$\{D_{1q}, D_{2q}, D_{3q}\} = \{\mu(R(\alpha_q) + \alpha_q), 0, \lambda + (\lambda + 2\mu) R(\alpha_q) \alpha_q\} \tag{15}$$

$$R(\alpha_q) = \frac{\lambda + \left(2 + \alpha_q^2\right) \mu - c^2 \rho}{\alpha_q (\lambda + \mu)} \tag{16}$$

obtained from Eq. (8).

Applying stress free boundary conditions, i.e., setting σ_{13}, σ_{23} and σ_{33} to zero at $x_3 = d/2$ and $x_3 = -d/2$, yields

$$\begin{bmatrix} e^{\frac{1}{2} i d \xi \alpha_1} \mu \alpha_1 & e^{\frac{1}{2} i d \xi \alpha_2} \mu \alpha_2 \\ e^{-\frac{1}{2} i d \xi \alpha_1} \mu \alpha_1 & e^{-\frac{1}{2} i d \xi \alpha_2} \mu \alpha_2 \end{bmatrix} \begin{bmatrix} U_{21} \\ U_{22} \end{bmatrix} = 0 \tag{17}$$

for SH waves and

$$\begin{bmatrix} D_{13}E_3 & D_{14}E_4 & D_{15}E_5 & D_{16}E_6 \\ D_{33}E_3 & D_{34}E_4 & D_{35}E_5 & D_{36}E_6 \\ D_{13}\tilde{E}_3 & D_{14}\tilde{E}_4 & D_{15}\tilde{E}_5 & D_{16}\tilde{E}_6 \\ D_{33}\tilde{E}_3 & D_{34}\tilde{E}_4 & D_{35}\tilde{E}_5 & D_{36}\tilde{E}_6 \end{bmatrix} \begin{bmatrix} U_{13} \\ U_{14} \\ U_{15} \\ U_{16} \end{bmatrix} = 0 \tag{18}$$

for SV and L waves, where $E_q = e^{i\xi\alpha_q d/2}$ and $\tilde{E}_q = e^{-i\xi\alpha_q d/2}$. It should be noted that Eqs. (9) and (10) have the following solutions:

$$\alpha_1 = -\alpha_2 = \sqrt{\frac{c^2\rho}{\mu} - 1} = \sqrt{\frac{c^2}{{c_T}^2} - 1}, \tag{19}$$

$$\alpha_3 = -\alpha_4 = \sqrt{\frac{c^2\rho}{\mu} - 1} = \sqrt{\frac{c^2}{{c_T}^2} - 1}, \tag{20}$$

$$\alpha_5 = -\alpha_6 = \sqrt{\frac{c^2\rho}{\lambda + 2\mu} - 1} = \sqrt{\frac{c^2}{{c_L}^2} - 1}. \tag{21}$$

To find non-trivial solutions for the displacement amplitudes U_{nq}, both of the determinants of matrices in Eqs. (17) and (18) should go to zero. Using the symmetries in α_q presented above with some trigonometric reduction, we obtain the following equations:

$$\sin(d\xi\alpha_3) = 0 \tag{22}$$

corresponding to the SH modes,

$$\frac{\tan\left(\frac{d\xi\alpha_3}{2}\right)}{\tan\left(\frac{d\xi\alpha_5}{2}\right)} = -\frac{4\alpha_3\alpha_5}{\left(-1+\alpha_3^2\right)^2} \tag{23}$$

corresponding to the symmetric modes, and

$$\frac{\tan\left(\frac{d\xi\alpha_3}{2}\right)}{\tan\left(\frac{d\xi\alpha_5}{2}\right)} = -\frac{\left(-1+\alpha_3^2\right)^2}{4\alpha_3\alpha_5} \tag{24}$$

corresponding to the antisymmetric modes. Substituting $p = \xi\alpha_3$, $q = \xi\alpha_5$ and $h = d/2$ produces an equivalent set of equations as presented in Rose [5]:

$$\left(\frac{n\pi}{2}\right)^2 = (\omega h/c_t)^2 - (kh)^2 \tag{25}$$

corresponding to the SH modes,

$$\frac{\tan(qh)}{\tan(ph)} = -\frac{4k^2pq}{(q^2-k^2)^2} \tag{26}$$

corresponding to the symmetric modes, and

$$\frac{\tan(qh)}{\tan(ph)} = -\frac{(q^2-k^2)^2}{4k^2pq} \tag{27}$$

Table 1: Nominal parameters for 7075 Aluminum.

Parameter	**Value**
λ	54.9 GPa
μ	26.5 GPa
ρ	2800 kg/m^3
c_T	3076.4 m/s
c_L	6207.7 m/s

corresponding to the antisymmetric modes. The SH modes are obtained by iterating n over 0,1,2...etc. The equations above are essentially relations between wave-velocity (c), wave-number (ξ) and frequency ($\omega = c\xi$). They characterize wave propagation in an isotropic plate with parameters c_L, c_T and d. Dispersion curves are a plot of these wave number-frequency relations. Curves for aluminum 7075 with nominal parameters listed in Table 1 are presented in Figures 2, 3 and 4. The plots show that there are an infinite number of continuous curves in the $K - \omega$ plane that constitute the set of possible solutions to the Rayleigh-Lamb equations. Each of these lines is referred to as a mode. At any given time, there may be any number of modes propagating in the plate and all but the SH0 mode are dispersive, i.e., the velocity of wave is dependent on its temporal frequency.

1.2 Wave Propagation in Anisotropic Materials

The equations that govern dynamics for anisotropic materials [2] [5] are the stress equations of motion

$$\sigma_{ij,j} + \rho f_i = \rho \ddot{u}_i, \tag{28}$$

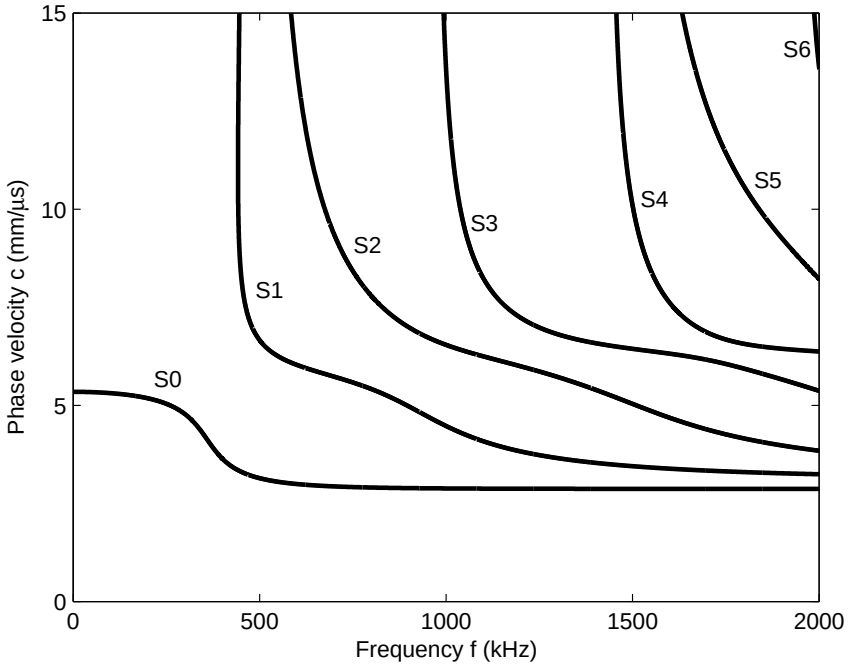

Figure 2: Symmetric modes for aluminum 7075 plate of thickness 6.35 mm.

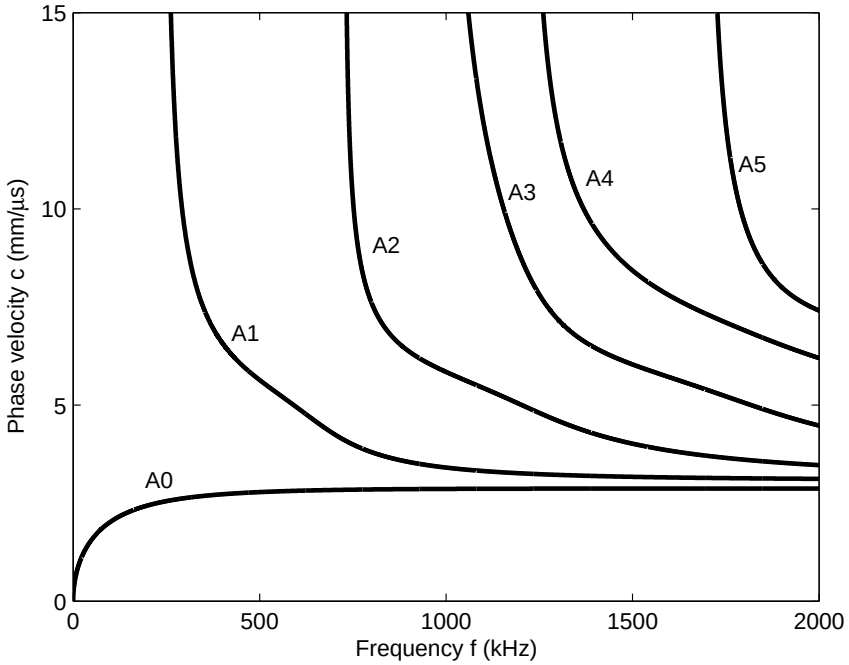

Figure 3: Antisymmetric modes for aluminum 7075 plate of thickness 6.35 mm.

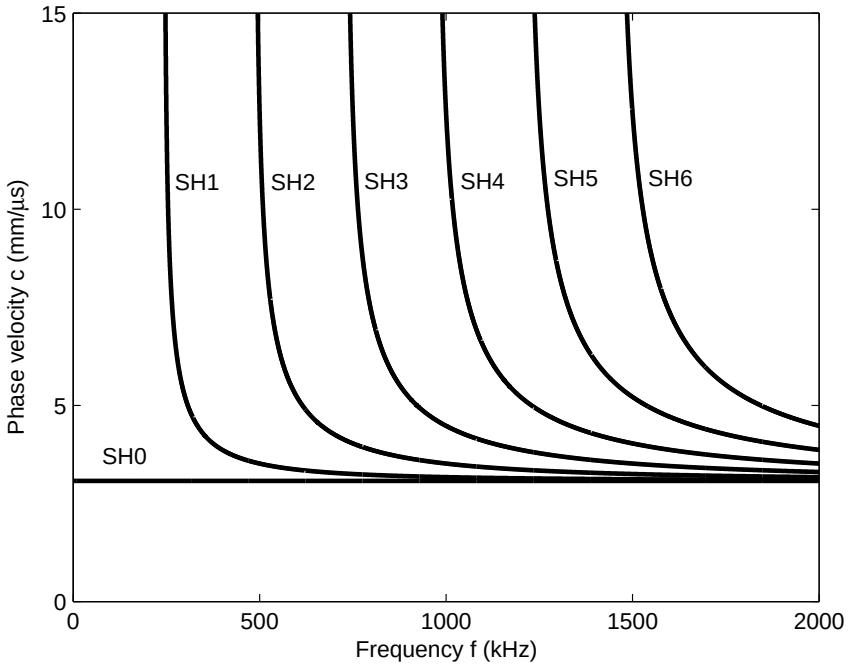

Figure 4: SH modes for aluminum 7075 plate of thickness 6.35 mm.

the tensor form of Hooke's law based on the assumptions of linear elasticity

$$\sigma_{ij} = C_{ijkl}\epsilon_{ij}, \tag{29}$$

and the linear strain-displacement relation

$$\epsilon_{ij} = \frac{1}{2}(u_{i,j} + u_{j,i}). \tag{30}$$

where $\boldsymbol{\sigma}$ is the Cauchy stress tensor, $\boldsymbol{\epsilon}$ is the infinitesimal or Cauchy strain tensor, ρ is the material density, C_{ijkl} are the coefficients of the stiffness tensor, and $\boldsymbol{u}$ can represent the displacement in either the material or spatial descriptions of the system. These systems are equivalent under the assumptions used for linearization [2]. The external forces on the material particles are represented by $\boldsymbol{f}$ and are assumed to be zero. The second derivative of $\boldsymbol{u}$ with respect to time is represented by $\ddot{\boldsymbol{u}}$.

Also, it can be shown using conservation of angular momentum and arguments from thermodynamics that the tensors have the following symmetries [6, Section

3.2.8]:

$$\sigma_{ij} = \sigma_{ji}, \tag{31}$$

$$\epsilon_{ij} = \epsilon_{ji}, \tag{32}$$

$$C_{ijkl} = C_{ijlk} = C_{jikl} = C_{klij}. \tag{33}$$

Combining the equations above results in the equation of elastodynamics for anisotropic materials

$$C_{ijkl} u_{k,jl} = \rho \ddot{u}_i. \tag{34}$$

This equation represents a system of three coupled equations for displacements u_1, u_2 and u_3.

The symmetries in Eq. (33) also allow us to compactly represent the stiffness tensor using the Voigt notation. Pairs of first two and second two subscripts are collapsed using the following rule 11 $\rightarrow$ 1, 22 $\rightarrow$ 2, 33 $\rightarrow$ 3, 23 $\rightarrow$ 4, 13 $\rightarrow$ 5, 12 $\rightarrow$ 6. This notation allows us to represent elements of the tensor C_{ijkl} as elements of a matrix C_{mn}. Following are matrices corresponding to different types of material symmetries [5] [7]. Since the stiffness matrices are symmetric, only the elements above the principle diagonal of the matrix are listed.

$$\begin{bmatrix} C_{11} & C_{12} & C_{13} & C_{14} & C_{15} & C_{16} \\ & C_{22} & C_{23} & C_{24} & C_{25} & C_{26} \\ & & C_{33} & C_{34} & C_{35} & C_{36} \\ & & & C_{44} & C_{45} & C_{46} \\ & & & & C_{55} & C_{56} \\ & & & & & C_{66} \end{bmatrix} \tag{35}$$

Triclinic Symmetry

21 Constants

$$\begin{bmatrix} C_{11} & C_{12} & C_{13} & 0 & C_{15} & 0 \\ & C_{22} & C_{23} & 0 & C_{25} & 0 \\ & & C_{33} & 0 & C_{35} & 0 \\ & & & C_{44} & 0 & C_{46} \\ & & & & C_{55} & 0 \\ & & & & & C_{66} \end{bmatrix} \tag{36}$$

Monoclinic Symmetry

13 Constants

$$\begin{bmatrix} C_{11} & C_{12} & C_{12} & 0 & 0 & 0 \\ & C_{11} & C_{12} & 0 & 0 & 0 \\ & & C_{11} & 0 & 0 & 0 \\ & & & \frac{1}{2}(C_{11}-C_{12}) & 0 & 0 \\ & & & & \frac{1}{2}(C_{11}-C_{12}) & 0 \\ & & & & & \frac{1}{2}(C_{11}-C_{12}) \end{bmatrix} \tag{37}$$

Isotropic

2 Constants $C_{11} = \lambda + 2\mu$ and $C_{12} = \lambda$

1.2.1 Bulk Waves in Unbounded Anisotropic Media

In Section 1.1.1 Helmholtz decomposition was used to show that there are two independent types of wave propagation if the material is isotropic. Helmholtz decomposition is in general not possible for anisotropic materials because there is a coupling between shear and longitudinal motion. Following the developments in Rose and Kline [5, 8] we start by assuming a plane harmonic traveling wave solution of the form

$$u_i = A_i e^{i(k_j x_j - \omega t)}, \tag{38}$$

where $\boldsymbol{u}$ is the particle displacement vector, $A_i = A\alpha_i$, A is the amplitude of displacement, $\boldsymbol{\alpha}$ is a unit-vector that represents the direction of particle displacement,

$\boldsymbol{k}$ is the wave number vector and ω is the angular frequency. All quantities are with respect to the standard Cartesian frame of reference (x_1, x_2, x_3). This plane harmonic solution must satisfy the equations of motion and substituting Eq. (38) into Eq. (34) results in the Christoffel equation:

$$(\Gamma_{im} - \rho c^2 \delta_{im}) u_m = 0, \tag{39}$$

where $\Gamma_{im} = C_{iklm} n_k n_l$. The Christoffel acoustic tensor is represented by $\mathbf{\Gamma}$, n_k and n_l are the direction cosines of the normal to the wavefront, i.e., $k_p = |\boldsymbol{k}| n_p$, and $c = \omega/k$ is the phase velocity. For any non-trivial solution i.e., non-zero displacements, the determinant of the coefficient matrix in the expression above must go to zero,

$$|\Gamma_{im} - \rho c^2 \delta_{im}| = 0. \tag{40}$$

This equation is essentially a relation between the material properties, the direction of wave propagation and the velocity of the wave. It is evident that unlike the isotropic case in Section 1.1.1, the velocities are now a function of direction of propagation. Also, the particle displacements are not necessarily perpendicular or parallel to the direction of propagation.

1.2.2 Waves in Anisotropic Plates

Dispersion relations for materials of monoclinic and higher symmetry have been derived in an important paper by Nayfeh and Chimenti [9]. Presented here is a brief description of the derivation and a numerical method to find the dispersion curves. The theory for stressed plates in later sections is based upon ideas from this derivation.

1.2.2.1 Derivation for a Generally Anisotropic Plate

Consider an infinite anisotropic plate of triclinic symmetry having thickness d whose normal is aligned with the x_3' axes of a reference Cartesian coordinate system $x_i' =$

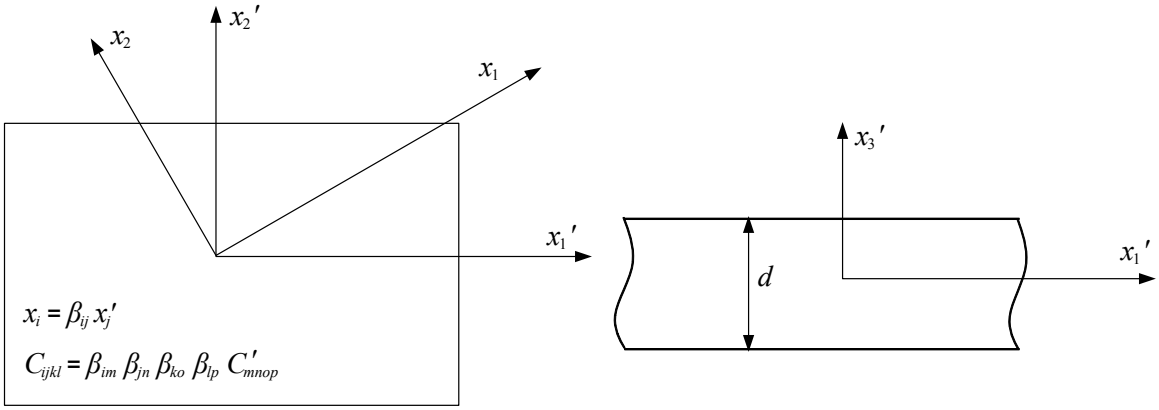

Figure 5: Anisotropic plate coordinate system.

(x_1', x_2', x_3') as shown in Figure 5. Symbols of all quantities belonging to this system of reference are primed. The mid-plane of the plate is chosen to coincide with the $x_1' - x_2'$ plane. To study the propagation of plane waves in the plate along a direction that makes an arbitrary azimuthal angle ϕ with the x_1'-axis, we conduct our analysis in a transformed coordinate system x_i formed by a rotation of the orthogonal reference axes x_1', x_2' about the x_3' direction through this angle ϕ. This coordinate transformation can be written as

$$x_i = \beta_{ij} x_j', \tag{41}$$

where $\boldsymbol{\beta}$ is a rotation matrix and β_{ij} is the cosine of the angle between the x_i and x_j' axis. The stresses, strains and stiffness tensor in the two systems are related by

$$\sigma_{ij} = \beta_{im}\beta_{jn}\sigma'_{mn}, \tag{42}$$

$$\epsilon_{ij} = \beta_{im}\beta_{jn}\epsilon'_{mn}, \tag{43}$$

and

$$C_{ijkl} = \beta_{im}\beta_{jn}\beta_{ko}\beta_{lp}C'_{mnop}. \tag{44}$$

We will work only in the rotated (unprimed) coordinate system. All quantities from this point on are in this system. Consider again, a solution with the form of harmonic waves. All possible harmonic waves must have wave number vectors that are in the

$x_1 - x_3$ plane and travel with the same velocity with respect to the x_1 axis. For justification see Henneke (1972) and Jones (1971) [10, 11]. The general form of the solution is

$$u_j = U_j e^{i\xi(x_1+\alpha x_3-ct)}. \tag{45}$$

Substituting this equation in the equation of elastodynamics (Eq. (34)) gives a form of the Christoffel equations:

$$K_{mn}(\alpha)U_n = 0. \tag{46}$$

The coefficients of the matrix $\boldsymbol{K}$ using the contracted Voigt notation are given by:

$$\begin{aligned}
K_{11} &= C_{11} - \rho c^2 + 2C_{15}\alpha + C_{55}\alpha^2, \\
K_{12} &= C_{16} + (C_{14} + C_{56})\alpha + C_{45}\alpha^2, \\
K_{13} &= C_{15} + (C_{13} + C_{55})\alpha + C_{35}\alpha^2, \\
K_{22} &= C_{66} - \rho c^2 + 2C_46\alpha + C_{44}\alpha^2, \\
K_{23} &= C_{56} + (C_{36} + C_{45})\alpha + C_{34}\alpha^2, \\
K_{33} &= C_{55} - \rho c^2 + 2C_{35}\alpha + C_{33}\alpha^2.
\end{aligned} \tag{47}$$

For existence of non-trivial solutions, the determinant of $\boldsymbol{K}$ must go to zero as noted in Section 1.2.1. This produces a 6^{th} order equation in α with six solutions α_q, $q = 1...6$, corresponding to each of the six possible partial waves for the given guided wave velocity c:

$$P_6\alpha^6 + P_5\alpha^5 + P_4\alpha^4 + P_3\alpha^3 + P_2\alpha^2 + P_1\alpha + P_0 = 0, \tag{48}$$

where the coefficients (not given here) are a function of material properties and velocity of propagation of the guided wave c. Using Eq. (46), displacement ratios $V_q = U_{2q}/U_{1q}$ and $W_q = U_{3q}/U_{1q}$ can be defined as

$$V_q(\alpha_q) = \frac{K_{11}(\alpha_q)K_{23}(\alpha_q) - K_{13}(\alpha_q)K_{12}(\alpha_q)}{K_{13}(\alpha_q)K_{22}(\alpha_q) - K_{12}(\alpha_q)K_{23}(\alpha_q)} \tag{49}$$

and

$$W_q(\alpha_q) = \frac{K_{11}(\alpha_q)K_{23}(\alpha_q) - K_{13}(\alpha_q)K_{12}(\alpha_q)}{K_{12}(\alpha_q)K_{33}(\alpha_q) - K_{23}(\alpha_q)K_{13}(\alpha_q)}. \tag{50}$$

Using V and W as defined above with stress strain relations in Eq. (29), we can write the total displacements and stresses by superposition as

$$\begin{aligned}\{u_1, u_2, u_3\} &= \sum_{q=3}^{6} \{1, V(\alpha_q), W(\alpha_q)\} U_{1q} e^{i\xi(x_1+\alpha_q x_3 - ct)}, \\ \{\sigma_{33}, \sigma_{13}, \sigma_{23}\} &= \sum_{q=3}^{6} i\xi \{D_{1q}, D_{2q}, D_{3q}\} U_{1q} e^{i\xi(x_1+\alpha_q x_3 - ct)}.\end{aligned} \tag{51}$$

The stress amplitudes D_{mn} are given by:

$$\begin{aligned}D_{1q} &= [C_{13} + \alpha_q C_{35} + (C_{36} + \alpha_q C_{34})V_q + (C_{35} + \alpha_q C_{33})W_q], \\ D_{2q} &= [C_{15} + \alpha_q C_{55} + (C_{56} + \alpha_q C_{45})V_q + (C_{55} + \alpha_q C_{35})W_q], \\ D_{3q} &= [C_{14} + \alpha_q C_{45} + (C_{46} + \alpha_q C_{44})V_q + (C_{45} + \alpha_q C_{34})W_q].\end{aligned} \tag{52}$$

Applying stress free boundary conditions, i.e., setting σ_{13}, σ_{23} and σ_{33} to zero at $x_3 = d/2$ and $x_3 = -d/2$ results in six equations relating displacement amplitudes $U_{11}, U_{12}, \ldots, U_{16}$ whose determinant of coefficients must go to zero for nontrivial solutions.

$$\begin{vmatrix} D_{11}E_1 & D_{12}E_2 & D_{13}E_3 & D_{14}E_4 & D_{15}E_5 & D_{16}E_6 \\ D_{21}E_1 & D_{22}E_2 & D_{23}E_3 & D_{24}E_4 & D_{25}E_5 & D_{26}E_6 \\ D_{31}E_1 & D_{32}E_2 & D_{33}E_3 & D_{34}E_4 & D_{35}E_5 & D_{36}E_6 \\ D_{11}\tilde{E}_1 & D_{12}\tilde{E}_2 & D_{13}\tilde{E}_3 & D_{14}\tilde{E}_4 & D_{15}\tilde{E}_5 & D_{16}\tilde{E}_6 \\ D_{21}\tilde{E}_1 & D_{22}\tilde{E}_2 & D_{23}\tilde{E}_3 & D_{24}\tilde{E}_4 & D_{25}\tilde{E}_5 & D_{26}\tilde{E}_6 \\ D_{31}\tilde{E}_1 & D_{32}\tilde{E}_2 & D_{33}\tilde{E}_3 & D_{34}\tilde{E}_4 & D_{35}\tilde{E}_5 & D_{36}\tilde{E}_6 \end{vmatrix} = 0 \tag{53}$$

where $E_q = e^{i\xi\alpha_q d/2}$ and $\tilde{E}_q = e^{-i\xi\alpha_q d/2}$. The values of α are in general complex, which means the determinant is complex valued. Solving for the values of ξ and c that satisfy Eq. (53) can be a difficult numerical problem.

1.2.2.2 Special Case of Monoclinic Symmetry

If the material has monoclinic or higher symmetry, we can show that Eq. (53) decouples into a much simpler form that is numerically tractable and offers some insight into wave propagation in the plate. Starting with the assumption that the plane

of mirror symmetry of this material is placed parallel to the plane of the plate, the following constants go to zero for all azimuthal angles:

$$C_{14} = C_{24} = C_{34} = C_{15} = C_{25} = C_{35} = C_{46} = C_{56} = 0. \tag{54}$$

This reduction in terms simplifies Eqs. (47) and (48), resulting in symmetry properties that will help break down the determinant in Eq. (53). Equation (47) now becomes:

$$\begin{aligned} K_{11} &= C_{11} - \rho c^2 + C_{55}\alpha^2, \\ K_{12} &= C_{16} + C_{45}\alpha^2, \\ K_{13} &= (C_{13} + C_{55})\alpha, \\ K_{22} &= C_{66} - \rho c^2 + C_{44}\alpha^2, \\ K_{23} &= (C_{36} + C_{45})\alpha, \\ K_{33} &= C_{55} - \rho c^2 + C_{33}\alpha^2. \end{aligned} \tag{55}$$

Coefficients P_5, P_3, P_1 in Eq. (48) go to zero, resulting in

$$P_6\alpha^6 + P_4\alpha^4 + P_2\alpha^2 + P_0 = 0, \tag{56}$$

where the coefficients are listed in Appendix (A.1). This simplification results in six solutions with the following properties:

$$\alpha_2 = -\alpha_1, \alpha_4 = -\alpha_3, \alpha_6 = -\alpha_5. \tag{57}$$

Futher, the stress amplitudes D_{mn} are now given by:

$$\begin{aligned} D_{1q} &= C_{13} + C_{36}V_q + C_{33}\alpha_q W_q, \\ D_{2q} &= C_{55}(\alpha_q + W_q) + C_{45}\alpha_q V_q, \\ D_{3q} &= C_{45}(\alpha_q + W_q) + C_{44}\alpha_q V_q. \end{aligned} \tag{58}$$

Incorporating Eq. (57) into Eqs. (49), (50) and (55) leads to the following symmetries:

$$V_{j+1} = V_j, \quad W_{j+1} = -W_j. \tag{59}$$

Incorporating Eqs. (57) and (59) into Eq. (58) leads to

$$D_{1j+1} = D_{1j}, \quad D_{2j+1} = -D_{2j}, \quad D_{3j+1} = -D_{3j}. \tag{60}$$

Applying row-column operations to the determinant of Eq. (52) in the presence of these symmetries allow us to decouple the determinant into two equations consisting of trigonometric functions. These equations are

$$f_s = D_{11}G_1 \cot(\gamma\alpha_1) + D_{13}G_3 \cot(\gamma\alpha_3) + D_{15}G_5 \cot(\gamma\alpha_5) = 0 \tag{61}$$

for the symmetric modes and,

$$f_a = D_{11}G_1 \tan(\gamma\alpha_1) + D_{13}G_3 \tan(\gamma\alpha_3) + D_{15}G_5 \tan(\gamma\alpha_5) = 0 \tag{62}$$

for the antisymmetric modes, where

$$\begin{aligned} G_1 &= D_{23}D_{35} - D_{33}D_{25}, \\ G_3 &= D_{31}D_{25} - D_{21}D_{35}, \\ G_5 &= D_{21}D_{33} - D_{31}D_{23}, \\ \gamma &= \frac{\xi d}{2} = \frac{\omega d}{2c}. \end{aligned} \tag{63}$$

These are expressions that relate the guided wave velocity c to the wavelength ξ and describe entirely the dispersive behaviour of any wave as it propagates through the plate. It can be shown that these equations can under restricted conditions be applied to materials with higher symmetry (orthotropic, transversely isotropic etc.), however, this is beyond the scope of this dissertation.

1.2.2.3 Numerical Solution

Equations (61) and (62) look deceptivesly simple. Several numerical considerations have to be made in order to solve these equations to obtain dispersion curves. Commercial tools [12] are available to generate dispersion curves for anisotropic materials, however these only work for stress-free materials of orthotropic and higher symmetries. A numerical method was developed to solve dispersion equations for materials

Table 2: Material constants for a transversely isotropic (graphite-epoxy) material.

Parameter	**Value**
C'_{11}	155.6 GPa
C'_{12}	3.7 GPa
C'_{13}	3.7 GPa
C'_{22}	15.95 GPa
C'_{23}	4.33 GPa
C'_{33}	15.95 GPa
C'_{44}	5.81 GPa
C'_{55}	7.46 GPa
C'_{66}	7.46 GPa
ρ	1600 kg/m^3

of monoclinic symmetry and later augmented to solve the equations for the case of biaxially stressed isotropic materials discussed in later sections. The similarity between the two cases is a result of the fact that the final expressions for both cases have the same canonical form (although the expressions for Ds, Gs etc. are different) and a description of the numerical method will be omitted here to avoid repetition (see Section 5.3 for details).

1.2.2.4 Dispersion Curves

A few examples of dispersion curves are presented here for materials with different symmetries. The curves are represented by black lines against a color-map of the function $\log|f_s|$ (Eq. (61)) for symmetric modes and $\log|f_a|$ (Eq. (62)) for antisymmetric modes. Figures 6 and 7 present dispersion curves for a transversely isotropic

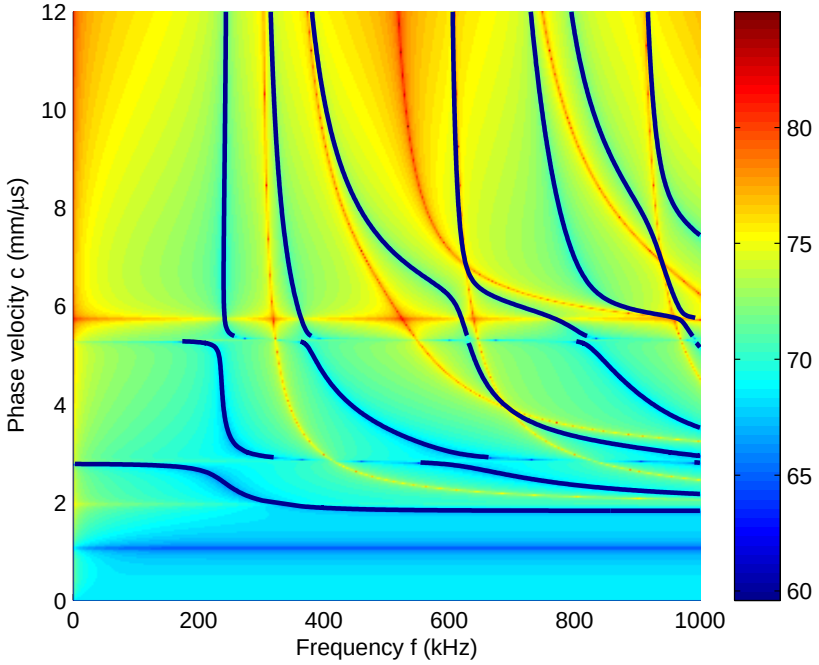

Figure 6: Symmetric modes for a transversely isotropic (graphite-epoxy) plate of thickness 6.35 mm at $\phi = 45°$.

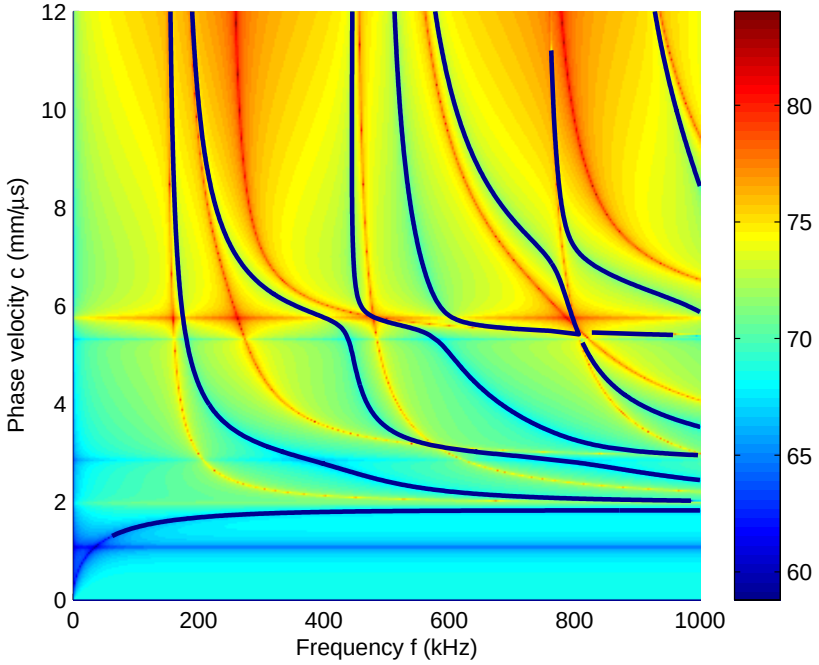

Figure 7: Antisymmetric modes for a transversely isotropic (graphite-epoxy) plate of thickness 6.35 mm at $\phi = 45°$.

Table 3: Material constants for an orthotropic (fictitious) material.

Parameter	**Value**
C'_{11}	128 GPa
C'_{12}	7 GPa
C'_{13}	6 GPa
C'_{22}	72 GPa
C'_{23}	5 GPa
C'_{33}	32 GPa
C'_{44}	18 GPa
C'_{55}	12.25 GPa
C'_{66}	8 GPa
ρ	2000 kg/m^3

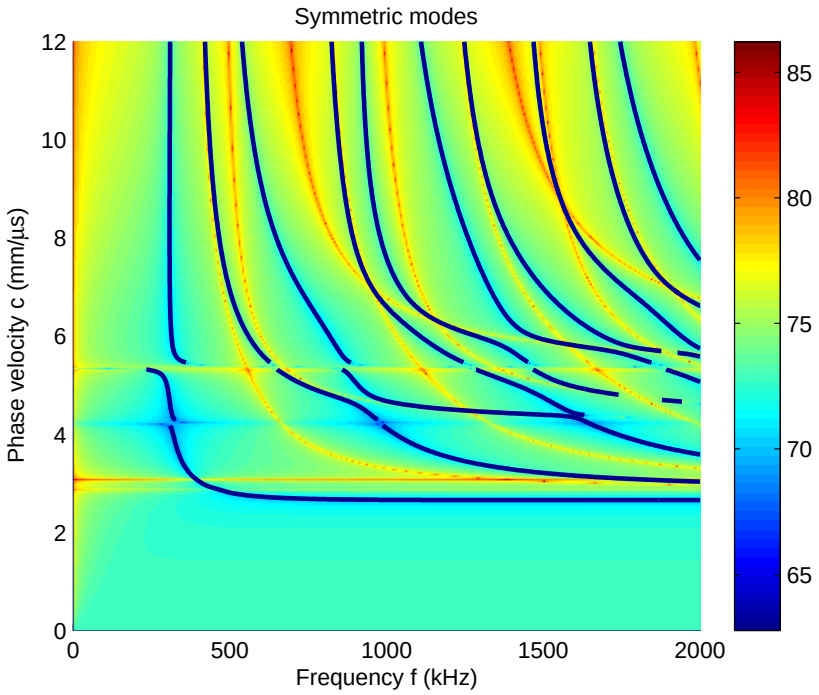

Figure 8: Symmetric modes for a fictitious orthotropic plate of thickness 6.35 mm at $\phi = 45°$.

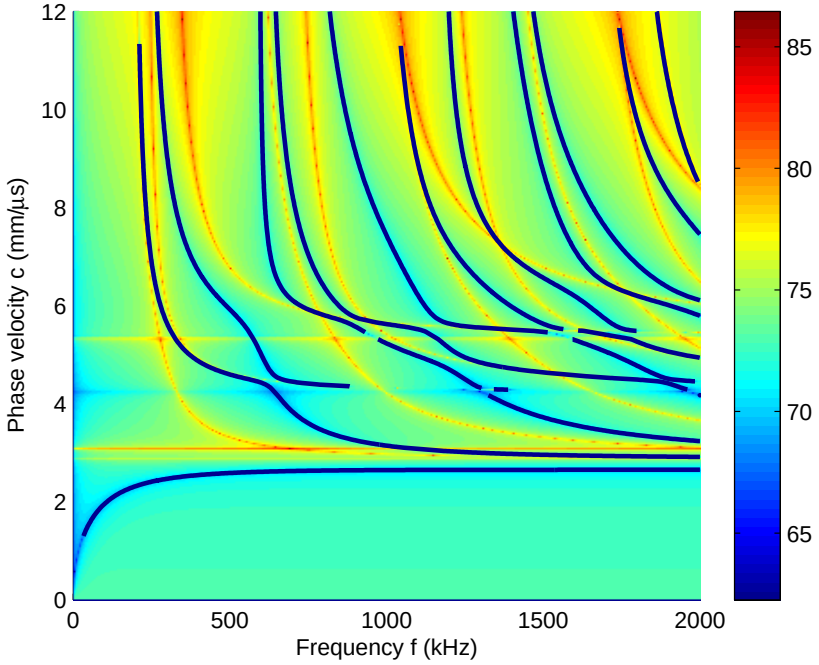

Figure 9: Antisymmetric modes for a fictitious orthotropic plate of thickness 6.35 mm at $\phi = 45°$.

(graphite-epoxy) plate of thickness 6.35 mm with material constants presented in Table 2. Figures 8 and 9 present dispersion curves for a orthotropic (fictitious) plate of thickness 6.35 mm with material parameters presented in Table 3. All material constants used in this section are the same as the ones used by Nayfeh and Chimenti [9]. "They were selected to model materials of interest where values were readily available". All curves are continuous in the $f - c$ plane, however, they appear discontinuous on the plots because of sudden changes in direction in some areas making it difficult for the algorithm to determine the best way to connect the roots of f_s and f_a. The results obtained agree with that of Nayfeh and Chimenti [9] and ones generated with commercial applications such as Disperse [12]. This validates the numerical method.

CHAPTER II

OVERVIEW OF ACOUSTOELASTICITY

Acoustoelasticity is a nonlinear phenomenon of interest in ultrasonics because it explains changes in wave speed of bulk waves as a function of applied stress. This chapter introduces and reviews the theory of acoustoelasticity in preparation for Chapter 3, where equations for the specific case of biaxial load are derived.

2.1 Nonlinear Ultrasonics

As a result of the linear stress-strain model assumed throughout Chapter 1, the relations between fields variables associated with the waves (displacement, strains, stresses) were also linear. Linearity greatly simplifies the analysis of dynamics in the material. However, these assumptions are only valid for media that are stress-free and have small perturbations. Nonlinear ultrasonics involves the use of nonlinear relations between field variables associated with ultrasonic waves and encompasses a broader range of phenomena [13, 14, 15, 16, 17]. Phenomena of interest in literature include acoustoelasticity, harmonic generation and finite amplitude effects [13]. Only acoustoelasticity is of interest in this dissertation.

2.2 Third Order Elastic Constants

In Chapter 1 we used second order elastic constants λ and μ as parameters to describe the linear stress-strain relation in an isotropic medium. For nonlinear characterization, however we need additional third order elastic constants (TOECs). TOECs are related to material anharmonicity and inter-atomic bonding forces that are inherently nonlinear [18].

Following the development in References [19, 15], for hyperelastic materials, the

strain energy function U can be expressed as a power series in strain:

$$U = \frac{1}{2!}C^{(2)}_{ijkl}E_{ij}E_{kl} + \frac{1}{3!}C^{(3)}_{ijklmn}E_{ij}E_{kl}E_{mn} + ..., \tag{64}$$

where $\boldsymbol{E}$ is the Lagrangian strain tensor and $\boldsymbol{C^{(2)}}, \boldsymbol{C^{(3)}}$ etc. are tensors of increasing order that are the coefficients of the series expansion. The stresses are related to the strain energy by

$$T_{ij} = \frac{\partial U}{\partial E_{ij}}, \tag{65}$$

where $\boldsymbol{T}$ is the second Piola-Kirchhoff stress tensor. Combining Eqs. (64) and (65) yields the stress strain relation:

$$T_{ij} = C^{(2)}_{ijkl}E_{kl} + C^{(3)}_{ijklmn}E_{kl}E_{mn} + ... \tag{66}$$

As noted before, $C^{(2)}_{ijkl}$ are the second order constants, which for isotropic materials are given by

$$C_{ijkl} = \lambda\delta_{ij} + \mu(\delta_{ik}\delta_{jl} + \delta_{il}\delta_{jk}), \tag{67}$$

where λ and μ are Lamé constants and δ is the Kronecker delta function given by

$$\delta_{ij} = \begin{cases} 1 \text{ if } i = j \\ 0 \text{ if } i \neq j \end{cases} \tag{68}$$

C_{ijklmn} represent 729 third order elastic constants. Due to symmetry, this reduces to 56 constants. Further, for isotropic materials, there are just three independent constants [15]. The 6th order tensor C_{ijklmn} for isotropic materials can be represented in terms of the Murnaghan constants l, m and n [20] as

$$\begin{aligned} C_{ijklmn} =& 2\left(l - m + \frac{n}{2}\right)\delta_{ij}\delta_{kl}\delta_{mn} + 2\left(m - \frac{n}{2}\right)(\delta_{ij}I_{klmn} + \delta_{kl}I_{mnij} + \delta_{mn}I_{ijkl}) \\ &+ \frac{n}{2}(\delta_{ik}I_{jlmn} + \delta_{il}I_{jkmn} + \delta_{jk}I_{ilmn} + \delta_{jl}I_{ikmn}), \end{aligned} \tag{69}$$

where

$$I_{ijkl} = \frac{(\delta_{ik}\delta_{jl} + \delta_{il}\delta_{jk})}{2}. \tag{70}$$

To summarize, Eq. (66) is the non-linear relation between stress and strain, and higher order stiffness tensors $C^{(3)}$, $C^{(4)}$ etc. are required to describe a relation between the two.

2.3 Acoustoelasticity

Acoustoelasticity is the stress dependence of acoustic wave velocity in solid media. The theory of acoustoelasticity was developed in 1953 by Hughes and Kelly [21] based on the Murnaghan theory of finite deformations for predeformed but initially isotropic solids. Acoustoelastic theory has since been generalized by Toupin and Berstein [19] in 1961 and Thurston and Brugger in 1964 [22] to materials of arbitrary symmetry. Acoustoelasticity has also been used extensively to study applied and residual stresses [23, 24, 25, 26].

2.3.1 Equations of Motion

The theory of acoustoelasticity for bulk waves is well developed [21] [27] [28]. We use some of the results from acoustoelasticity to describe the incremental stresses, strains and displacements in stressed media. Following the derivations of Pao et al. [27], coordinates of a material point in the natural, initial and final states are represented by the position vectors $\boldsymbol{\xi}, \boldsymbol{X}, \boldsymbol{x}$, respectively. Components of quantities referring to the natural state are given by Greek subscripts, those referring to the initial state are given by uppercase Roman subscripts, and those referring to the final state by lowercase Roman subscripts. Thus ξ_α, X_J and x_j are components of the position vectors in the natural, initial and final systems, respectively.

As shown in Figure 10, the deformation from natural to the initial states is static and the the displacement of the particles is denoted by $\boldsymbol{u^i}$. The displacements from the natural to the final sates is represented by the vector $\boldsymbol{u^f}$. These are related to the position vectors by

$$\boldsymbol{u^i}(\xi) = \boldsymbol{X} - \boldsymbol{\xi}, \tag{71}$$

and

$$\boldsymbol{u^f}(\xi, t) = \boldsymbol{x} - \boldsymbol{\xi}. \tag{72}$$

The difference between these two vectors is the dynamic displacement from the initial

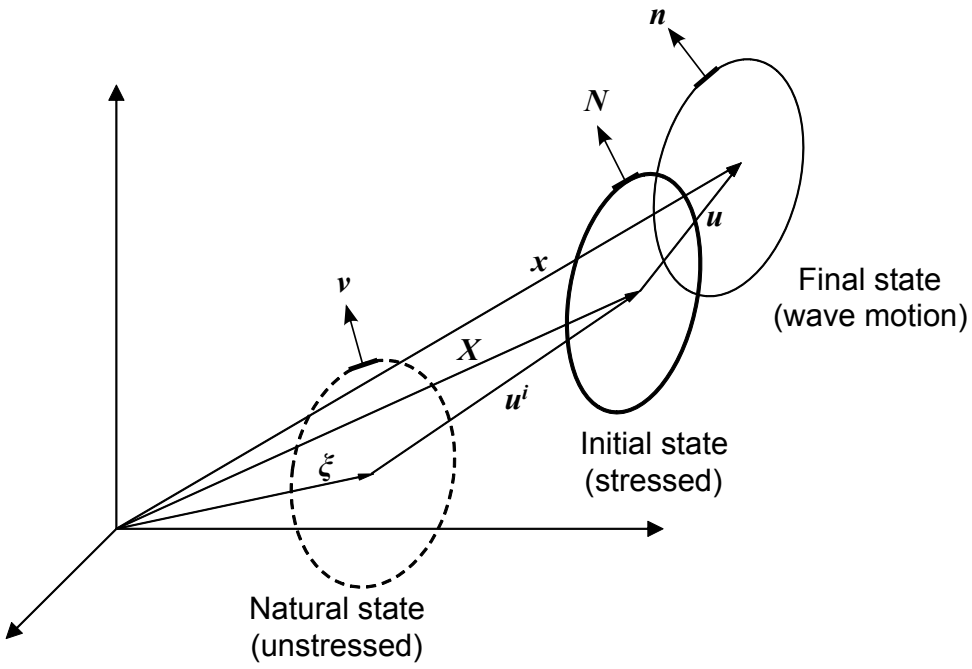

Figure 10: Coordinates of a material point at natural ($\boldsymbol{\xi}$), initial ($\boldsymbol{X}$) and final ($\boldsymbol{x}$) configuration of a predeformed body [28].

to the final state,

$$\boldsymbol{u}(\xi, t) = \boldsymbol{x} - \boldsymbol{X} = \boldsymbol{u^f} - \boldsymbol{u^i}. \tag{73}$$

The Lagrangian strain tensors in the initial and final states are defined as

$$\begin{aligned} E^i_{\alpha\beta} &= \frac{1}{2}\left(\frac{\partial u^i_\alpha}{\partial \xi_\beta} + \frac{\partial u^i_\beta}{\partial \xi_\alpha} + \frac{\partial u^i_\lambda}{\partial \xi_\alpha}\frac{\partial u^i_\lambda}{\partial \xi_\beta}\right), \\ E^f_{\alpha\beta} &= \frac{1}{2}\left(\frac{\partial u^f_\alpha}{\partial \xi_\beta} + \frac{\partial u^f_\beta}{\partial \xi_\alpha} + \frac{\partial u^f_\lambda}{\partial \xi_\alpha}\frac{\partial u^f_\lambda}{\partial \xi_\beta}\right). \end{aligned} \tag{74}$$

If the superposed dynamic motion is small, i.e.,

$$\|u_\alpha\| \ll \|u^i_\alpha\|, \quad \|E^f_{\alpha\beta} - E^i_{\alpha\beta}\| \ll \|E^i_{\alpha\beta}\|. \tag{75}$$

then the difference between the two strain tensors is given approximately by

$$E_{\alpha\beta} = E^f_{\alpha\beta} - E^i_{\alpha\beta} = \frac{1}{2}\left(\frac{\partial u_\alpha}{\partial \xi_\beta} + \frac{\partial u_\beta}{\partial \xi_\alpha} + \frac{\partial u^i_\lambda}{\partial \xi_\alpha}\frac{\partial u_\lambda}{\partial \xi_\beta} + \frac{\partial u^i_\lambda}{\partial \xi_\beta}\frac{\partial u_\lambda}{\partial \xi_\alpha}\right). \tag{76}$$

Stress tensors can be defined relative to different configurations. The Cauchy stress tensor $\boldsymbol{t}$, for example, describes the stresses relative to the present configuration while

the Kirchhoff (or the second Piola-Kirchhoff) stress tensor $\boldsymbol{T}$ describes the stresses relative to some reference configuration. These definitions allow us to write equations with reference to one of three configurations that were mentioned before. Therefore using the notation from the beginning of the section, the Kirchhoff stress components at the initial state that refers to the natural coordinate system are $T^i_{\alpha\beta}$, which are the force per unit predeformed area with an outernormal $\boldsymbol{v}$ as shown in Figure 10. Similarly, components of the Kirchhoff stress tensor in the final state relative to the undeformed configuration are represented by $T^f_{\alpha\beta}$. In general, different types of stress tensors are related by deformation gradients and determinant of Jacobians. However, in the presentation that follows, only Kirchhoff stress tensors relative to the undeformed (or natural) state will be used. For details refer to [27] [16].

The equation of equilibrium for the static predeformation is given by

$$\frac{\partial}{\partial \xi_\beta}\left[T^i_{\beta\alpha} + T^i_{\beta\gamma}\frac{\partial u^i_\alpha}{\partial \xi_\gamma}\right] = 0. \tag{77}$$

The equations of motion for the final state can be expressed as

$$\frac{\partial}{\partial \xi_\beta}\left[T^f_{\beta\alpha} + T^f_{\beta\gamma}\frac{\partial u^f_\alpha}{\partial \xi_\gamma}\right] = \rho^0\frac{\partial^2 u^f_\alpha}{\partial t^2}. \tag{78}$$

Subtracting the two equations above and dropping $T_{\beta\gamma}\frac{\partial u_\alpha}{\partial \xi_\gamma}$ [27],

$$\frac{\partial}{\partial \xi_\beta}\left[T_{\alpha\beta} + T^i_{\beta\gamma}\frac{\partial u_\alpha}{\partial \xi_\gamma} + T_{\beta\gamma}\frac{\partial u^i_\alpha}{\partial \xi_\gamma}\right] = \rho^0\frac{\partial^2 u_\alpha}{\partial t^2}. \tag{79}$$

The relation above is the equation of motion for the incremental displacement $\boldsymbol{u}(\xi, t)$ in natural coordinates. However, a constitutive relation is also required to express the stresses as a function of displacements. This is already available in Eq. (66). Neglecting higher order terms in the expansion we have the following stress-strain relations:

$$T^i_{\alpha\beta} = C_{\alpha\beta\gamma\delta}E^i_{\gamma\delta} + \frac{1}{2}C_{\alpha\beta\gamma\delta\epsilon\eta}E^i_{\gamma\delta}E^i_{\epsilon\eta}, \tag{80}$$

$$T^f_{\alpha\beta} = C_{\alpha\beta\gamma\delta}E^f_{\gamma\delta} + \frac{1}{2}C_{\alpha\beta\gamma\delta\epsilon\eta}E^f_{\gamma\delta}E^f_{\epsilon\eta}. \tag{81}$$

Subtracting the final stress from the initial to get the incremental stress,

$$\begin{aligned}
T_{\alpha\beta} &= T^f_{\alpha\beta} - T^i_{\alpha\beta} \\
&= C_{\alpha\beta\gamma\delta}E^f_{\gamma\delta} + \frac{1}{2}C_{\alpha\beta\gamma\delta\epsilon\eta}E^f_{\gamma\delta}E^f_{\epsilon\eta} - C_{\alpha\beta\gamma\delta}E^i_{\gamma\delta} - \frac{1}{2}C_{\alpha\beta\gamma\delta\epsilon\eta}E^i_{\gamma\delta}E^i_{\epsilon\eta} \\
&= C_{\alpha\beta\gamma\delta}E_{\gamma\delta} + \frac{1}{2}C_{\alpha\beta\gamma\delta\epsilon\eta}[(E^f_{\gamma\delta}E^f_{\epsilon\eta}) - E^i_{\gamma\delta}E^i_{\epsilon\eta}] \\
&= C_{\alpha\beta\gamma\delta}E_{\gamma\delta} + \frac{1}{2}C_{\alpha\beta\gamma\delta\epsilon\eta}[(E^i_{\gamma\delta}E^i_{\epsilon\eta} + E^i_{\gamma\delta}E_{\epsilon\eta} + E_{\gamma\delta}E^i_{\epsilon\eta} + E_{\gamma\delta}E_{\epsilon\eta}) - E^i_{\gamma\delta}E^i_{\epsilon\eta}] \\
&= C_{\alpha\beta\gamma\delta}E_{\gamma\delta} + C_{\alpha\beta\gamma\delta\epsilon\eta}[E^i_{\gamma\delta}E_{\epsilon\eta} + \frac{1}{2}E_{\gamma\delta}E_{\epsilon\eta}].
\end{aligned} \tag{82}$$

Under the assumption that the dynamic disturbance is small compared to the pre-deformation, the second term inside the brackets can be neglected because it is a product of two small quantities (see Eq. (75)). "To be consistent with the cubic polynomial approximation of the strain energy function, the Lagrangian strains are approximated by infinitesimal (or Cauchy) strain tensors" [27] to give

$$T_{\alpha\beta} = C_{\alpha\beta\gamma\delta}E_{\gamma\delta} + C_{\alpha\beta\gamma\delta\epsilon\eta}e^i_{\gamma\delta}e_{\epsilon\eta}, \tag{83}$$

where

$$\begin{aligned}
e_{\alpha\beta} &= \frac{1}{2}\left[\frac{\partial u_\alpha}{\partial \xi_\beta} + \frac{\partial u_\beta}{\partial \xi_\alpha}\right], \\
e^i_{\alpha\beta} &= \frac{1}{2}\left[\frac{\partial u^i_\alpha}{\partial \xi_\beta} + \frac{\partial u^i_\beta}{\partial \xi_\alpha}\right].
\end{aligned} \tag{84}$$

Substituting this in Eq. (79) gives

$$\frac{\partial}{\partial \xi_\beta}\left[T^i_{\gamma\beta}\frac{\partial u_\alpha}{\partial \xi_\gamma} + \Gamma_{\alpha\beta\gamma\delta}\frac{\partial u_\gamma}{\partial \xi_\delta}\right] = \rho^0\frac{\partial^2 u_\alpha}{\partial t^2}, \tag{85}$$

where

$$\Gamma_{\alpha\beta\gamma\delta} = C_{\alpha\beta\gamma\delta} + C_{\alpha\beta\rho\delta}\frac{\partial u^i_\gamma}{\partial \xi_\rho} + C_{\rho\beta\gamma\delta}\frac{\partial u^i_\alpha}{\partial \xi_\rho} + C_{\alpha\beta\gamma\delta\epsilon\eta}e^i_{\epsilon\eta}. \tag{86}$$

Plane waves can only propagate in homogeneous media because constant characteristic wave speeds are required on the entire wavefront. However, from the equation above we see that the wavespeeds change from point to point depending on the value of initial stress $\boldsymbol{t^i}$ and initial displacement gradient $\boldsymbol{\partial u^i/\partial \xi}$. As a result these equations

do not admit plate wave solutions unless these coefficients are constants with respect to the three axis, i.e., $\boldsymbol{t^i}$ and $\boldsymbol{\partial u^i/\partial \xi}$ are constant through out the body. In this case of homogeneous predeformation, the equation of motion in natural cooridantes is given by

$$A_{\alpha\beta\gamma\delta}\frac{\partial^2 u_\gamma}{\partial\xi_\beta\partial\xi_\delta} = \rho^0\frac{\partial^2 u_\alpha}{\partial t^2}, \tag{87}$$

where the coefficients $A_{\alpha\beta\gamma\delta}$, now spatially independent, are given by

$$A_{\alpha\beta\gamma\delta} = T^i_{\beta\delta}\delta_{\alpha\gamma} + \Gamma_{\alpha\beta\gamma\delta}. \tag{88}$$

2.3.2 Bulk Waves

Linearization of the wave equation in the previous section now allows us to use a method similar to the one presented in Section 1.2.1 to characterize bulk wave propagation in a homogeneous medium in a uniform stress field. The stressed material is not necessarily isotropic since an arbitrary uniform stress field can be applied. In general this means that Helmoltz decomposition will not yield a direct solution. Starting with a plane harmonic traveling wave solution of the form

$$u_\alpha = A_\alpha e^{i(k_\beta\xi_\beta - \omega t)}, \tag{89}$$

where $\boldsymbol{u}$ is the particle displacement vector, $A_\alpha = Ad_\alpha$, A is the amplitude of displacement, $\boldsymbol{d}$ is a unit-vector that represents the direction of particle displacement, $\boldsymbol{k}$ is the wave vector and ω is the angular frequency. All quantities are with respect to the standard Cartesian frame of reference (ξ_1, ξ_2, ξ_3). Substituting Eq. (89) into Eq. (87) gives us the Christoffel equation

$$(\Delta_{\alpha\delta} - \rho c^2\delta_{\alpha\delta})u_\delta = 0, \tag{90}$$

where $\Delta_{\alpha\delta} = A_{\alpha\beta\gamma\delta}n_\beta n_\gamma$. The acoustic tensor is represented by $\boldsymbol{\Delta}$, n_β and n_γ are the direction cosines of the normal to the wavefront, i.e., $k_\alpha = |\boldsymbol{k}|n_\alpha$. For any non-trivial solution such that the displacements are non-zero, the determinant of the coefficient

matrix in the expression above must go to zero,

$$|\Delta_{\alpha\delta} - \rho c^2 \delta_{\alpha\delta}| = 0. \tag{91}$$

This is again a relation between the material properties, applied stresses, direction of wave propagation and the velocity of the wave. It is evident that the velocities are now a function of direction of propagation and the applied stress. Also, particle displacements are not necessarily perpendicular or parallel to the direction of propagation.

CHAPTER III

ACOUSTOELASTIC CONSTANTS FOR ISOTROPIC MEDIA WITH BIAXIAL INITIAL STRESS

In Chapter 2 a linear wave equation was obtained to represent dynamics for a homogeneous body under an uniform stress field. Since the case of interest in this dissertation is that of biaxial initial stresses in a isotropic medium, equations of motion and stress strain relations from Chapter 2 are specialized for this purpose.

3.1 Equations of Motion

Following the work of Muir [29], coefficients $A_{\alpha\beta\gamma\delta}$ in Eq. (87) for the specific case of a biaxial load are derived. As the derivation will show, some of coefficients for this case are zero and this has substantial implications in the theory for plate waves. For the non-zero coefficients, it will provide us with expressions allowing us to perform numerical computations.

First, Eq. (80) has to be modified for small predeformations. Under this assumption, the strains are small and can be approximated by the Cauchy strain tensor. Also product of two small stains in the second term can be neglected, producing the following stress strain relation [28]:

$$T^i_{\alpha\beta} = C_{\alpha\beta\gamma\delta} e^i_{\gamma\delta}. \tag{92}$$

Eq. (88) then becomes

$$A_{\alpha\beta\gamma\delta} = C_{\beta\delta\lambda\rho} e^i_{\lambda\rho} \delta_{\alpha\gamma} + C_{\alpha\beta\gamma\delta} + C_{\alpha\beta\rho\delta} \frac{\partial u^i_\gamma}{\partial \xi_\rho} + C_{\rho\beta\gamma\delta} \frac{\partial u^i_\alpha}{\partial \xi_\rho} + C_{\alpha\beta\gamma\delta\epsilon\eta} e^i_{\epsilon\eta}. \tag{93}$$

For a medium with stresses σ_{11} along ξ_1 and σ_{22} along ξ_2 the Kirchhoff stress tensor

in the natural system is

$$T^i_{\alpha\beta} = \begin{bmatrix} \sigma_{11} & 0 & 0 \\ 0 & \sigma_{22} & 0 \\ 0 & 0 & 0 \end{bmatrix}. \tag{94}$$

The linear relation in Eq. (92) can be rewritten using Voight notation to give

$$\begin{bmatrix} T^i_1 \\ T^i_2 \\ T^i_3 \\ T^i_4 \\ T^i_5 \\ T^i_6 \end{bmatrix} = \begin{bmatrix} C_{11} & C_{12} & C_{13} & 0 & 0 & 0 \\ C_{21} & C_{22} & C_{23} & 0 & 0 & 0 \\ C_{31} & C_{32} & C_{33} & 0 & 0 & 0 \\ 0 & 0 & 0 & 2C_{44} & 0 & 0 \\ 0 & 0 & 0 & 0 & 2C_{55} & 0 \\ 0 & 0 & 0 & 0 & 0 & 2C_{66} \end{bmatrix} \begin{bmatrix} e^i_1 \\ e^i_2 \\ e^i_3 \\ e^i_4 \\ e^i_5 \\ e^i_6 \end{bmatrix}. \tag{95}$$

The multiplicative factors of 2 appear on the shear terms as a result of the conversion from 4th other tensor to a matrix using Voight notation. C_{44} corresponds to 4 different constants ($C_{2323}, C_{2332}, C_{3223}, C_{3232}$) while C_{11} corresponds to only C_{1111}, etc. Inverting this relation, and using Eq. (67) gives

$$\begin{aligned} e^i_1 &= \frac{(\lambda+\mu)\sigma 11}{3\lambda\mu + 2\mu^2} - \frac{\lambda\sigma 22}{6\lambda\mu + 4\mu^2}, \\ e^i_2 &= -\frac{\lambda\sigma 11}{6\lambda\mu + 4\mu^2} + \frac{(\lambda+\mu)\sigma 22}{3\lambda\mu + 2\mu^2}, \\ e^i_3 &= -\frac{\lambda\sigma 11}{6\lambda\mu + 4\mu^2} - \frac{\lambda\sigma 22}{6\lambda\mu + 4\mu^2}, \\ e^i_4 &= 0, \\ e^i_5 &= 0, \\ e^i_6 &= 0. \end{aligned} \tag{96}$$

Next, we note that the rotation terms are zero for this stress configuration:

$$r^i_{ij} = \frac{1}{2}\left[\frac{\partial u^i_i}{\partial \xi_j} - \frac{\partial u^i_j}{\partial \xi_i}\right] = 0. \tag{97}$$

Also, since

$$\frac{\partial u^i_\gamma}{\partial \xi_j} = r^i_{ij} + e^i_{ij} = e^i_{ij}, \tag{98}$$

Eq. (93) can be re-written as

$$A_{\alpha\beta\gamma\delta} = C_{\beta\delta\lambda\rho}e^i_{\lambda\rho}\delta_{\alpha\gamma} + C_{\alpha\beta\gamma\delta} + C_{\alpha\beta\rho\delta}e^i_{\gamma\rho} + C_{\rho\beta\gamma\delta}e^i_{\alpha\rho} + C_{\alpha\beta\gamma\delta\epsilon\eta}e^i_{\epsilon\eta}. \tag{99}$$

We now have everything needed to compute expressions for the $\boldsymbol{A}$ tensor from Eqs. (67) and (96). For example, the expression for A_{1111} is

$$\begin{aligned} A_{1111} = \; & \frac{\mu(\lambda+2\mu)(3\lambda+2\mu) + (2\lambda^2+9\lambda\mu+4m(\lambda+\mu)+2\mu(l+3\mu))\,\sigma_{11}}{\mu(3\lambda+2\mu)} \\ & - \frac{(-2l\mu+\lambda(2m+\lambda+2\mu))\sigma_{22}}{\mu(3\lambda+2\mu)} \end{aligned} \tag{100}$$

The expressions for the remaining coefficients are listed in Appendix B.1. These constants, along with Eq. (87), represent the acoustoelastic equations of motion for biaxially loaded media.

3.2 Stress-Strain Relation

In this section we consider the incremental stress-strain relation. Starting with Eq. (84),

$$T_{\alpha\beta} = C_{\alpha\beta\gamma\delta}E_{\gamma\delta} + C_{\alpha\beta\gamma\delta\epsilon\eta}e^i_{\gamma\delta}e_{\epsilon\eta}. \tag{101}$$

Using Eq. (76) leads to

$$T_{\alpha\beta} = C_{\alpha\beta\gamma\delta}\frac{1}{2}\left(\frac{\partial u_\gamma}{\partial\xi_\delta} + \frac{\partial u_\delta}{\partial\xi_\gamma} + \frac{\partial u^i_\lambda}{\partial\xi_\gamma}\frac{\partial u_\lambda}{\partial\xi_\delta} + \frac{\partial u^i_\lambda}{\partial\xi_\delta}\frac{\partial u_\lambda}{\partial\xi_\gamma}\right) + C_{\alpha\beta\gamma\delta\epsilon\eta}e^i_{\gamma\delta}\frac{1}{2}\left(\frac{\partial u_\epsilon}{\partial\xi_\eta} + \frac{\partial u_\eta}{\partial\xi_\epsilon}\right). \tag{102}$$

Using symmetries in the second and third order elastic constants, $C_{\alpha\beta\gamma\delta\epsilon\eta} = C_{\alpha\beta\gamma\delta\eta\epsilon}$ and $C_{\alpha\beta\gamma\delta} = C_{\alpha\beta\delta\gamma}$,

$$T_{\alpha\beta} = C_{\alpha\beta\gamma\delta}\frac{\partial u_\gamma}{\partial\xi_\delta} + C_{\alpha\beta\gamma\delta}\frac{\partial u^i_\lambda}{\partial\xi_\gamma}\frac{\partial u_\lambda}{\partial\xi_\delta} + C_{\alpha\beta\gamma\delta\epsilon\eta}e^i_{\gamma\delta}\frac{\partial u_\epsilon}{\partial\xi_\eta}. \tag{103}$$

Rewriting indices and using $C_{\alpha\beta\gamma\delta\epsilon\eta} = C_{\alpha\beta\epsilon\eta\gamma\delta}$,

$$\begin{aligned} T_{\alpha\beta} &= C_{\alpha\beta\gamma\delta}\frac{\partial u_\gamma}{\partial\xi_\delta} + C_{\alpha\beta\lambda\delta}\frac{\partial u^i_\gamma}{\partial\xi_\lambda}\frac{\partial u_\gamma}{\partial\xi_\delta} + C_{\alpha\beta\gamma\delta\epsilon\eta}e^i_{\epsilon\eta}\frac{\partial u_\gamma}{\partial\xi_\delta} \\ &= \left(C_{\alpha\beta\gamma\delta} + C_{\alpha\beta\lambda\delta}\frac{\partial u^i_\gamma}{\partial\xi_\lambda} + C_{\alpha\beta\gamma\delta\epsilon\eta}e^i_{\epsilon\eta}\right)\frac{\partial u_\gamma}{\partial\xi_\delta}. \end{aligned} \tag{104}$$

Using Eq. (98),

$$\begin{aligned} T_{\alpha\beta} &= \left(C_{\alpha\beta\gamma\delta} + C_{\alpha\beta\lambda\delta}e^{i}_{\gamma\lambda} + C_{\alpha\beta\gamma\delta\epsilon\eta}e^{i}_{\epsilon\eta}\right)\frac{\partial u_\gamma}{\partial \xi_\delta} \\ &= B_{\alpha\beta\gamma\delta}\frac{\partial u_\gamma}{\partial \xi_\delta}. \end{aligned} \tag{105}$$

The equation above is the relation between the incremental stresses and displacements. It should be emphasised that the stress ($\boldsymbol{T}$) tensor and displacement ($\boldsymbol{u}$) vector in the equation above correspond to the incremental wave motion and do not include the effects of static predeformation. The coefficients $B_{\alpha\beta\gamma\delta}$ are constant and can be computed using Eqs. (67), (69) and (96). B_{1111}, for example, is given by

$$\begin{aligned} B_{1111} =& \frac{2\mu(\lambda+2\mu)(3\lambda+2\mu) + 2(2l\mu + (\lambda+\mu)(4m+\lambda+2\mu))\sigma_{11}}{2\mu(3\lambda+2\mu)} \\ &- \frac{(-4l\mu + \lambda(4m+\lambda+2\mu))\sigma_{22}}{2\mu(3\lambda+2\mu)}. \end{aligned} \tag{106}$$

The remaining coefficients are listed in Appendix B.2.

It is important to note that since the relation is linear, the strain tensor $\boldsymbol{e^i}$, the stress tensor $\boldsymbol{T^i}$, and the tensors $\boldsymbol{A}$ and $\boldsymbol{B}$ all follow the rules of tensor rotation, which means that a rotation matrix can be applied to any tensor to rotate the material in space.

CHAPTER IV

DISPERSION CURVES USING EFFECTIVE ELASTIC CONSTANTS

From symmetry considerations alone, it is expected that under a biaxial load the propagation of Lamb waves in the plate will be anisotropic. However, the type of anisotropy exhibited is important. In this chapter an attempt is made to draw parallels between two cases: (1) a material with monoclinic symmetry and (2) an isotropic material with a uniaxial stress applied in a direction parallel to the plane of the plate. Since a numerical method for monoclinic materials has already been developed in Section 1.2.2, similarities between the two cases would yield an approximate solution for the case of isotropic plates under uniaxial stress. It will also enable the use of existing commercial applications such as Disperse [12] to generate dispersion curves for stressed plates.

4.1 Symmetry in the A Tensor

The equation of motion in anisotropic materials, Eq. (34), is analogous to the equation of motion in a material under uniform stress, Eq. (87). The equations are exactly the same, expect for the tensors $\boldsymbol{C}$ and $\boldsymbol{A}$, which capture information about the symmetry of the material. Also, it should be noted the the following symmetries of the $\boldsymbol{C}$ tensor are integral to the theory for anisotropic materials in Section 1.2.2.

$$C_{ijkl} = C_{ijlk} = C_{jikl} = C_{klij}. \tag{107}$$

It allows us to use Voight notation to give the following representation of the stiffness matrix for monoclinic materials with a $\xi_1 - \xi_2$ plane of symmetry [30, 5, 7]:

$$\begin{bmatrix} C_{11} & C_{12} & C_{13} & 0 & C_{15} & 0 \\ & C_{22} & C_{23} & 0 & C_{25} & 0 \\ & & C_{33} & 0 & C_{35} & 0 \\ & & & C_{44} & 0 & C_{46} \\ & & & & C_{55} & 0 \\ & & & & & C_{66} \end{bmatrix}. \tag{108}$$

It is shown in Section 1.2.2.2 that in a plate made of a monoclinic material where the plane of monoclinic symmetry is parallel to the plane of the plate, bulk waves traveling with opposing ξ_3 wave numbers have the same velocity, giving rise to symmetric and antisymmetric Lamb modes. The case of monoclinic symmetry is a more general case of a material that is transversely isotropic about the ξ_1 axis. The stiffness matrix for this type of material is represented by [30, 5, 7]:

$$\begin{bmatrix} C_{11} & C_{12} & C_{12} & 0 & 0 & 0 \\ & C_{22} & C_{23} & 0 & 0 & 0 \\ & & C_{22} & 0 & 0 & 0 \\ & & & \frac{1}{2}(C_{22} - C_{23}) & 0 & 0 \\ & & & & C_{55} & 0 \\ & & & & & C_{55} \end{bmatrix}. \tag{109}$$

Also, a uniaxial load along the ξ_1 axis is expected to result in wave propagation that is symmetric about this axis. In other words the material is in some sense transversely isotropic about the ξ_1 axis. The symmetries in the $\boldsymbol{A}$ tensor using expressions from

B.1 for a uniaxial load ($\sigma_{22} = 0$) are:

$$\begin{bmatrix} A_{11} & A_{12} & A_{12} & 0 & 0 & 0 \\ & A_{22} & A_{23} & 0 & 0 & 0 \\ & & A_{22} & 0 & 0 & 0 \\ & & & \frac{1}{2}(A_{22} - A_{23}) & 0 & 0 \\ & & & & \text{Split} & 0 \\ & & & & & \text{Split} \end{bmatrix}. \tag{110}$$

The form is exactly the same as that of the transversely isotropic material except that the coefficients corresponding to A_{55} and A_{66} do not have unique values and each of them splits into two values in the following fashion:

$$\begin{aligned} A_{55}^{(1)} &= A_{1313} = A_{3131} = \mu + \frac{(n\lambda + 4\mu(m + 2(\lambda + \mu)))\sigma_{11}}{4\mu(3\lambda + 2\mu)}. \\ A_{55}^{(2)} &= A_{1331} = A_{3113} = \mu + \frac{(n\lambda + 2\mu(2m + \lambda + 2\mu))\sigma_{11}}{4\mu(3\lambda + 2\mu)}. \\ A_{66}^{(1)} &= A_{1212} = A_{2121} = \mu + \frac{(n\lambda + 4\mu(m + 2(\lambda + \mu)))\sigma_{11}}{4\mu(3\lambda + 2\mu)}. \\ A_{66}^{(2)} &= A_{2112} = A_{1221} = \mu + \frac{(n\lambda + 2\mu(2m + \lambda + 2\mu))\sigma_{11}}{4\mu(3\lambda + 2\mu)}. \end{aligned} \tag{111}$$

4.2 Selecting Effective Elastic Constants

From the similarities of a uniaxially loaded material to a transversely isotropic material, a new tensor $\boldsymbol{A'}$ can be constructed such that the degenerations in the coefficients are avoided. In literature, these new constants are called the effective elastic constants (EECs) [31] [32]. Further, this new tensor can be used with Eqs. (61) and (62) to obtain dispersion curves for a stressed plate. However, these are transcendental equations and thus choosing appropriate values for the coefficients that split is analytically infeasible.

It should also be noted that avoiding degenerations in constants of the stiffness matrix by changing values in the corresponding 4th order tensor means that some of the information contained in the stiffness tensor is lost. Also, the stress-strain

relations for an unstressed transversely isotropic plate (Eq. (29)) are different from those of a stressed plate (Eq. (105)), resulting in different analyses while applying boundary conditions. As a result, this method is an approximation and is proposed because (1) it simplifies the mathematics and (2) existing methods and tools used to compute dispersion curves in anisotropic plates [12] can be used for new applications involving stressed plates.

Duquennoy et al. [32] state that the coefficients $A_{55}^{(2)}$ and $A_{66}^{(2)}$ can be neglected altogether, after which a classic second order formalism can be applied by replacing the second order constants with EECs. "The perturbation linked to the presence of residual or applied stress is fully integrated in the EEC". In this treatment, however, we follow a different approach by examining the difference in the two elastic constants,

$$\begin{aligned} A_{55}^{(1)} - A_{55}^{(2)} &= \frac{\sigma_{11}}{2}, \\ A_{66}^{(1)} - A_{66}^{(2)} &= \frac{\sigma_{11}}{2}. \end{aligned} \tag{112}$$

We note that the difference is half the applied stress. The applied stress has to be lower than the yield stress of the material to avoid plastic deformations. The yield stress for aluminum, for example, is hundreds of MPa and is typically two orders of magnitude lower than the material constants, which are of the order of tens of GPa. An assumption of small applied stress is also consistent with the small strain assumption in development of acoustoelastic theory in Chapter 3. This could indicate that using either of the values may not have a significant effect on computation of dispersion curves. Also, if we choose EEC $A'_{55} = A_{55}^{(1)}$, then A'_{66} should be equal to $A_{66}^{(1)}$ to retain transversely isotropic symmetry for the stiffness matrix in Eq. (109). The choice of $A'_{55} = A'_{66} = A_{55}^{(1)}$ will be referred to as case I, while $A'_{55} = A'_{66} = A_{55}^{(2)}$ will be referred to as case II.

The derivation for monoclinic materials required the rotation of the stiffness matrix to obtain dispersion curves at varying in-plane angles of propagation. Therefore, before we proceed, the effect of rotation on the splits must also be considered. To

derive dispersion relations, a rotation of the stiffness tensor about the ξ_3 axis is required. Rotation of the $\boldsymbol{A}$ tensor produces additional split coefficients A_{44} and the pair A_{45}/A_{54} as shown below:

$$\begin{bmatrix} A_{11}^{\phi} & A_{12}^{\phi} & A_{13}^{\phi} & 0 & 0 & 0 \\ & A_{22}^{\phi} & A_{23}^{\phi} & 0 & 0 & 0 \\ & & A_{33}^{\phi} & 0 & 0 & 0 \\ & & & \text{Split} & \text{Split} & 0 \\ & & & & \text{Split} & 0 \\ & & & & & \text{Split} \end{bmatrix}, \tag{113}$$

where

$$\begin{aligned} A_{44}^{\phi(1)} &= A_{2323}^{\phi} = A_{3232}^{\phi} = \mu + \frac{(n\lambda + 4\mu(m + 2(\lambda + \mu)))\sigma_{11}}{4\mu(3\lambda + 2\mu)}, \\ A_{44}^{\phi(2)} &= A_{2332}^{\phi} = A_{3223}^{\phi} = \mu + \frac{(n\lambda + 2\mu(2m + \lambda + 2\mu))\sigma_{11}}{4\mu(3\lambda + 2\mu)}, \\ A_{45}^{\phi(1)} &= A_{2313}^{\phi} = A_{3231}^{\phi} = \mu + \frac{(n\lambda + 4\mu(m + 2(\lambda + \mu)))\sigma_{11}}{4\mu(3\lambda + 2\mu)} = A_{1323}^{\phi} = A_{3132}^{\phi} = A_{54}^{\phi(1)}, \\ A_{45}^{\phi(2)} &= A_{2331}^{\phi} = A_{3213}^{\phi} = \mu + \frac{(n\lambda + 2\mu(2m + \lambda + 2\mu))\sigma_{11}}{4\mu(3\lambda + 2\mu)} = A_{1332}^{\phi} = A_{3123}^{\phi} = A_{54}^{\phi(2)}. \end{aligned} \tag{114}$$

It can be verified that if EECs are selected such that $A'_{55} = A_{55}^{(n)}$ and $A'_{66} = A_{66}^{(n)}$, then after rotation through an angle ϕ, $A_{44}^{'\phi}$ will take on a value of $A_{44}^{\phi(n)}$ and $A_{45}^{'\phi} = A_{54}^{'\phi} = A_{45}^{\phi(n)}$, where $n = 1$ or 2. In other words, selection of A'_{55} and A'_{66} in this manner also "bounds" $A_{44}^{'\phi}, A_{45}^{'\phi}$ and $A_{54}^{'\phi}$ to the splits in $A_{44}^{\phi}, A_{45}^{\phi}$ and A_{54}^{ϕ} respectively.

4.3 Numerical Results

This section presents dispersion curves generated using EECs with the numerical method of Section 1.2.2.3. Material constants from Table 4 are used along with a plate thickness of 6.35 mm and a uniaxial stress of $\sigma_{11} = 120$ MPa. The EECs were generated by using the expressions for the $\boldsymbol{A}$ tensor in Appendix B.1 along with

Table 4: Material parameters used to generate dispersion curves. TOECs obtained by Stobbe [33].

Parameter	**Value**
l	-252.2 GPa
m	-324.9 GPa
n	-351.2 GPa
λ	54.9 GPa
μ	26.5 GPa
ρ^0	2800 kg/m^3

constants for the two cases from the previous section. All coefficients have units of GPa.

- Case I : $A'_{55} = A^{(1)}_{55}$ and $A'_{66} = A^{(1)}_{66}$:

$$\boldsymbol{A'} = \begin{bmatrix} 105.91 & 54.513 & 54.513 & 0 & 0 & 0 \\ & 108.24 & 55.065 & 0 & 0 & 0 \\ & & 108.24 & 0 & 0 & 0 \\ & & & 26.588 & 0 & 0 \\ & & & & 26.310 & 0 \\ & & & & & 26.310 \end{bmatrix}. \tag{115}$$

- Case II : $A'_{55} = A^{(2)}_{55}$ and $A'_{66} = A^{(2)}_{66}$:

$$\boldsymbol{A'} = \begin{bmatrix} 105.91 & 54.513 & 54.513 & 0 & 0 & 0 \\ & 108.24 & 55.065 & 0 & 0 & 0 \\ & & 108.24 & 0 & 0 & 0 \\ & & & 26.588 & 0 & 0 \\ & & & & 26.250 & 0 \\ & & & & & 26.250 \end{bmatrix}. \tag{116}$$

4.3.1 Dispersion Curves

Figures 11 and 12 present dispersion curves for cases I and II listed in the previous section for a uniaxial load of 120 MPa along the ξ_1 direction and at an azimuthal angle of $\phi = 45°$ (arbitrary selected).

4.3.2 Angle Dependence

The change of phase velocity with variation in angle of propagation is presented in Figure 13. Angle dependence of phase velocity is expected as the applied stress field is anisotropic. S1 curves using the EEC method have been plotted for an applied stress of $\sigma_{11} = 120$ MPa, zoomed in to a frequency region of 600 kHz to match experiments in later sections. The solid lines represent curves for case I, while the dashed lines are that of case II. The trends for change in phase velocity with angle are the same for both cases, however, there are noticeable changes in phase velocity at this scale (about 2 m/s for the 40° case). It is difficult to justify remarks about the significance of these changes without first considering the application for which these curves are needed. Also, the difference in phase velocities vary between modes and frequency regions of interest.

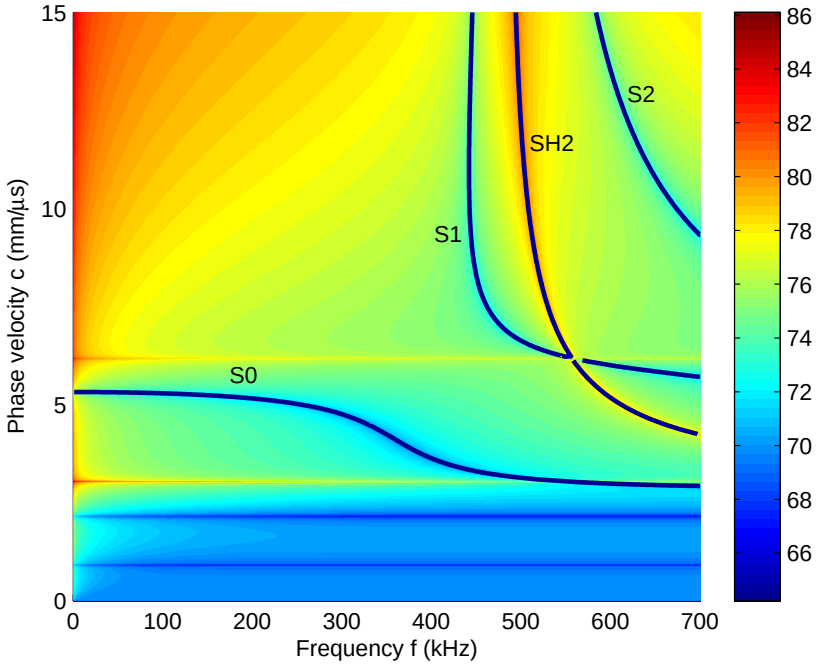

(a) Symmetric modes.

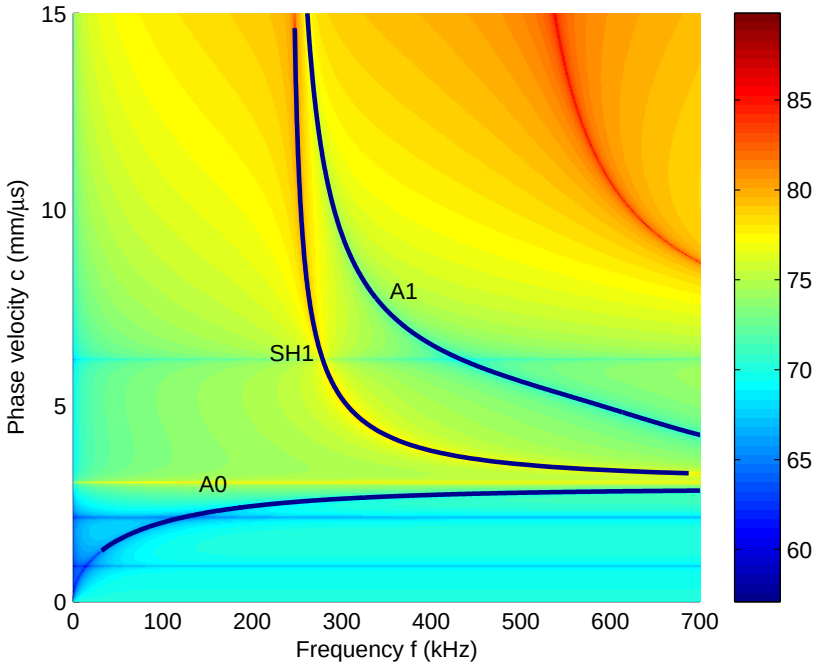

(b) Antisymmetric modes.

Figure 11: Dispersion curves for a stressed aluminum plate generated using EECs from case I with $\sigma_{11} = 120$ MPa and $\phi = 45°$.

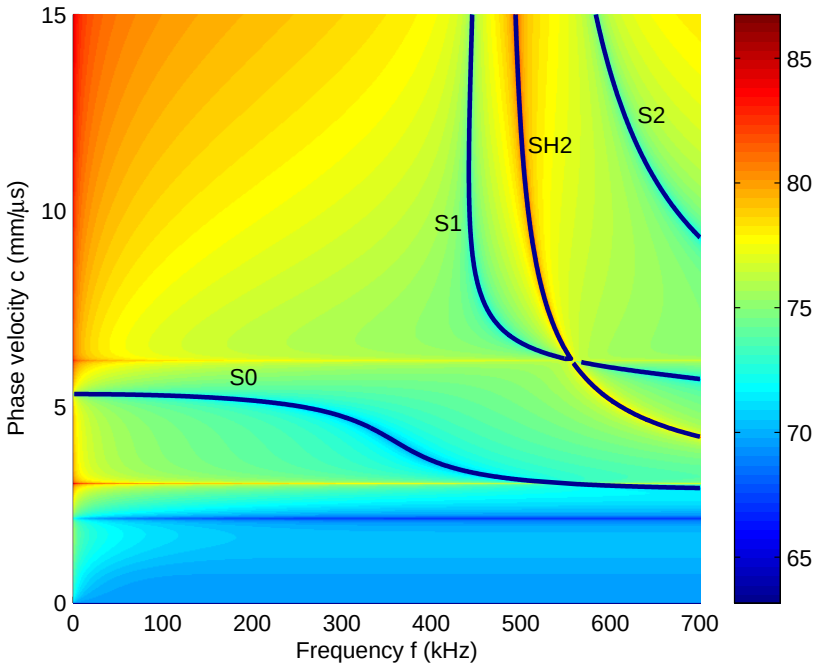

(a) Symmetric modes.

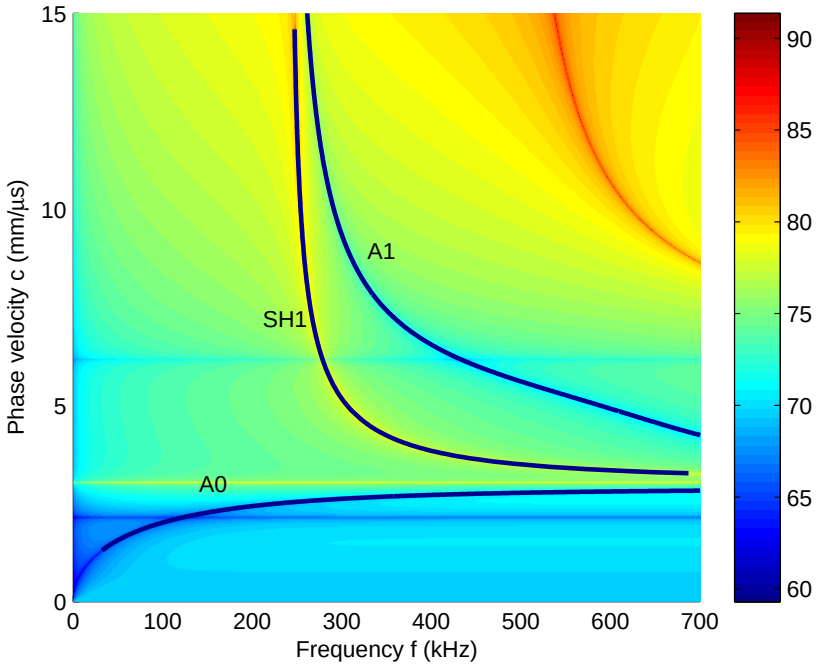

(b) Antisymmetric modes.

Figure 12: Dispersion curves for a stressed aluminum plate generated using EECs from case II with $\sigma_{11} = 120$ MPa and $\phi = 45°$.

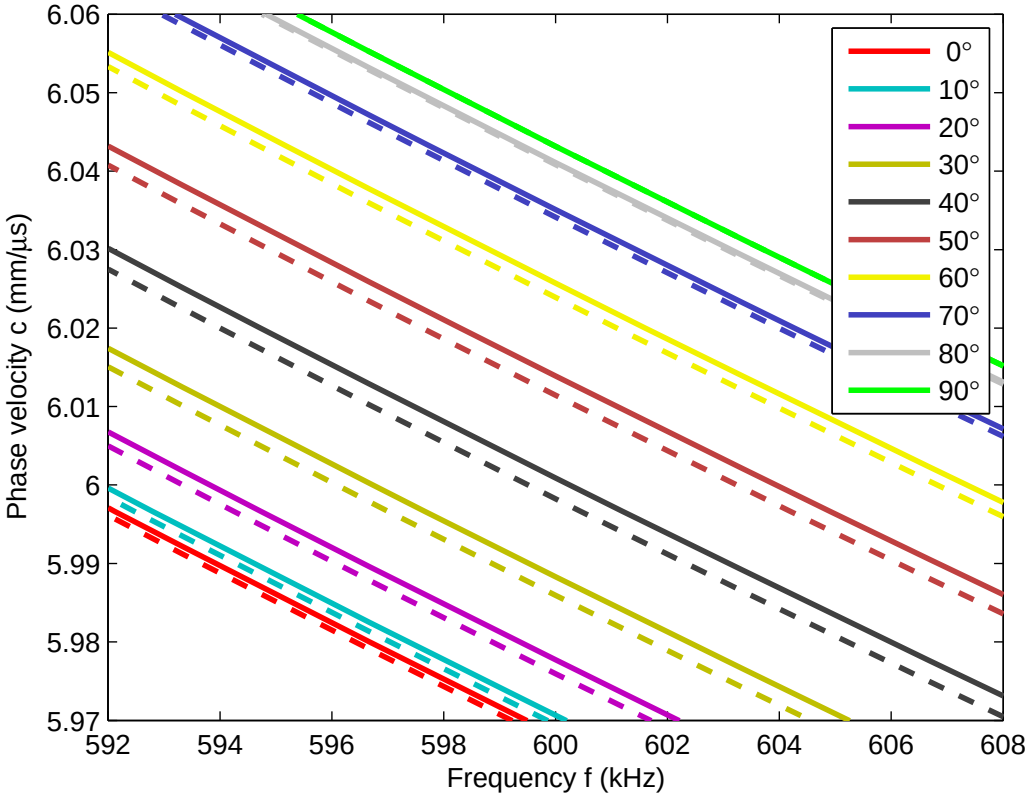

Figure 13: Angle dependence of S1 mode dispersion curve generated using EECs for $\sigma_{11} = 120$ MPa. Curves for case I are solid lines and case II are dashed lines.

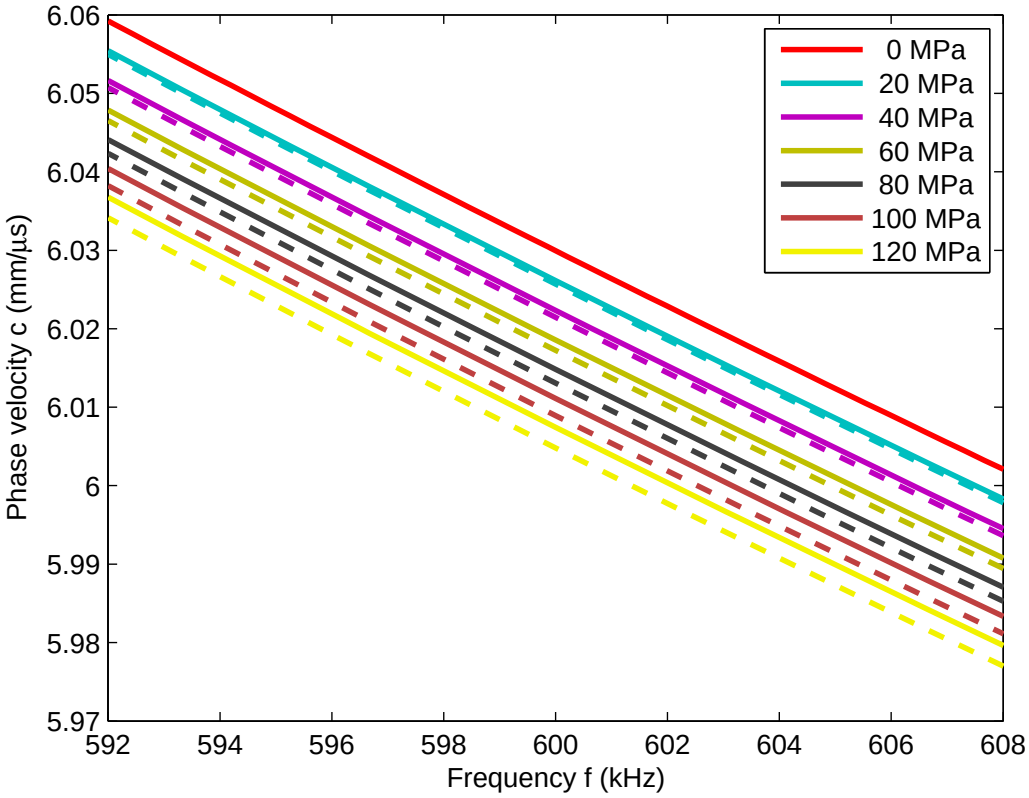

Figure 14: Stress dependence of S1 mode dispersion curve generated using EECs for $\phi = 45°$. Curves for case I are solid lines and case II are dashed lines.

4.3.3 Stress Dependence

The stress dependence of phase velocities using the EEC method at an angle of $\phi = 45°$ is presented in Figure 14. Curves for the S1 mode zoomed in to a frequency region of 600 kHz are plotted to match experiments in later sections. The solid lines represent curves for case I, while the dashed lines are that of case II. Just as was the case for angle dependence, the trends for change in phase velocity with stress are the same for both cases, however, there are noticeable changes in phase velocity at this scale (about 2 m/s for the 120 MPa). Also, the magnitude of change in phase velocities varies between modes and frequency regions of interest. A significant feature of this plot is that the phase velocities seem to vary linearly with stress as they do for acoustoelastic bulk waves.

CHAPTER V

DISPERSION CURVES BASED ON ACOUSTOELASTIC THEORY

As noted in Chapter 3, the presence of stress fields in isotropic media results in a nonlinear wave equation and a nonlinear stress-strain relation. However, under assumptions of a small homogeneous pre-deformation in a homogeneous medium, it is possible to linearize both of these relations. Since the theory for Lamb waves in unstressed media rely on the linearity of these relations, we can now ask if it is possible to develop theory for Lamb waves in stressed media under these assumptions.

There are a few papers in the literature on generating dispersion curves for stressed media. Lematre et al. [34] apply a full 4th order tensor approach to obtain dispersion curves along the principle stress direction for uniaxial loading that also included the piezoelectric effect. Considered here is a similar methodology that specifically addresses an extension to an arbitrary direction of propagation under bi-axial loading.

This method requires modifying the work of Nayfeh and Chimenti [9] using the full 4th order tensors $\boldsymbol{A}$ and $\boldsymbol{B}$ in the absence of symmetry that exists for $\boldsymbol{C}$ in stress-free media. In particular, expressions for the bulk wave velocities have to be found using the theory of acoustoelasticity in Chapter 2. These bulk wave velocities allow expressions for plate wave velocities to be developed in terms of the constants $A_{\alpha\beta\gamma\delta}$ and $B_{\alpha\beta\gamma\delta}$.

5.1 Derivation

Consider an infinite isotropic plate having thickness d whose normal is aligned with the x_3' axis of a reference Cartesian coordinate system $x_i' = (x_1', x_2', x_3')$ as shown in

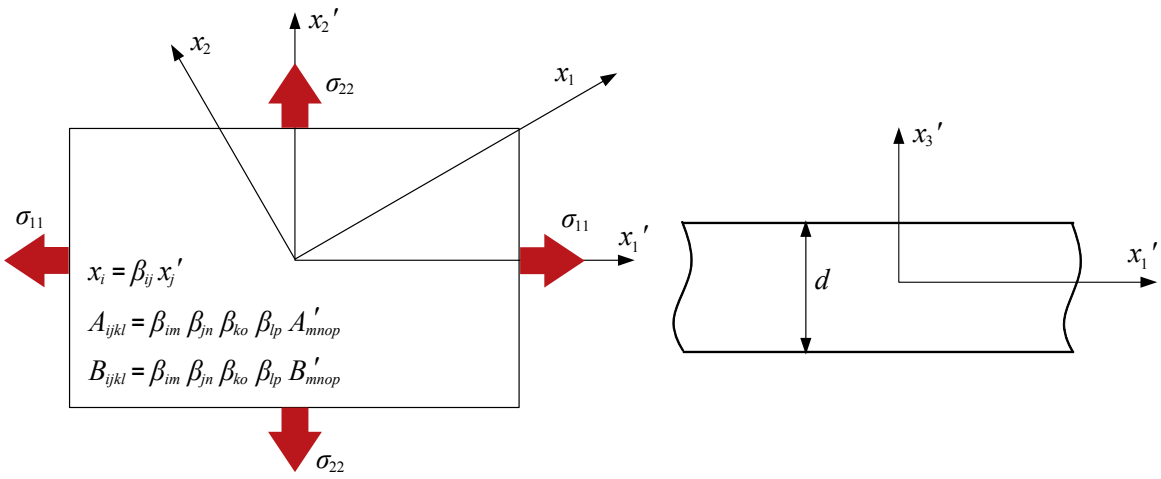

Figure 15: Plate coordinate system.

Figure 15. Assume also that the applied stresses are σ_{11} and σ_{22} along x_1' and x_2' respectively (force per unit area with reference to the natural state). The mid-plane of the plate is chosen to coincide with the $x_1' - x_2'$ plane. Since the stresses are expected to make Lamb wave propagation in the plate anisotropic, to study the propagation of plane waves along a direction that makes an arbitrary azimuthal angle ϕ with the x_1'-axis, we conduct our analysis in a transformed coordinate system x_i formed by a rotation of the orthogonal reference axes x_1', x_2' about the x_3' direction through the angle ϕ. This coordinate transformation can be written as

$$x_i = \beta_{ij} x_j', \tag{117}$$

where $\boldsymbol{\beta}$ is a rotation matrix and β_{ij} is the cosine of the angle between the x_i and x_j' axis. Note that we will be working entirely in the natural system and Greek subscripts used in Chapters 2 and 3 will be replaced with Roman letters for clarity of presentation. All quantities (stresses, strains, displacements etc.) are in the natural coordinate system and the natural coordinates of the material particles ξ_i are replaced with x_i. As we noted in Section 3.2 the stresses, strains and tensors $\boldsymbol{A}$ and $\boldsymbol{B}$ can be rotated using rotation matrices:

$$T_{ij} = \beta_{ik}\beta_{jl}T'_{kl}, \tag{118}$$

$$\epsilon_{ij} = \beta_{ik}\beta_{jk}\epsilon'_{kl}, \tag{119}$$

$$A_{ijkl} = \beta_{im}\beta_{jn}\beta_{ko}\beta_{lp}A'_{mnop}, \tag{120}$$

$$B_{ijkl} = \beta_{im}\beta_{jn}\beta_{ko}\beta_{lp}B'_{mnop}. \tag{121}$$

Acoustoelastic Lamb wave propagation requires solving the wave equation for the incremental displacements as given by Eq. (87) with a stress-strain relation given by Eq. (105), $\boldsymbol{A}$ tensor given by Eq. (99), and subject to stress-free boundary conditions. This problem differs from Lamb wave propagation in anisotropic media in two regards: (1) the acoustic tensor $\boldsymbol{A}$ does not have the same symmetries as the stiffness tensor $\boldsymbol{C}$, and (2) the stress-strain relation is different, leading to different analysis while evaluating the boundary condition.

Solutions in the form of harmonic waves are considered again. All possible harmonic waves have a wave number vector in the same plane and travel with the same velocity with respect to the x_1 axis. The general form is

$$u_j = U_j e^{i\xi(x_1+\alpha x_3-ct)}. \tag{122}$$

Substituting this equation in the equation of motion (Eq. (87) gives a form of the Christoffel equations:

$$K_{mn}(\alpha)U_n = 0, \tag{123}$$

where

$$
\begin{aligned}
K_{11} &= c^2\rho^0 - A_{1111} - \alpha^2 A_{1313}, \\
K_{12} &= -A_{1112} - \alpha^2 A_{1323}, \\
K_{13} &= -\alpha(A_{1133} + A_{1331}), \\
K_{21} &= -A_{1112} - \alpha^2 A_{1323}, \\
K_{22} &= c^2\rho^0 - A_{1212} - \alpha^2 A_{2323}, \\
K_{23} &= -\alpha(A_{1233} + A_{1332}), \\
K_{31} &= -\alpha(A_{1133} + A_{1331}), \\
K_{32} &= -\alpha(A_{1233} + A_{1332}), \\
K_{33} &= c^2\rho^0 - A_{1313} - \alpha^2 A_{3333}.
\end{aligned}
\tag{124}
$$

For existence of non-trivial solutions, $|K_{mn}|$ must go to zero, which produces a 6^{th} order equation in α with six solutions α_q, $q = 1...6$. Coefficients P_5, P_3, P_1 in the 6^{th} order equation in α go to zero, resulting in

$$P_6\alpha^6 + P_4\alpha^4 + P_2\alpha^2 + P_0 = 0, \tag{125}$$

where the coefficients are listed in Appendix C.1. The six solutions to this equation corresponding to the six possible partial waves (for a given guided wave velocity c) have the following properties:

$$\alpha_2 = -\alpha_1, \quad \alpha_4 = -\alpha_3 \text{ and } \alpha_6 = -\alpha_5. \tag{126}$$

The displacement ratios $V_q = U_{2q}/U_{1q}$ and $W_q = U_{3q}/U_{1q}$ are defined as

$$V_q(\alpha_q) = \frac{K_{11}(\alpha_q)K_{23}(\alpha_q) - K_{13}(\alpha_q)K_{12}(\alpha_q)}{K_{13}(\alpha_q)K_{22}(\alpha_q) - K_{12}(\alpha_q)K_{23}(\alpha_q)} \tag{127}$$

and

$$W_q(\alpha_q) = \frac{K_{11}(\alpha_q)K_{23}(\alpha_q) - K_{13}(\alpha_q)K_{12}(\alpha_q)}{K_{12}(\alpha_q)K_{33}(\alpha_q) - K_{23}(\alpha_q)K_{13}(\alpha_q)}, \tag{128}$$

where again the index q goes from 1 to 6 and corresponds to the six different partial waves that can exist for the given c. Using V and W as defined above, the total displacements can be written as

$$\{u_1, u_2, u_3\} = \sum_{q=1}^{6} \{1, V(\alpha_q), W(\alpha_q)\} U_{1q} e^{i\xi(x_1 + \alpha_q x_3 - ct)}. \tag{129}$$

Using the stress-displacement relations in Eq. (105) and superposition the stresses are

$$\{T_{33}, T_{13}, T_{23}\} = \sum_{q=1}^{6} i\xi \{D_{1q}, D_{2q}, D_{3q}\} U_{1q} e^{i\xi(x_1 + \alpha_q x_3 - ct)}, \tag{130}$$

where

$$\begin{aligned} D_{1q} &= B_{3311} + B_{3312} V_q + \alpha_q B_{3333} W_q, \\ D_{2q} &= \alpha_q (B_{1313} + B_{1323} V_q) + B_{1331} W_q, \\ D_{3q} &= \alpha_q (B_{1323} + B_{2323} V_q) + B_{1332} W_q. \end{aligned} \tag{131}$$

Applying stress free boundary conditions, i.e., setting T_{13}, T_{23} and T_{33} to zero at $x_3 = d/2$ and $x_3 = -d/2$, gives us six equations relating amplitudes $U_{11}, U_{12}, \ldots, U_{16}$ of the bulk waves, whose determinant of coefficients must go to zero for nontrivial solutions.

$$\begin{vmatrix} D_{11}E_1 & D_{12}E_2 & D_{13}E_3 & D_{14}E_4 & D_{15}E_5 & D_{16}E_6 \\ D_{21}E_1 & D_{22}E_2 & D_{23}E_3 & D_{24}E_4 & D_{25}E_5 & D_{26}E_6 \\ D_{31}E_1 & D_{32}E_2 & D_{33}E_3 & D_{34}E_4 & D_{35}E_5 & D_{36}E_6 \\ D_{11}\tilde{E}_1 & D_{12}\tilde{E}_2 & D_{13}\tilde{E}_3 & D_{14}\tilde{E}_4 & D_{15}\tilde{E}_5 & D_{16}\tilde{E}_6 \\ D_{21}\tilde{E}_1 & D_{22}\tilde{E}_2 & D_{23}\tilde{E}_3 & D_{24}\tilde{E}_4 & D_{25}\tilde{E}_5 & D_{26}\tilde{E}_6 \\ D_{31}\tilde{E}_1 & D_{32}\tilde{E}_2 & D_{33}\tilde{E}_3 & D_{34}\tilde{E}_4 & D_{35}\tilde{E}_5 & D_{36}\tilde{E}_6 \end{vmatrix} = 0, \tag{132}$$

where $E_q = e^{i\xi\alpha_q d/2}$ and $\tilde{E}_q = e^{-i\xi\alpha_q d/2}$.

Incorporating Eq. (126) in Eqs. (127), (128) and (131) yields the following symmetries:

$$\begin{aligned} V_{j+1} = V_j, \quad W_{j+1} = -W_j \\ D_{1j+1} = D_{1j}, \quad D_{2j+1} = -D_{2j}, \quad D_{3j+1} = -D_{3j}. \end{aligned} \tag{133}$$

Applying row-column operations to the determinant in the presence of these symmetries allow us to decouple the determinant. The column operations are (C_m is the mth column):

$$\begin{aligned} C_1^{\text{new}} &= C_1 + C_2, \\ C_3^{\text{new}} &= C_3 + C_4, \\ C_5^{\text{new}} &= C_5 + C_6, \\ C_2^{\text{new}} &= C_1 - C_2, \\ C_4^{\text{new}} &= C_3 - C_4, \\ C_6^{\text{new}} &= C_5 - C_6. \end{aligned} \tag{134}$$

followed by row operations (R_m is the mth row):

$$\begin{aligned} R_1^{\text{new}} &= R_1 - R_4, \\ R_2^{\text{new}} &= R_2 + R_5, \\ R_3^{\text{new}} &= R_3 + R_6, \\ R_4^{\text{new}} &= R_4 + R_1, \\ R_5^{\text{new}} &= R_5 - R_2, \\ R_6^{\text{new}} &= R_6 - R_3. \end{aligned} \tag{135}$$

to give

$$\begin{vmatrix} 0 & 0 & 0 & \sin(\gamma\alpha_3)D_{13} & \sin(\gamma\alpha_1)D_{11} & \sin(\gamma\alpha_5)D_{15} \\ 0 & 0 & 0 & \cos(\gamma\alpha_3)D_{23} & \cos(\gamma\alpha_1)D_{21} & \cos(\gamma\alpha_5)D_{25} \\ 0 & 0 & 0 & \cos(\gamma\alpha_3)D_{33} & \cos(\gamma\alpha_1)D_{31} & \cos(\gamma\alpha_5)D_{35} \\ \cos(\gamma\alpha_1)D_{11} & \cos(\gamma\alpha_5)D_{15} & \cos(\gamma\alpha_3)D_{13} & 0 & 0 & 0 \\ \sin(\gamma\alpha_1)D_{21} & \sin(\gamma\alpha_5)D_{25} & \sin(\gamma\alpha_3)D_{23} & 0 & 0 & 0 \\ \sin(\gamma\alpha_1)D_{31} & \sin(\gamma\alpha_5)D_{35} & \sin(\gamma\alpha_3)D_{33} & 0 & 0 & 0 \end{vmatrix} = 0, \tag{136}$$

where

$$\gamma = \frac{\xi d}{2} = \frac{\omega d}{2c}. \tag{137}$$

The determinant decouples into two separate equations,

$$D_{11}G_1 \cot(\gamma\alpha_1) + D_{13}G_3 \cot(\gamma\alpha_3) + D_{15}G_5 \cot(\gamma\alpha_5) = 0 \tag{138}$$

for the symmetric modes and

$$D_{11}G_1 \tan(\gamma\alpha_1) + D_{13}G_3 \tan(\gamma\alpha_3) + D_{15}G_5 \tan(\gamma\alpha_5) = 0 \tag{139}$$

for the antisymmetric modes, where

$$\begin{aligned} G_1 &= D_{23}D_{35} - D_{33}D_{25}, \\ G_3 &= D_{31}D_{25} - D_{21}D_{35}, \\ G_5 &= D_{21}D_{33} - D_{31}D_{23}. \end{aligned} \tag{140}$$

These are expressions that relate the wave velocity c to the wavelength ξ and describe entirely the dispersive behavior of any wave as it propagates through the plate. It is important to note that since the analysis was performed in the natural coordinate system, the wave velocity (c) obtained is the rate at which a disturbance travels with respect to the natural coordinates of the material points. In general the velocities in the natural and initial coordinate system are different because of the stretching of material as it goes from its natural to predeformed states.

5.2 SH Modes

In Chapter 1, Eqs. (22) for SH modes are decoupled from the ones for symmetric and antisymmetric modes, which are composed of L and SV waves (Eqs. (23) and (24)). However, when stress is applied, Eq. (136) shows that SH modes are no longer independent and these modes will have particle displacements in x_1 or x_3 directions also. However, for small stresses these modes will have displacements that are mostly in the x_2 direction. This is related to the phenomenon of birefringence of bulk waves in the presence of stress fields and further discussion is beyond the scope of this thesis.

5.3 Numerical Solution

Eqs. (138) and (139) are transcendental equations and several numerical considerations have to be made to solve these equations to obtain dispersion curves. The method is outlined in this section followed by some results for several different cases.

5.3.1 Method

The first step is to pick a plate wave velocity c and find the corresponding α_q from the polynomial in Eq. (125). Next, express Eq. (138) as

$$\begin{aligned} f_s(\omega, c) &= D_{11}G_1(\alpha_3, \alpha_5)\cot(\gamma\alpha_1) + D_{13}G_3(\alpha_1, \alpha_5)\cot(\gamma\alpha_3) + D_{15}G_5(\alpha_1, \alpha_3)\cot(\gamma\alpha_5) \\ &= D_{11}H_1(\alpha_1, \alpha_3, \alpha_5) + D_{13}H_3(\alpha_1, \alpha_3, \alpha_5) + D_{15}H_5(\alpha_1, \alpha_3, \alpha_5) = 0. \end{aligned} \tag{141}$$

For real α_q, all Ds, Gs and cotangent functions are real and therefore f_s is real. D_{1q} is even in α_q, D_{2q} and D_{3q} are odd in α_q, which implies $G_n(\alpha_p, \alpha_q)$ is odd in both α_p and α_q. Since $\cot(\gamma\alpha_q)$ is odd in α_q, $H_n(\alpha_p, \alpha_q, \alpha_r)$ is odd in all three α. For odd functions, the Taylor series has only odd terms and this implies that for imaginary arguments, the value of the odd functions is always imaginary. By carefully analyzing the symmetries for all terms it can be seen that for a mixture of real and imaginary αs, f_s has a value that is purely imaginary or purely real. Next, based on the values of α, we pick one of two root finding algorithms:

- For values of c that produce purely imaginary and real values of α:

  Sweep across ω and find pairs of ω values where the value of f_s changes sign (this is not a problem since f_s values at all ω for this value of c are real or all imaginary). Each of the pairs thus obtained mark intervals in which solutions to the equation $f_s = 0$ are guaranteed to exist (and these intervals can be arbitrary small). These ω, c pairs constitute points of the dispersion curves. Any real value of α will produce infinities in the cotangent functions. Since a

sign change occurs at an infinity, these are actually false roots that must be accounted for by excluding pairs of ω values that correspond to multiples of $n\pi$ in the cotangent functions. Cotangents with imaginary values of α do not produce any infinities.

- For values of c with any complex values of α:

  Ds and Gs are complex valued and therefore f_s is complex valued. Sweep across ω for pairs of ω that switch sign for both real and imaginary components together. Also project real and imaginary components of the function value f_s on the $\theta = 45°$ and $\theta = 135°$ lines and check for sign changes in both projected values. This finds roots that occur when the curve of f_s as a function of ω is tangential to either the real or imaginary axis. Either a sign change in both real and imaginary components or ones in both projected values yields a interval with a solution. In general for this case, it is possible to get false solutions but these can be discarded later. Cotangents corresponding to complex and imaginary values of α do not produce any infinities.

Finally, points that are nearby in the set of solutions are connected to obtain dispersion curves. The exact same method applies to the function for antisymmetric modes f_a.

5.3.2 Dispersion Curves

The numerical method summarized above is used to generate dispersion curves for an aluminum plate of thickness 6.35 mm with material constants given in Table 4. The applied loads are assumed to be $\sigma_{11} = 120$ MPa and $\sigma_{22} = 0$. Figure 16 presents these results and also demonstrates the fact that the SH modes are no longer independent and are present as a part of Eqs. (138) and (139). The dispersion curves are presented as solid lines against a color map of $\log|f_s|$ and $\log|f_a|$.

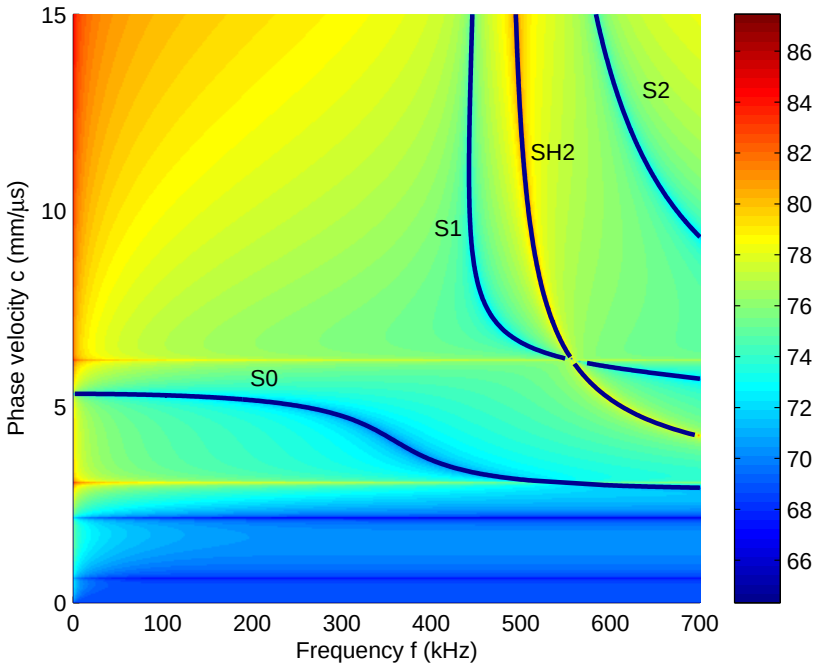

(a) Symmetric modes.

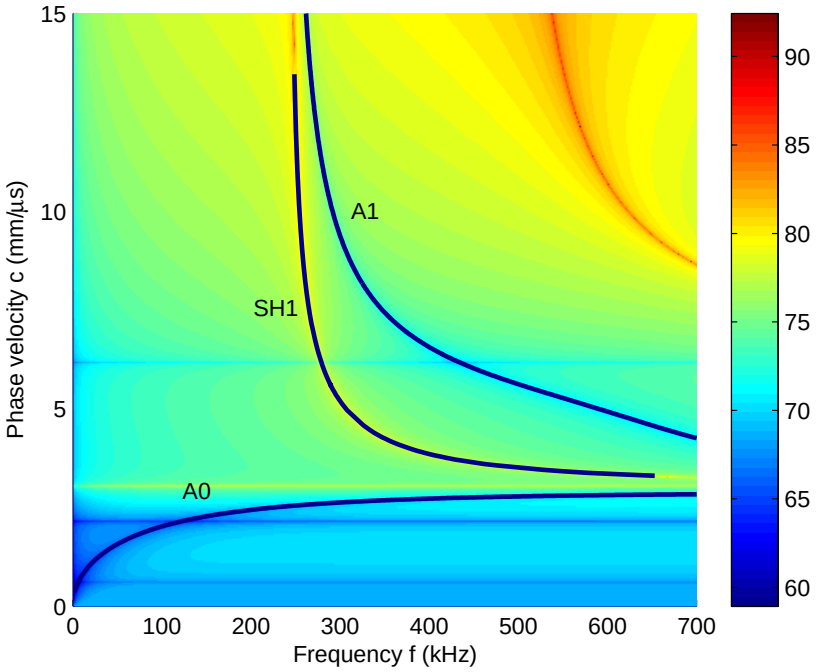

(b) Antisymmetric modes.

Figure 16: Dispersion curves generated using theory for a stressed aluminum plate with $\sigma_{11} = 120$ MPa and $\phi = 45°$ (SH0 mode not shown).

5.3.3 Angle Dependence

To demonstrate the dependence of wave velocity on the direction of propagation, a comparison of S1 modes about 600 kHz propagating at varying angles with respect to the x_1' axis is presented in Figure 17(a). Material constants from Table 4 are used with plate thickness of 6.35 mm and uniaxial stress $\sigma_{11} = 120$ MPa. The change is about 80 m/s between angles of 0 and 90°. The change in phase velocity with angle fits well to a $\sin(2\phi)$ curve as it does for acoustoelastic bulk waves and this is illustrated for 600 kHz in Figure 17(b).

The magnitude of induced anisotropy varies with mode and frequency range of interest. As a result, certain frequency regions can be very favourable for NDE/SHM applications. This is illustrated for the low frequency A0 mode at $\sigma_{11} = 600$ MPa (chosen to exaggerate anisotropy for illustration) in Figure 18. The curves corresponding to different angles cross at a frequency of around 32.1 kHz. This makes it a region of isotropic behaviour for A0 Lamb waves, even under the effects of applied uniaxial stress. However, the phase velocity at this frequency does vary from the velocity in the absence of applied stress.

5.3.4 Stress Dependence

To demonstrate the dependence of wave velocity on the applied load, dispersion curves for the S1 mode about 600 kHz for an aluminum plate of thickness 6.35 mm with material constants from Table 4 at varying applied stresses are presented in Figure 19(a). All curves are at an angle of $\phi = 45°$. The change in phase velocity is about 25 m/s for an applied stress of 120 MPa. Significantly, the variation of phase velocity with small changes in applied load is linear as it is for acoustoelastic bulk wave propagation and this is illustrated for a frequency of 600 kHz in Figure 19(b).

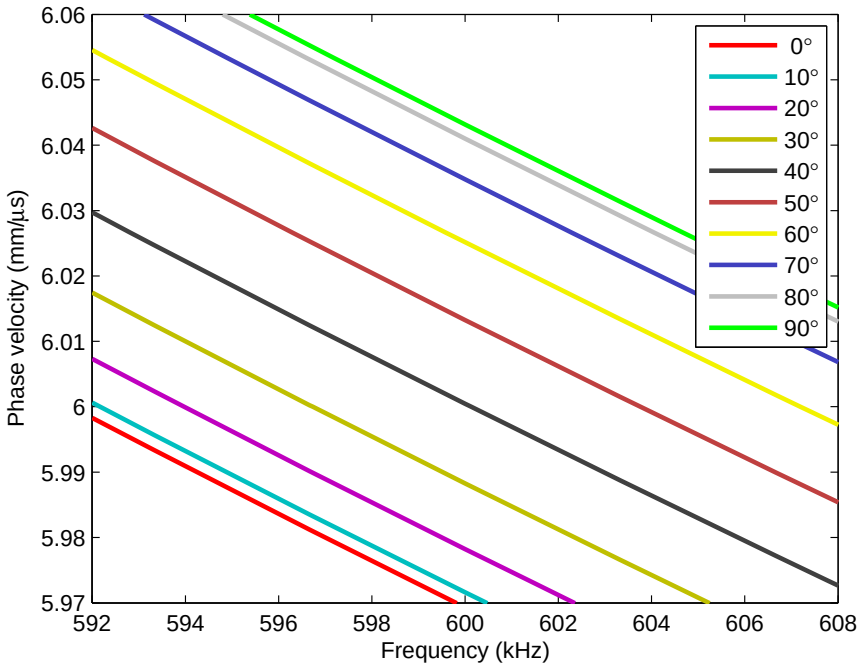

(a) Angle dependence of dispersion curves.

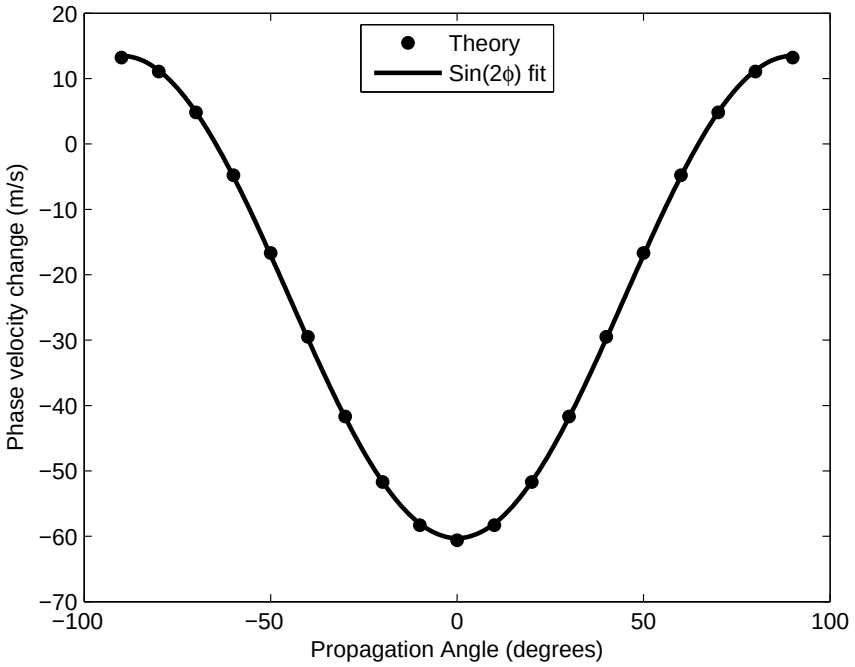

(b) Variation of phase velocity at 600 kHz to demonstrate $\sin(2\phi)$ dependence.

Figure 17: S1 mode phase velocities using theory for a uniaxial load of $\sigma_{11} = 120$ MPa for an aluminum plate.

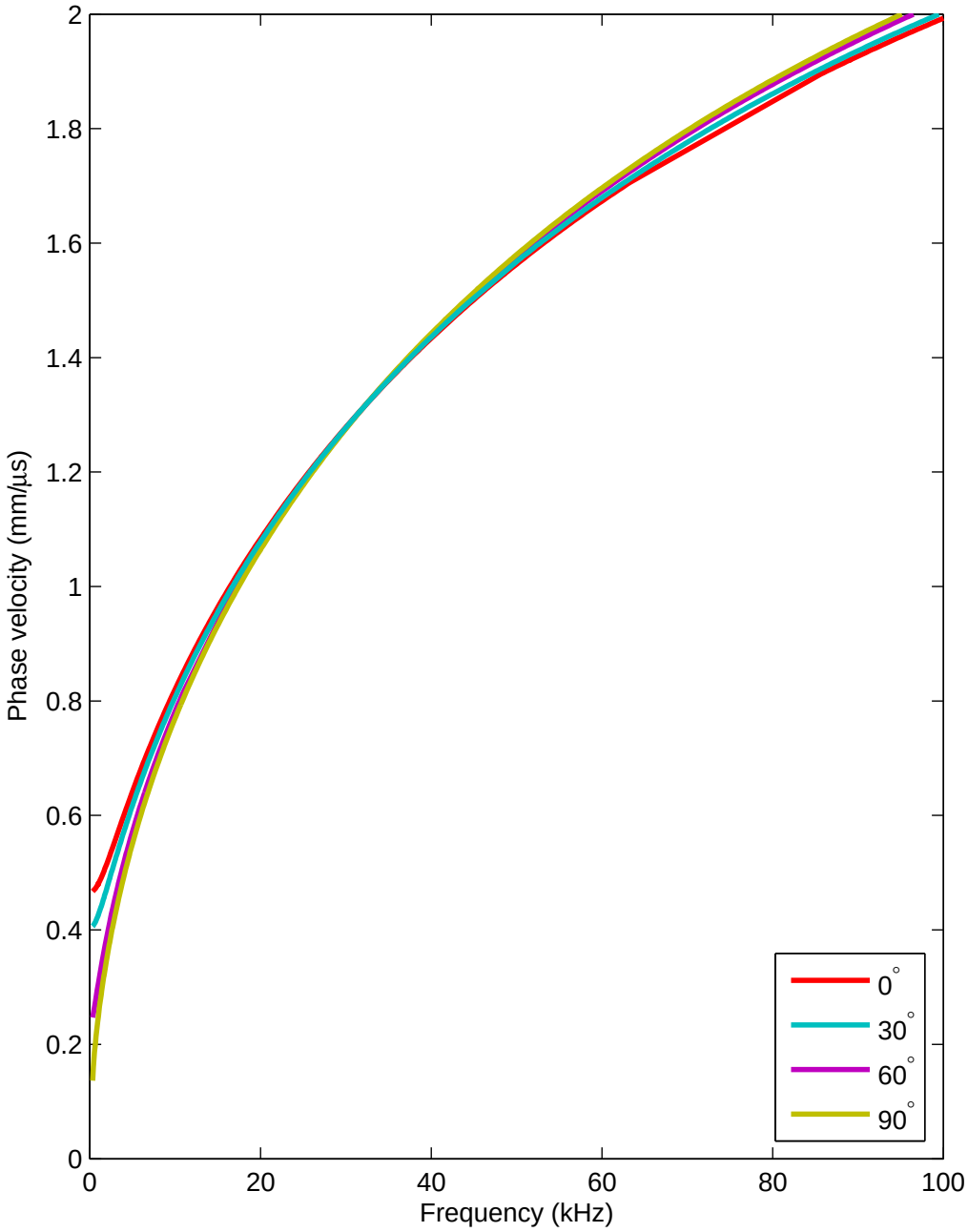

Figure 18: A0 mode phase velocities using theory for a uniaxial load of $\sigma_{11} = 600$ MPa to demonstrate the mode and frequency dependence of the degree of anisotropy.

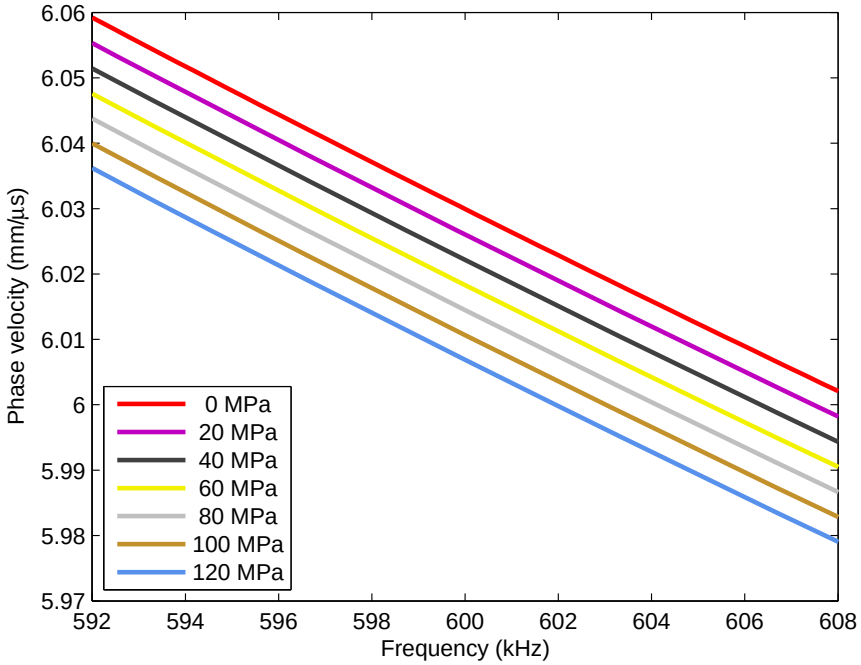

(a) Stress dependence of dispersion curves.

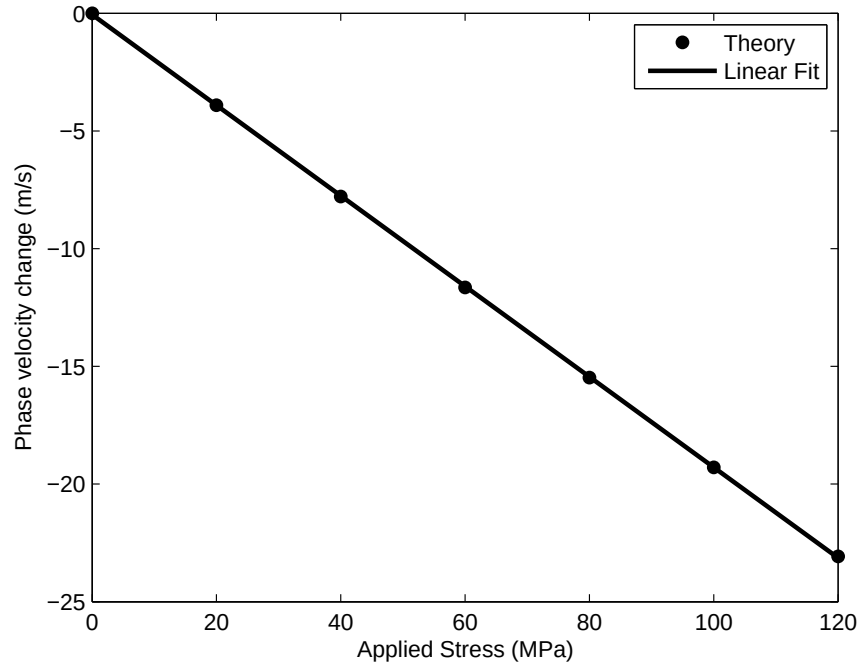

(b) Variation of phase velocity at 600 kHz to demonstrate linear dependence with stress.

Figure 19: S1 mode phase velocities using theory at a propagation angle of $\phi = 45°$ for an aluminum plate.

CHAPTER VI

COMPARISON AND EXPERIMENTAL VERIFICATION

6.1 EECs and Theoretical Solution

It is difficult to analytically compare results from acoustoelastic theory to the EEC method because the dispersion relations are not in closed form and the expressions for the constants A_{ijkl} are complicated. This section contains numerical comparisons for different cases.

6.1.1 Dispersion Curves

Presented in Figure 20 is a comparison of dispersion curves generated using the EEC method (case I) with ones from theory for a uniaxial load of $\sigma_{11} = 120$ MPa at $\phi = 45°$. They are in very close agreement and finer details are illustrated in the following sections.

6.1.2 Angle Dependence

Presented in Figure 21 is a comparison of the angle dependence of S1 mode phase velocities using the EEC method with ones from theory for a load of $\sigma_{11} = 120$ MPa. Solid lines represent theory solutions while dashed lines represent EEC curves. For this mode and range of frequencies, the EEC dispersion curves are in close agreement with theory. There is a difference of about 1 m/s in direction of applied stress for case I and 2 m/s for case II. However, this conclusion should not be generalized because the deviation of EECs from theory is dependent on the mode and frequency range under consideration. Figure 22 illustrates this for a frequency range of 980 kHz where the deviation is higher and in the opposite direction for some of the angles. Also, the deviation from theory is maximum at the angle of applied stress (0° in this example)

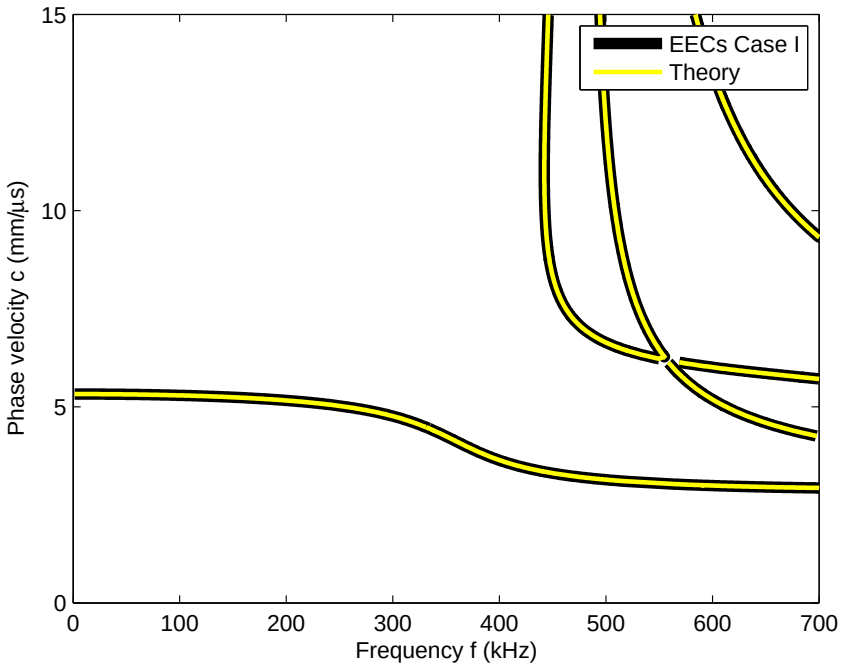

(a) Symmetric modes.

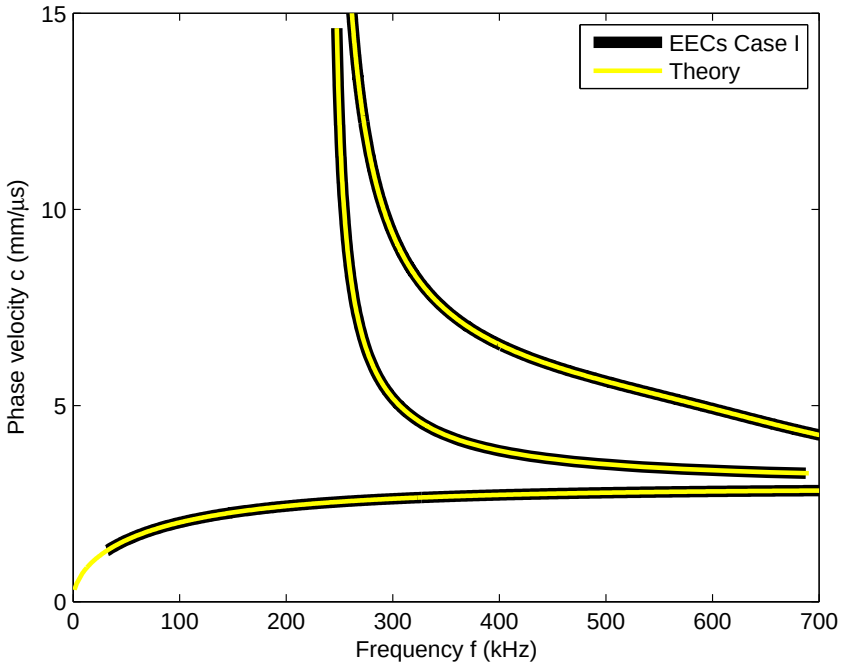

(b) Antisymmetric modes.

Figure 20: Dispersion curves generated using EECs from case I compared against ones from theory for $\sigma_{11} = 120$ MPa and $\phi = 45°$.

and zero perpendicular to it for both cases.

6.1.3 Stress Dependence

Presented in Figure 23 is a comparison of the stress dependence of S1 mode phase velocities using the EEC method with ones from theory for a fixed angle of $\phi = 45°$. Solid lines represent theory solutions while dashed lines represent EEC curves. Again, as in the case of angle dependence, case I is in closer agreement with theory (less than 1 m/s deviation for case I). This should not be generalized and an increase in velocity deviation at 980 kHz is illustrated in Figure 24. The deviation from theory increases with an increase in applied load and falls to zero for zero applied load. This is to be expected because both the EEC method and theory degenerate to the case of Rayleigh-Lamb equations for a case of zero stress. As before, the magnitude of the deviation from theory changes with mode and frequency range for a given value of applied stress.

6.2 Experimental Verification

Experimental data were collected using PZT transducers bonded to an aluminum plate subjected to uniaxial loads. These data were analyzed to obtain changes in phase velocity as a function of both load and direction of propagation [35].

6.2.1 Experimental Data Set

Ultrasonic signals were recorded from waves propagating between pairs of piezoelectric transducers mounted on a standard 6061 aluminum plate of thickness 6.35 mm under varying uniaxial stresses ($\sigma_{11} \neq 0, \sigma_{22} = 0$). The experimental setup and transducer locations are shown in Figure 25 and the experiment parameters are listed in Table 5. Of the 45 possible transducer pair combinations, data from only 9 of them are used. The combinations used are marked (boxed) in Table 6 along with the angles between them. They are selected to maximize the distance between transducers pairs

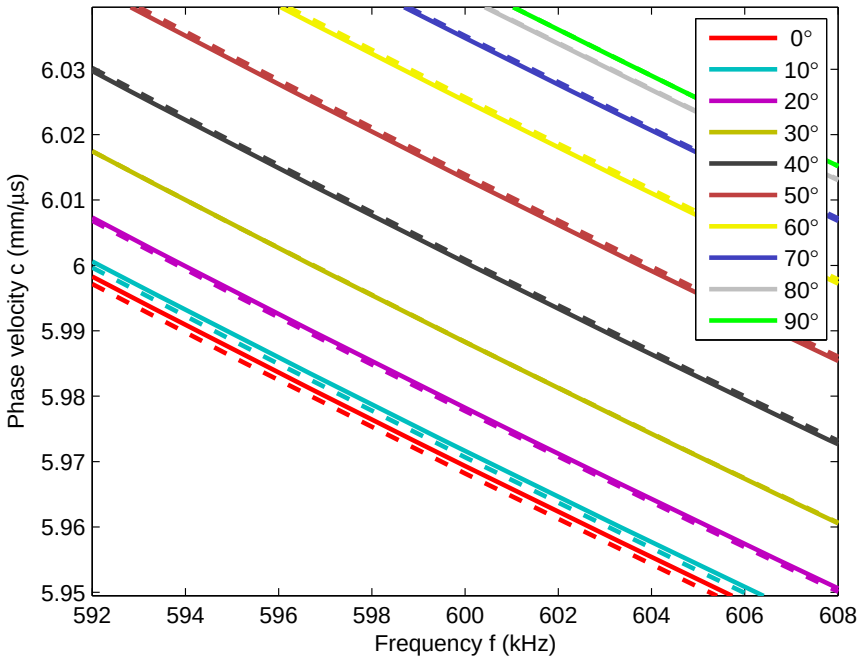

(a) Theory vs. EEC case I.

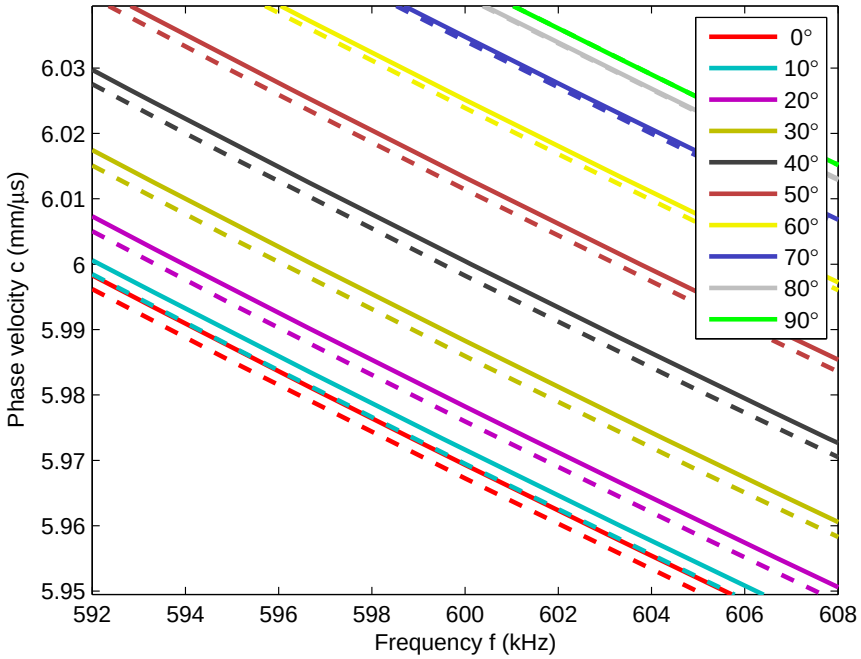

(b) Theory vs. EEC case II.

Figure 21: Comparison of angle dependence of S1 mode for a uniaxial load of $\sigma_{11} = 120$ MPa. Theoretical solution is represented by solid lines while EEC solution by dashed lines.

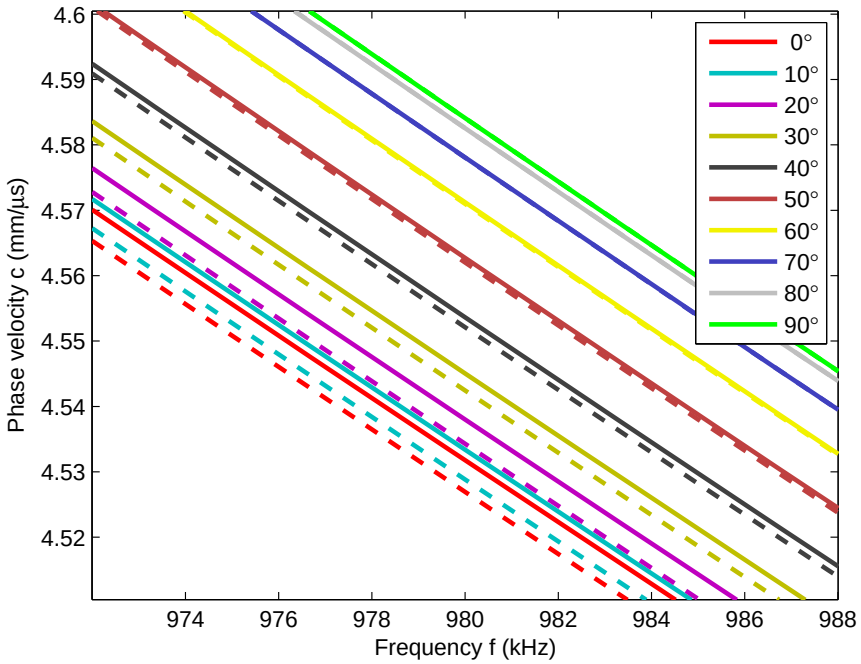

Figure 22: Comparison of angle dependence of S1 mode for a uniaxial load of $\sigma_{11} = 120$ MPa about a frequency of 980 kHz. Theoretical solution is represented by solid lines while EECs case I solution by dashed lines.

and provide data from all possible angles. All transducers are at a distance of 109 mm from the center of the plate (in the undeformed state). All parameters have been selected to maximize mode separation for the S1 mode at 600 kHz and only this mode is considered here.

6.2.2 Data Analysis

For a plane wave, the time t for a constant phase point to travel a distance d is

$$t = \frac{d}{c_p}, \tag{142}$$

where c_p is the phase velocity. An applied stress causes two effects that change the time t for a given point. First is a change in phase velocity c_p and second, a change in distance between the transducers due to the induced strain. For small changes in

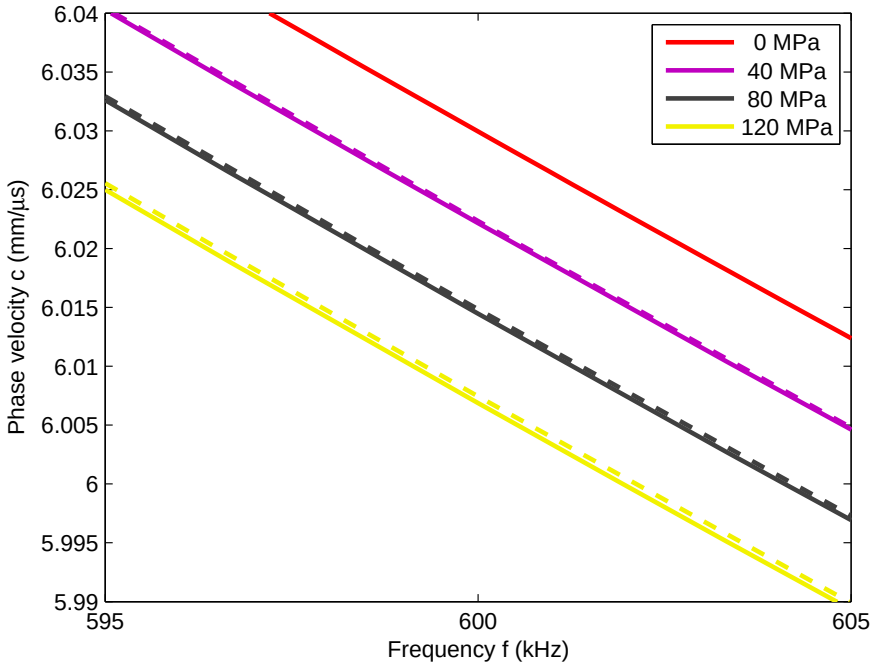

(a) Theory vs EEC case I.

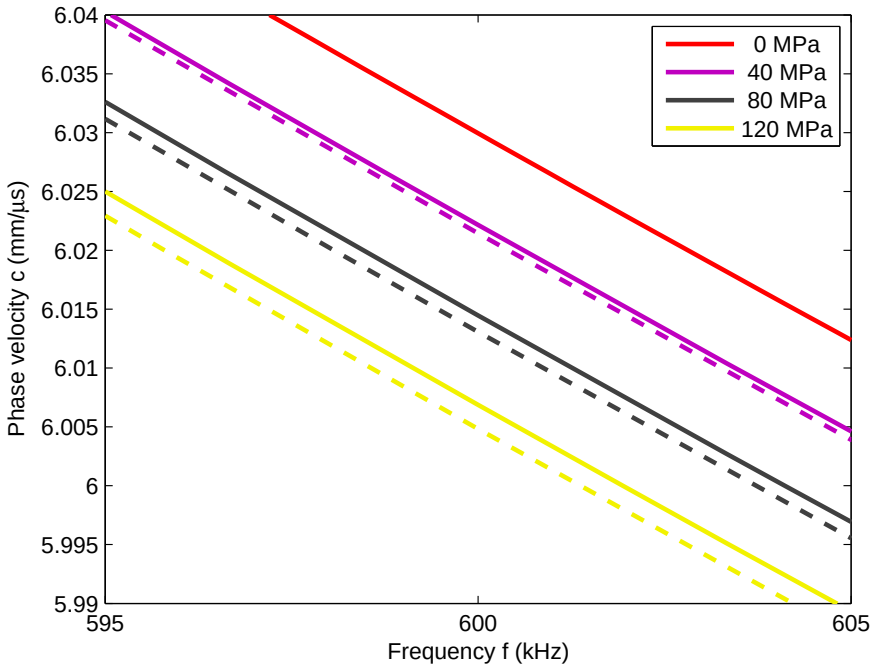

(b) Theory vs EEC case II.

Figure 23: Comparison of stress dependence of S1 mode for a uniaxial load ($\sigma_{22} = 0$) at $\phi = 45°$. Theoretical solution is represented by solid lines while EECs solution by dashed lines.

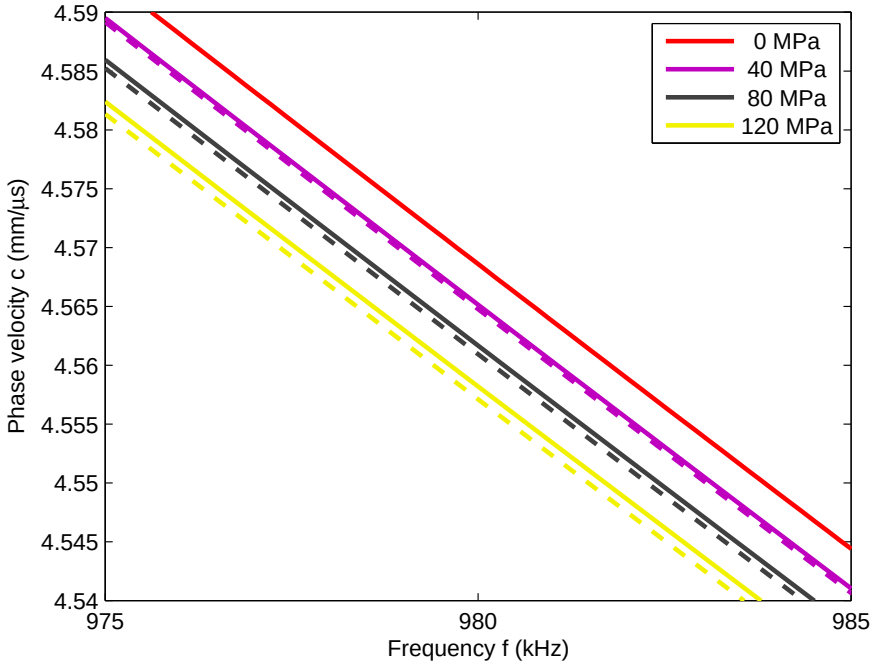

Figure 24: Comparison of stress dependence of S1 mode for a uniaxial load ($\sigma_{22} = 0$) at $\phi = 45°$ about a frequency of 980 kHz. Theoretical solution is represented by solid lines while EECs case I solution by dashed lines.

Table 5: Data acquisition parameters.

Parameter	**Value**
Specimen	610 mm × 305 mm × 6.35 mm aluminum 6061 plate
Load	0 to 57.5 MPa with 5.75 MPa increment.
Excitation	± 10 V 5-cycle Hanning windowed cosine pulse
Excitation frequency	600 kHz
Measurement time	500 us
Sampling rate	20 MHz
Averaging	50 times
Repetition time	50 ms
Amplifier gain	40 db

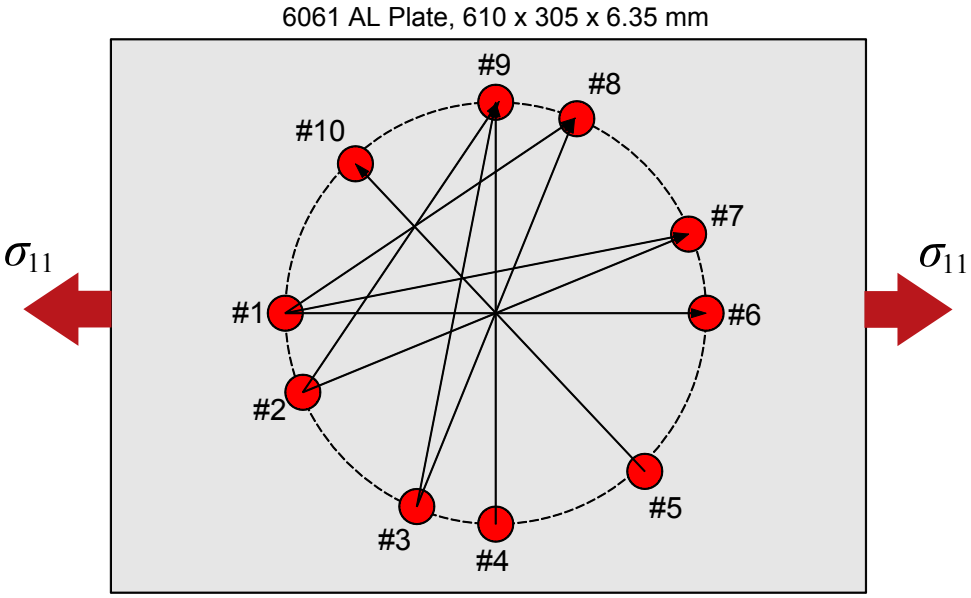

(a) Transducer locations.

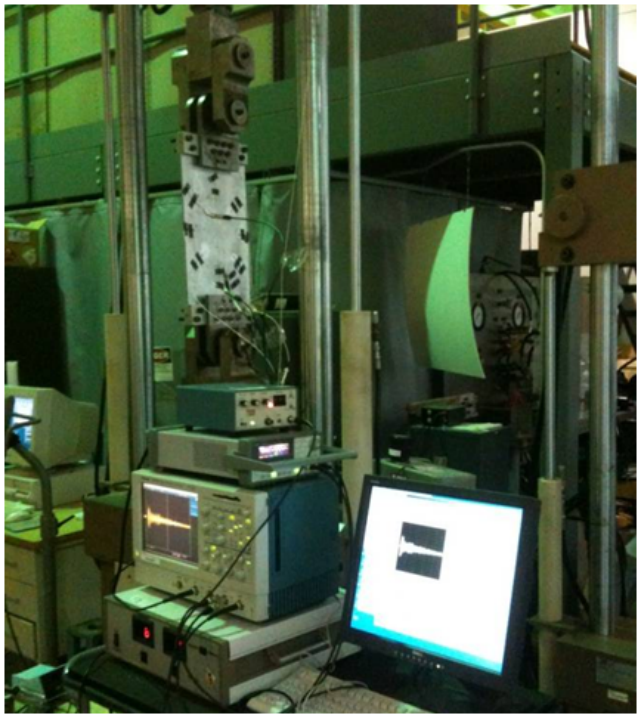

(b) Plate in the loading fixture.

Figure 25: Experimental setup.

Table 6: Transducer pairs and angles.

No.	**1**	**2**	**3**	**4**	**5**	**6**	**7**	**8**	**9**	**10**
1		78.75	56.25	45	22.5	0	11.25	33.75	45	67.5
2			45	33.75	11.25	11.25	22.5	45	56.25	78.75
3				11.25	11.25	33.75	45	67.5	78.75	78.75
4					22.5	45	56.25	78.75	90	67.5
5						67.5	78.75	78.75	67.5	45
6							78.75	56.25	45	22.5
7								45	33.75	11.25
8									11.25	11.25
9										22.5

phase-velocity and strain, the change in arrival time can be approximated by:

$$\begin{aligned} \Delta t &= \frac{\partial t}{\partial d}\Delta d + \frac{\partial t}{\partial c_p}\Delta c_p \\ &= \frac{\Delta d}{c_p^0} - \frac{d^0 \Delta c_p}{(c_p^0)^2}, \end{aligned} \tag{143}$$

where c_p^0 and d^0 are the phase velocity and distance between the transducers in the natural state. The change in distance is

$$\Delta d = \epsilon d^0, \tag{144}$$

where ϵ is the strain along the direction of propagation and finally,

$$\Delta c_p = \frac{c_p^0 \Delta d}{d^0} - \frac{(c_p^0)^2 \Delta t}{d^0}. \tag{145}$$

For natural coordinates, Δd is 0. Therefore for a computation of change in phase velocity, only the time shift of arrival is needed. The time shifts are calculated by tracking a zero-crossing in the center of the first arrival as a function of load. The

time delays are expected to be small compared to the period of the signal to avoid ambiguity of change in phase. Figure 26 shows the time delays at different angles and the change in phase velocity at different angles as compared with theory. There is fair agreement considering the uncertainty in third order elastic constants, nominal phase velocities, and separation distances [29].

6.3 Ray tracing simulation

A ray-tracing model can be constructed to study the effects of stress on pulse propagation through plates. Ray-tracing models are approximate simulations of wave-propagation that include only far-field behaviour.

6.3.1 Design

Consider an excitation signal $s(t)$ applied to an infinite plate at position $\mathbf{p^s}$. The response of this plate to the signal at a point $\mathbf{p_i}$ is given by:

$$s_i(t) = \frac{\mathcal{F}^{-1}\left[S(\omega)e^{-i\omega|\mathbf{p_i}-\mathbf{p^s}|/c(\omega)}\right]}{\sqrt{|\mathbf{p_i}-\mathbf{p^s}|}}, \tag{146}$$

where $S(\omega)$ is the Fourier transform of $s(t)$, $c(\omega)$ is the dispersion curve, the term $\omega|\mathbf{p_i}-\mathbf{p^s}|/c(\omega)$ applies a frequency dependent phase shift to the signal i.e., it effects "dispersion" and the term $\sqrt{|\mathbf{p_i}-\mathbf{p^s}|}$ is included because the far-field decays as the square-root of the distance (otherwise known as geometric spreading). $s(t)$ can be any of the fields associated with the traveling wave. It is most convenient to think of it as the particle velocity in a specific direction (e.g. in-plane or out of plane). This model will then give the signal shapes and relative amplitudes of velocity at any arbitrary point $\mathbf{p_i}$ sufficiently far away from the source.

6.3.2 Plots

Figure 27 presents plots of a Hanning windowed pulse with parameters listed in Table 5 traveling at at an angle of 45° relative to the applied stress through a distance of

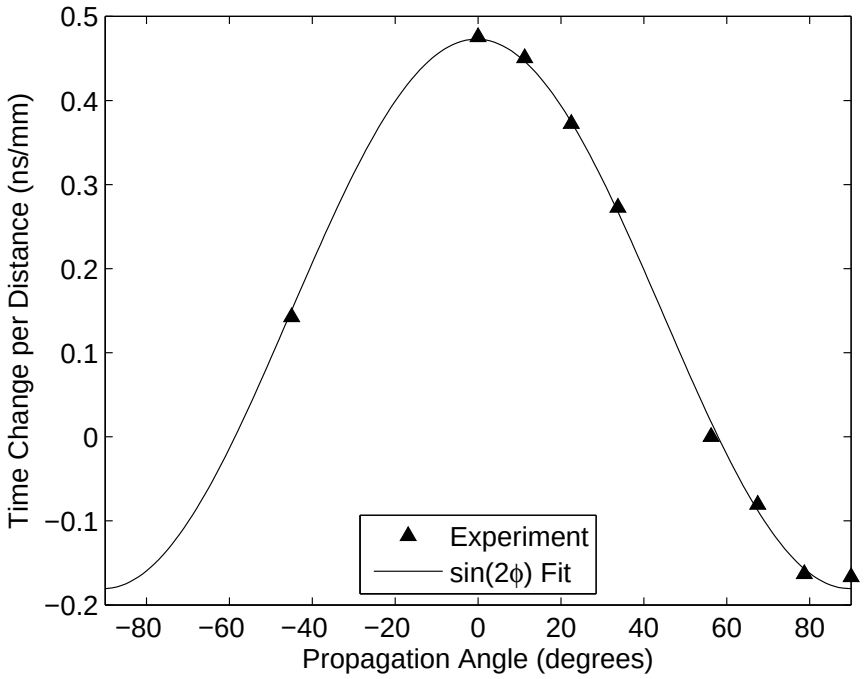

(a) Time shifts.

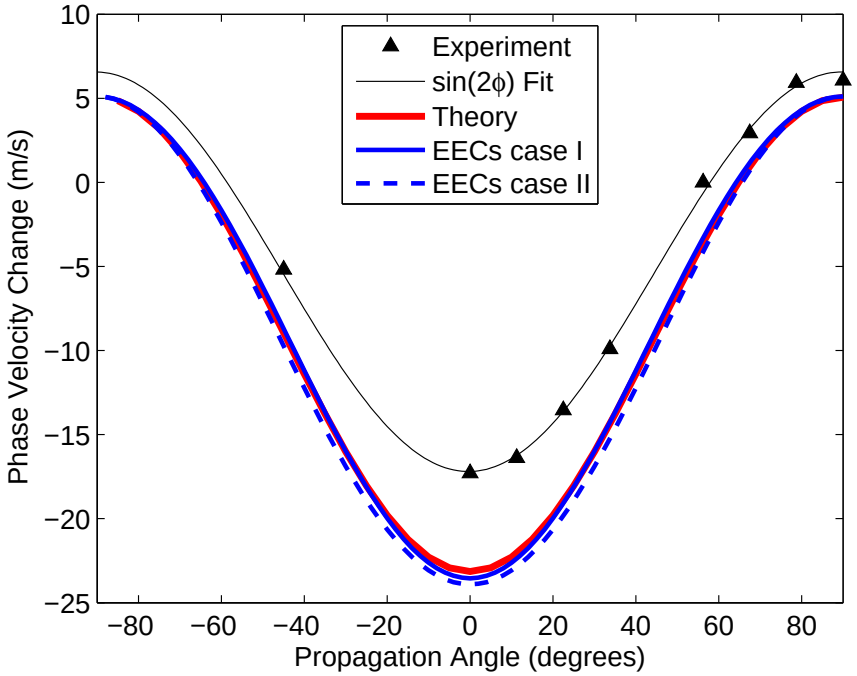

(b) Phase velocity change.

Figure 26: Phase velocity change for $c_p^0 = 6029.9$ m/s and $\sigma_{11} = 46$ MPa.

218 mm. It compares results for zero load, the theoretical solution, EEC case I and EEC case II for an applied uniaxial stress of $\sigma_{11} = 46$ MPa to match the experiment in Section 6.2. Several inferences can be made. First, the effect of dispersion on the no load waveform is significantly different from the others and changes in dispersion (due to the applied stresses) to a 1^{st} order are manifested as time shifts. This implies that the applied stress has a significant impact that cannot be ignored for structural health monitoring applications that use this kind of information. Second, for this case of small applied stress and the frequency range of 600 kHz, the signal generated using both EEC methods are in close agreement with that of theory.

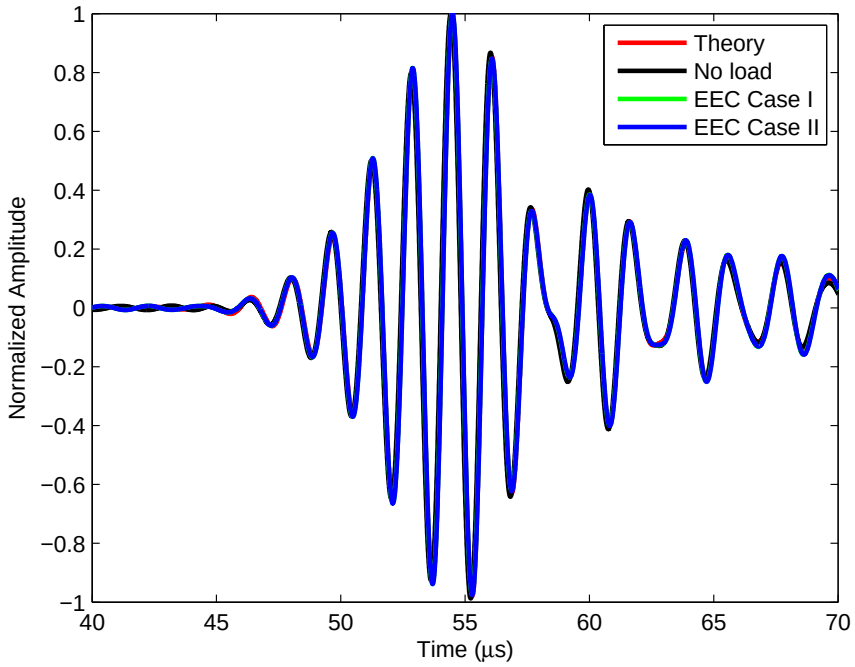

(a) First arrivals.

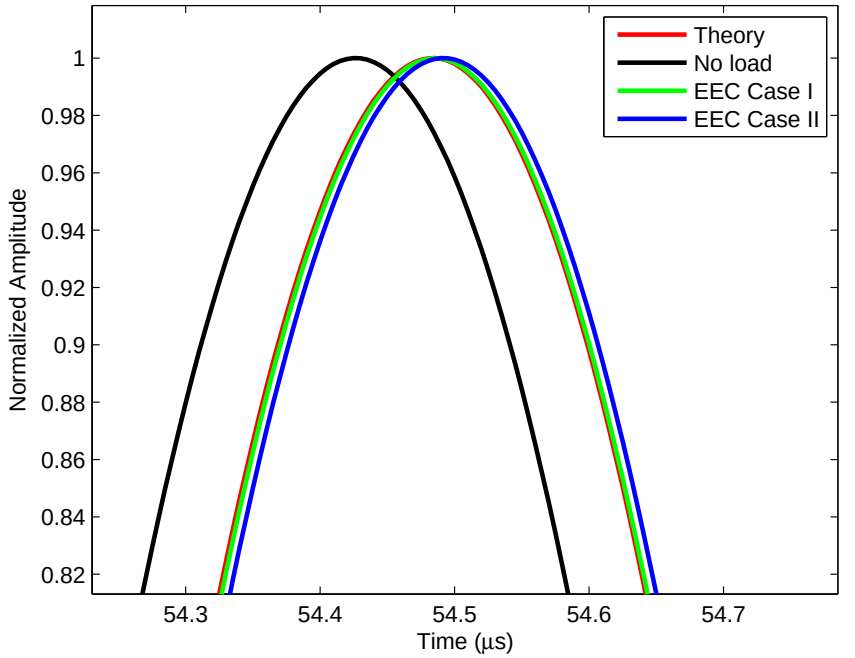

(b) Magnified view.

Figure 27: Simulated waveforms under an applied uniaxial stress of $\sigma_{11} = 46$ MPa.

CHAPTER VII

CONCLUSION AND RECOMMENDATIONS

The acoustoelastic theory for Lamb waves in an isotropic plate under small, uniform, biaxial stress fields has been developed. It was shown that the theory is similar to that of anisotropic materials of monoclinic symmetry although the numerical computation is more involved. The theory presents insight into the nature of wave propagation under the influence of pre-existing stresses and as a result, coupling of SH modes with the symmetric and antisymmetric modes. The numerical method and results have been presented for varying angles and frequencies of several Lamb modes. An approximate method using effective elastic constants is also developed and can be used for numerical computation of dispersion curves using existing commercial applications [12] without the need for new code or algorithms. The deviation of phase velocities using the EEC method from theory is in general dependent on the mode and frequency range in consideration and the feasibility of its use should be determined from the sensitivity of the application to perturbation in phase velocities. NDE/SHM systems will certainly benefit from using EECs to account for the anisotropy in absence of the full blown theoretical solution. Experimental data shows fair agreement of the change in phase velocity with values computed from theory. However, an accurate comparison could not be made because of the uncertainty in determining the values of third order elastic constants.

Lamb waves are used for nondestructive evaluation and are proposed for structural health monitoring applications. The anisotropic effects due to pre-existing stresses are significant and cannot be ignored in this context. The theory presented in this dissertation can be used to augment existing NDE/SHM systems with more accurate

information about wave speed changes. Also, it was shown that some modes are less susceptible to the effects of stress in some frequency regions, which provides a basis for selection of operating points in the K-ω plane for these applications. Since the velocity is a function of the applied stresses, an inverse problem formulation may also allow the use of this theory to detect the state of stress in a structure from the measurement of changes in wave velocities at varying angles. High loads tend to couple the shear modes with the symmetric and antisymmetric modes. The implications of this phenomenon for excitability and losses due to mode conversion are yet to be explored. Recommendations for future work also include the design of a more accurate experiment to further validate the theoretical model.

Finally, there is scope for a more generalized theory. Preliminary investigation suggests that this theory can be extended to materials of monoclinic symmetry under uniform stress fields. Also, the method of EECs can be extended to biaxial stress fields by studying the symmetry in hexagonal point groups as opposed to transversely isotropic symmetry for uniaxial stress.

APPENDIX A

EXPRESSIONS FOR MONOCLINIC DISPERSION CURVES

A.1 Expressions for 6^{th} *order Polynomial in Eq.* (56)

$$
\begin{aligned}
P_6 = \;& C_{33}(C_{44}C_{55} - C_{45}^2) \\
P_4 = \;& (c^2\rho(-(C_{55}(C_{33} + C_{44}) + C_{33}C_{44} - C_{45}^2)) + C_{11}C_{33}C_{44} - C_{13}^2C_{44} \\
& + 2C_{13}C_{45}(C_{36} + C_{45}) - 2C_{13}C_{44}C_{55} - 2C_{16}C_{33}C_{45} + \\
& C_{33}C_{55}C_{66} - C_{36}^2C_{55}) \\
P_2 = \;& (c^4\rho^2(C_{33} + C_{44} + C_{55}) - C_{11}(c^2\rho(C_{33} + C_{44}) - C_{33}C_{66} + (C_{36} + C_{45})^2 \\
& - C_{44}C_{55}) + c^2\rho(C_{13}^2 + 2C_{13}C_{55} - C_{66}(C_{33} + C_{55}) + (C_{36} + C_{45})^2 \\
& - C_{44}C_{55}) + 2C_{16}(c^2C_{45}\rho + C_{13}(C_{36} + C_{45}) + C_{36}C_{55}) - C_{13}C_{66}(C_{13} \\
& + 2C_{55}) - C_{16}^2C_{33}) \\
P_0 = \;& -(C_{55} - c^2\rho)((C_{11} - c^2\rho)(c^2\rho - C_{66}) + C_{16}^2)
\end{aligned}
$$

APPENDIX B

ACOUSTOELASTIC EXPRESSIONS FOR A BIAXIAL LOAD

B.1 Expressions for A_{ijkl} presented in Eq. (99)

$$A_{1111} = \frac{\mu(\lambda+2\mu)(3\lambda+2\mu)+(2\lambda^2+9\lambda\mu+4m(\lambda+\mu)+2\mu(l+3\mu))\,\sigma_{11}}{\mu(3\lambda+2\mu)} - \frac{(-2l\mu+\lambda(2m+\lambda+2\mu))\sigma_{22}}{\mu(3\lambda+2\mu)}$$

$$A_{1112} = 0$$

$$A_{1113} = 0$$

$$A_{1121} = 0$$

$$A_{1122} = \frac{2\lambda\mu(3\lambda+2\mu)+(4l\mu+\lambda(2m-n+\lambda+2\mu))\,(\sigma_{11}+\sigma_{22})}{2\mu(3\lambda+2\mu)}$$

$$A_{1123} = 0$$

$$A_{1131} = 0$$

$$A_{1132} = 0$$

$$A_{1133} = \frac{2\lambda\mu(3\lambda+2\mu)+(4l\mu+\lambda(2m-n+\lambda+2\mu))\sigma_{11}}{2\mu(3\lambda+2\mu)} + \frac{2((n-\lambda)\lambda+(2l+n)\mu-2m(\lambda+\mu))\sigma_{22}}{2\mu(3\lambda+2\mu)}$$

$$A_{1211} = 0$$

$$A_{1212} = \frac{4\mu^2(3\lambda+2\mu)+(n\lambda+4\mu(m+2(\lambda+\mu)))\,(\sigma_{11}+\sigma_{22})}{4\mu(3\lambda+2\mu)}$$

$$A_{1213} = 0$$

$$A_{1221} = \frac{4\mu^2(3\lambda+2\mu)+(n\lambda+2\mu(2m+\lambda+2\mu))\,(\sigma_{11}+\sigma_{22})}{4\mu(3\lambda+2\mu)}$$

$$A_{1222} = 0$$

$$A_{1223} = 0$$

$$A_{1231} = 0$$

$$A_{1232} = 0$$

$$A_{1233} = 0$$

$$A_{1311} = 0$$

$$A_{1312} = 0$$

$$A_{1313} = \frac{4\mu^2(3\lambda+2\mu)+(n\lambda+4\mu(m+2(\lambda+\mu)))\sigma_{11}-2(n\lambda+(-2m+n+2\lambda)\mu)\sigma_{22}}{4\mu(3\lambda+2\mu)}$$

$$A_{1321} = 0$$

$$A_{1322} = 0$$

$$A_{1323} = 0$$

$$A_{1331} = \frac{4\mu^2(3\lambda+2\mu)+(n\lambda+2\mu(2m+\lambda+2\mu))\sigma_{11}-2(n\lambda+(-2m+n+2\lambda)\mu)\sigma_{22}}{4\mu(3\lambda+2\mu)}$$

$$A_{1332} = 0$$

$$A_{1333} = 0$$

$$A_{2111} = 0$$

$$A_{2112} = \frac{4\mu^2(3\lambda+2\mu)+(n\lambda+2\mu(2m+\lambda+2\mu))(\sigma_{11}+\sigma_{22})}{4\mu(3\lambda+2\mu)}$$

$$A_{2113} = 0$$

$$A_{2121} = \frac{4\mu^2(3\lambda+2\mu)+(n\lambda+4\mu(m+2(\lambda+\mu)))(\sigma_{11}+\sigma_{22})}{4\mu(3\lambda+2\mu)}$$

$$A_{2122} = 0$$

$$A_{2123} = 0$$

$$A_{2131} = 0$$

$$A_{2132} = 0$$

$$A_{2133} = 0$$

$$A_{2211} = \frac{2\lambda\mu(3\lambda+2\mu)+(4l\mu+\lambda(2m-n+\lambda+2\mu))\,(\sigma_{11}+\sigma_{22})}{2\mu(3\lambda+2\mu)}$$

$$A_{2212} = 0$$

$$A_{2213} = 0$$

$$A_{2221} = 0$$

$$A_{2222} = \frac{\mu(\lambda+2\mu)(3\lambda+2\mu)-(-2l\mu+\lambda(2m+\lambda+2\mu))\sigma_{11}}{\mu(3\lambda+2\mu)} + \frac{(2\lambda^2+9\lambda\mu+4m(\lambda+\mu)+2\mu(l+3\mu))\,\sigma_{22}}{\mu(3\lambda+2\mu)}$$

$$A_{2223} = 0$$

$$A_{2231} = 0$$

$$A_{2232} = 0$$

$$A_{2233} = \frac{2\lambda\mu(3\lambda+2\mu)+2((n-\lambda)\lambda+(2l+n)\mu-2m(\lambda+\mu))\sigma_{11}}{2\mu(3\lambda+2\mu)} + \frac{(4l\mu+\lambda(2m-n+\lambda+2\mu))\sigma_{22}}{2\mu(3\lambda+2\mu)}$$

$$A_{2311} = 0$$

$$A_{2312} = 0$$

$$A_{2313} = 0$$

$$A_{2321} = 0$$

$$A_{2322} = 0$$

$$A_{2323} = \frac{4\mu^2(3\lambda+2\mu)-2(2(-m+\lambda)\mu+n(\lambda+\mu))\sigma_{11}+(n\lambda+4\mu(m+2(\lambda+\mu)))\sigma_{22}}{4\mu(3\lambda+2\mu)}$$

$$A_{2331} = 0$$

$$A_{2332} = \frac{4\mu^2(3\lambda+2\mu)-2(2(-m+\lambda)\mu+n(\lambda+\mu))\sigma_{11}+(n\lambda+2\mu(2m+\lambda+2\mu))\sigma_{22}}{4\mu(3\lambda+2\mu)}$$

$$A_{2333} = 0$$

$$A_{3111} = 0$$

$$A_{3112} = 0$$

$$A_{3113} = \frac{4\mu^2(3\lambda+2\mu)+(n\lambda+2\mu(2m+\lambda+2\mu))\sigma_{11}-2(n\lambda+(-2m+n+2\lambda)\mu)\sigma_{22}}{4\mu(3\lambda+2\mu)}$$

$$A_{3121} = 0$$

$$A_{3122} = 0$$

$$A_{3123} = 0$$

$$A_{3131} = \frac{4\mu^2(3\lambda+2\mu)+(n\lambda+4\mu(m+2(\lambda+\mu)))\sigma_{11}-2(n\lambda+(-2m+n+2\lambda)\mu)\sigma_{22}}{4\mu(3\lambda+2\mu)}$$

$$A_{3132} = 0$$

$$A_{3133} = 0$$

$$A_{3211} = 0$$

$$A_{3212} = 0$$

$$A_{3213} = 0$$

$$A_{3221} = 0$$

$$A_{3222} = 0$$

$$A_{3223} = \frac{4\mu^2(3\lambda+2\mu)-2(2(-m+\lambda)\mu+n(\lambda+\mu))\sigma_{11}+(n\lambda+2\mu(2m+\lambda+2\mu))\sigma_{22}}{4\mu(3\lambda+2\mu)}$$

$$A_{3231} = 0$$

$$A_{3232} = \frac{4\mu^2(3\lambda+2\mu)-2(2(-m+\lambda)\mu+n(\lambda+\mu))\sigma_{11}+(n\lambda+4\mu(m+2(\lambda+\mu)))\sigma_{22}}{4\mu(3\lambda+2\mu)}$$

$$A_{3233} = 0$$

$$A_{3311} = \frac{2\lambda\mu(3\lambda+2\mu)+(4l\mu+\lambda(2m-n+\lambda+2\mu))\sigma_{11}}{2\mu(3\lambda+2\mu)} + \frac{2((n-\lambda)\lambda+(2l+n)\mu-2m(\lambda+\mu))\sigma_{22}}{2\mu(3\lambda+2\mu)}$$

$$A_{3312} = 0$$

$$A_{3313} = 0$$

$$A_{3321} = 0$$

$$A_{3322} = \frac{2\lambda\mu(3\lambda+2\mu)+2((n-\lambda)\lambda+(2l+n)\mu-2m(\lambda+\mu))\sigma_{11}}{2\mu(3\lambda+2\mu)}$$

$$+\frac{(4l\mu+\lambda(2m-n+\lambda+2\mu))\sigma_{22}}{2\mu(3\lambda+2\mu)}$$

$$A_{3323} = 0$$

$$A_{3331} = 0$$

$$A_{3332} = 0$$

$$A_{3333} = \frac{\mu(\lambda+2\mu)(3\lambda+2\mu)-(-2l\mu+\lambda(2m+\lambda+2\mu))(\sigma_{11}+\sigma_{22})}{\mu(3\lambda+2\mu)}$$

B.2 Expressions for B_{ijkl} presented in Eq. (105)

$$B_{1111} = \frac{2\mu(\lambda+2\mu)(3\lambda+2\mu)+2(2l\mu+(\lambda+\mu)(4m+\lambda+2\mu))\sigma_{11}}{2\mu(3\lambda+2\mu)} - \frac{(-4l\mu+\lambda(4m+\lambda+2\mu))\sigma_{22}}{2\mu(3\lambda+2\mu)}$$

$$B_{1112} = 0$$

$$B_{1113} = 0$$

$$B_{1121} = 0$$

$$B_{1122} = \frac{2\lambda\mu(3\lambda+2\mu)+(2m\lambda-\lambda(n+\lambda)+4l\mu)\sigma_{11}}{2\mu(3\lambda+2\mu)} + \frac{(4l\mu+\lambda(2m-n+2(\lambda+\mu)))\sigma_{22}}{2\mu(3\lambda+2\mu)}$$

$$B_{1123} = 0$$

$$B_{1131} = 0$$

$$B_{1132} = 0$$

$$B_{1133} = \frac{2\lambda\mu(3\lambda+2\mu)+(2m\lambda-\lambda(n+\lambda)+4l\mu)\sigma_{11}}{2\mu(3\lambda+2\mu)} - \frac{(\lambda^2-4l\mu+4m(\lambda+\mu)-2n(\lambda+\mu))\sigma_{22}}{2\mu(3\lambda+2\mu)}$$

$$B_{1211} = 0$$

$$B_{1212} = \frac{4\mu^2(3\lambda+2\mu)+(n\lambda+4\mu(m+\lambda+\mu))\sigma_{11}+(n\lambda+4m\mu-2\lambda\mu)\sigma_{22}}{4\mu(3\lambda+2\mu)}$$

$$B_{1213} = 0$$

$$B_{1221} = \frac{4\mu^2(3\lambda+2\mu)+(n\lambda+4m\mu-2\lambda\mu)\sigma_{11}+(n\lambda+4\mu(m+\lambda+\mu))\sigma_{22}}{4\mu(3\lambda+2\mu)}$$

$$B_{1222} = 0$$

$$B_{1223} = 0$$

$$B_{1231} = 0$$

$$B_{1232} = 0$$

$$B_{1233} = 0$$

$$B_{1311} = 0$$

$$B_{1312} = 0$$

$$B_{1313} = \frac{4\mu^2(3\lambda+2\mu)+(n\lambda+4\mu(m+\lambda+\mu))\sigma_{11}-2(n\lambda+(-2m+n+\lambda)\mu)\sigma_{22}}{4\mu(3\lambda+2\mu)}$$

$$B_{1321} = 0$$

$$B_{1322} = 0$$

$$B_{1323} = 0$$

$$B_{1331} = \frac{4\mu^2(3\lambda+2\mu)+(n\lambda+4m\mu-2\lambda\mu)\sigma_{11}-2(n\lambda+(-2m+n+\lambda)\mu)\sigma_{22}}{4\mu(3\lambda+2\mu)}$$

$$B_{1332} = 0$$

$$B_{1333} = 0$$

$$B_{2111} = 0$$

$$B_{2112} = \frac{4\mu^2(3\lambda+2\mu)+(n\lambda+4\mu(m+\lambda+\mu))\sigma_{11}+(n\lambda+4m\mu-2\lambda\mu)\sigma_{22}}{4\mu(3\lambda+2\mu)}$$

$$B_{2113} = 0$$

$$B_{2121} = \frac{4\mu^2(3\lambda+2\mu)+(n\lambda+4m\mu-2\lambda\mu)\sigma_{11}+(n\lambda+4\mu(m+\lambda+\mu))\sigma_{22}}{4\mu(3\lambda+2\mu)}$$

$$B_{2122} = 0$$

$$B_{2123} = 0$$

$$B_{2131} = 0$$

$$B_{2132} = 0$$

$$B_{2133} = 0$$

$$B_{2211} = \frac{2\lambda\mu(3\lambda+2\mu)+(4l\mu+\lambda(2m-n+2(\lambda+\mu)))\sigma_{11}}{2\mu(3\lambda+2\mu)} + \frac{(2m\lambda-\lambda(n+\lambda)+4l\mu)\sigma_{22}}{2\mu(3\lambda+2\mu)}$$

$$B_{2212} = 0$$

$$B_{2213} = 0$$

$$B_{2221} = 0$$

$$B_{2222} = \frac{2\mu(\lambda+2\mu)(3\lambda+2\mu)-(-4l\mu+\lambda(4m+\lambda+2\mu))\sigma_{11}}{2\mu(3\lambda+2\mu)} + \frac{2(2l\mu+(\lambda+\mu)(4m+\lambda+2\mu))\sigma_{22}}{2\mu(3\lambda+2\mu)}$$

$$B_{2223} = 0$$

$$B_{2231} = 0$$

$$B_{2232} = 0$$

$$B_{2233} = \frac{2\lambda\mu(3\lambda+2\mu)-(\lambda^2-4l\mu+4m(\lambda+\mu)-2n(\lambda+\mu))\,\sigma_{11}}{2\mu(3\lambda+2\mu)} + \frac{(2m\lambda-\lambda(n+\lambda)+4l\mu)\sigma_{22}}{2\mu(3\lambda+2\mu)}$$

$$B_{2311} = 0$$

$$B_{2312} = 0$$

$$B_{2313} = 0$$

$$B_{2321} = 0$$

$$B_{2322} = 0$$

$$B_{2323} = \frac{4\mu^2(3\lambda+2\mu)-2(n\lambda+(-2m+n+\lambda)\mu)\sigma_{11}+(n\lambda+4\mu(m+\lambda+\mu))\sigma_{22}}{4\mu(3\lambda+2\mu)}$$

$$B_{2331} = 0$$

$$B_{2332} = \frac{4\mu^2(3\lambda+2\mu)-2(n\lambda+(-2m+n+\lambda)\mu)\sigma_{11}+(n\lambda+4m\mu-2\lambda\mu)\sigma_{22}}{4\mu(3\lambda+2\mu)}$$

$$B_{2333} = 0$$

$$B_{3111} = 0$$

$$B_{3112} = 0$$

$$B_{3113} = \frac{4\mu^2(3\lambda+2\mu)+(n\lambda+4\mu(m+\lambda+\mu))\sigma_{11}-2(n\lambda+(-2m+n+\lambda)\mu)\sigma_{22}}{4\mu(3\lambda+2\mu)}$$

$$B_{3121} = 0$$

$$B_{3122} = 0$$

$$B_{3123} = 0$$

$$B_{3131} = \frac{4\mu^2(3\lambda+2\mu)+(n\lambda+4m\mu-2\lambda\mu)\sigma_{11}-2(n\lambda+(-2m+n+\lambda)\mu)\sigma_{22}}{4\mu(3\lambda+2\mu)}$$

$$B_{3132} = 0$$

$$B_{3133} = 0$$

$$B_{3211} = 0$$

$$B_{3212} = 0$$

$$B_{3213} = 0$$

$$B_{3221} = 0$$

$$B_{3222} = 0$$

$$B_{3223} = \frac{4\mu^2(3\lambda+2\mu)-2(n\lambda+(-2m+n+\lambda)\mu)\sigma_{11}+(n\lambda+4\mu(m+\lambda+\mu))\sigma_{22}}{4\mu(3\lambda+2\mu)}$$

$$B_{3231} = 0$$

$$B_{3232} = \frac{4\mu^2(3\lambda+2\mu)-2(n\lambda+(-2m+n+\lambda)\mu)\sigma_{11}+(n\lambda+4m\mu-2\lambda\mu)\sigma_{22}}{4\mu(3\lambda+2\mu)}$$

$$B_{3233} = 0$$

$$B_{3311} = \frac{2\lambda\mu(3\lambda+2\mu)+(4l\mu+\lambda(2m-n+2(\lambda+\mu)))\sigma_{11}}{2\mu(3\lambda+2\mu)} - \frac{(\lambda^2-4l\mu+4m(\lambda+\mu)-2n(\lambda+\mu))\,\sigma_{22}}{2\mu(3\lambda+2\mu)}$$

$$B_{3312} = 0$$

$$B_{3313} = 0$$

$$B_{3321} = 0$$

$$B_{3322} = \frac{2\lambda\mu(3\lambda + 2\mu) - (\lambda^2 - 4l\mu + 4m(\lambda + \mu) - 2n(\lambda + \mu))\,\sigma_{11}}{2\mu(3\lambda + 2\mu)} + \frac{(4l\mu + \lambda(2m - n + 2(\lambda + \mu)))\sigma_{22}}{2\mu(3\lambda + 2\mu)}$$

$$B_{3323} = 0$$

$$B_{3331} = 0$$

$$B_{3332} = 0$$

$$B_{3333} = \frac{2\mu(\lambda + 2\mu)(3\lambda + 2\mu) - (-4l\mu + \lambda(4m + \lambda + 2\mu))\,(\sigma_{11} + \sigma_{22})}{2\mu(3\lambda + 2\mu)}$$

APPENDIX C

EXPRESSIONS FOR DISPERSION CURVES UNDER BIAXIAL STRESSES

C.1 Expressions for 6^{th} *order Polynomial in Eq.* (125)

$$
\begin{aligned}
P_6 = \;& (A_{1323}^2 - A_{1313}A_{2323})A_{3333} \\
P_4 = \;& (A_{1233}^2 A_{1313} + A_{1313}A_{1323}^2 - 2A_{1133}A_{1323}A_{1332} - 2A_{1323}A_{1331}A_{1332} + A_{1313}A_{1332}^2 \\
& + 2A_{1233}(-A_{1323}(A_{1133} + A_{1331}) + A_{1313}A_{1332}) + A_{1133}^2 A_{2323} - A_{1313}^2 A_{2323} \\
& + 2A_{1133}A_{1331}A_{2323} + A_{1331}^2 A_{2323} - (A_{1212}A_{1313} - 2A_{1112}A_{1323} + A_{1111}A_{2323})A_{3333} \\
& + c^2\rho^0(-A_{1323}^2 + A_{1313}A_{2323} + (A_{1313} + A_{2323})A_{3333})) \\
P_2 = \;& (A_{1133}^2 A_{1212} + A_{1111}A_{1233}^2 - A_{1212}A_{1313}^2 + 2A_{1112}A_{1313}A_{1323} - 2A_{1112}A_{1233}A_{1331} \\
& + A_{1212}A_{1331}^2 + 2A_{1111}A_{1233}A_{1332} - 2A_{1112}A_{1331}A_{1332} + A_{1111}A_{1332}^2 - \\
& 2A_{1133}(-A_{1212}A_{1331} + A_{1112}(A_{1233} + A_{1332})) - A_{1111}A_{1313}A_{2323} + (A_{1112}^2 \\
& - A_{1111}A_{1212})A_{3333} - c^4\text{Density}^2(A_{1313} + A_{2323} + A_{3333}) + c^2\rho^0(-2A_{1112} \\
& A_{1323} - (A_{1133} + A_{1331})^2 - (A_{1233} + A_{1332})^2 + A_{1313}(A_{1212} + A_{1313} + A_{2323}) \\
& + A_{1212}A_{3333} + A_{1111}(A_{2323} + A_{3333}))) \\
P_0 = \;& (-A_{1112}^2 + (c^2\rho^0 - A_{1111})(c^2\text{Density} - A_{1212}))(c^2\rho^0 - A_{1313})
\end{aligned}
$$

REFERENCES

[1] Graff, K. F., *Wave Motion in Elastic Solids*. Dover Publications, 1991.

[2] Achenbach, J. D., *Wave Propagation in Elastic Solids*. American Elsevier Pub. Co., 1973.

[3] Pollard, H. F., *Sound Waves in Solids*. Pion, 1977.

[4] Kolsky, H., *Stress Waves in Solids*. Dover Publications, 2003.

[5] Rose, J. L., *Ultrasonic Waves in Solid Media*. Cambridge University Press, 34 ed., 1999.

[6] Bower, A. F., *Applied Mechanics of Solids*. CRC Press, 2009.

[7] Nye, J. F., *Physical Properties of Crystals*. Oxford University Press, 1964.

[8] Kline, R. A., *Nondestructive Characterization of Composite Media*. Technomic Publishing Company, 1992.

[9] Nayfeh, A. H. and Chimenti, D. E., "Free wave propagation in plates of general anisotropic media," *Journal of Applied Mechanics*, vol. 56, pp. 881–886, December 1989.

[10] Henneke, E. G., "Reflection-refraction of a stress wave at a plane boundary between anisotropic media," *Journal of the Acoustical Society of America*, vol. 51, no. 1B, pp. 210–217, 1972.

[11] Jones, A. T., "Exact natural frequencies and modal functions for a thick off-axis lamina," *Journal of Composite Materials*, vol. 5, no. 4, pp. 504–520, 1971.

[12] Pavlakovic, B. and Lowe, M. J. S., *Disperse User Manual*. Non Destructive Testing Laboratory, Imperial College, July 2003.

[13] Cantrell, J. H., *Ultrasonic Nondestructive Evaluation*, ch. Fundamentals and applications of nonlinear ultrasonic nondestructive evaluation, pp. 363–434, Kundu, T., ed. CRC Press, 2004.

[14] Drumheller, D., *Introduction to Wave Propagation in Nonlinear Fluids and Solids*. Cambridge University Press, 1998.

[15] Norris, A. N., *Nonlinear Acoustics*, ch. Finite amplitude waves in solids, pp. 263–277, Hamilton, M. F. and Blackstock, D. T., eds. Academic Press, New York, 1998.

[16] Ogden, R., *Nonlinear Elastic Deformations*. Dover Publications, 1997.

[17] Ogden, R., *Nonlinear Elasticity*, ch. Elements of theory of finite elasticity, pp. 1–47, Fu, Y. and Ogden, R., eds. Cambridge University Press, 2001.

[18] Crecraft, D. I., "The use of ultrasonics in stress analysis," *Strain*, vol. 1, no. 4, pp. 4–8, 1965.

[19] Toupin, R. A. and Bernstein, B., "Sound waves in deformed perfectly elastic materials. Acoustoelastic effect," *Journal of the Acoustical Society of America*, vol. 33, no. 2, pp. 216–225, 1961.

[20] Murnaghan, F. D., *Finite Deformation of an Elastic Solid*. John Wiley & Sons Inc, 1951.

[21] Hughes, D. S. and Kelly, J. L., "Second-order elastic deformation of solids," *Physical Review*, vol. 92, pp. 1145–1149, 1953.

[22] Thurston, R. N. and Brugger, K., "Third-order elastic constants and the velocity of small amplitude elastic waves in homogeneously stressed media," *Physical Review*, vol. 133, pp. 1604–1610, September 1964.

[23] Lee, Y.-C. and Kuo, S. H., "A new point contact surface acoustic wave transducer for measurement of acoustoelastic effect of polymethylmethacrylate," *IEEE Transactions on Ultrasonics, Ferroelectrics and Frequency Control*, vol. 51, pp. 114–120, January 2004.

[24] Duquennoy, M., Ouaftouh, M., Ourak, M., and Jenot, F., "Theoretical determination of Rayleigh wave acoustoelastic coefficients: comparison with experimental values," *Ultrasonics*, vol. 39, no. 8, pp. 575–583, 2002.

[25] Qu, J. and Liu, G., "Effects of residual stress on guided waves in layered media," in *Review of Progress in Quantitative Nondestructive Evaluation*, vol. 17, pp. 1635–1642, 1998.

[26] Fukuoka, H. and Toda, H., "Preliminary experiment on acoustoelasticity for stress analysis," *Archives of Mechanics*, vol. 29, no. 5, pp. 673–686, 1977.

[27] Pao, Y.-H., Sachse, W., and Fukuoka, H., *Physical Acoustics*, vol. 17, ch. Acoustoelasticity and Ultrasonic Measurements of Residual Stresses, pp. 61–143, Mason, W. and Thurston, R., eds. Academic Press, 1983.

[28] Pao, Y.-H. and Gamer, U., "Acoustoelastic waves in orthotropic media," *Journal of the Acoustical Society of America*, vol. 77, pp. 806–812, March 1985.

[29] Muir, D., *Determination of Third Order Elastic Constants via Ultrasonic Angle Beam Measurements*. PhD thesis, Georgia Institute of Technology, 2009.

[30] Conry, M., "Notes on wave propagation in anisotropic elastic solids," `http://80.68.92.234/anisotropic_with_lamb_waves.pdf`, April 2005.

[31] Prioul, R., Bakulinz, A., and Bakulin, V., "Nonlinear rock physics model for estimation of 3D subsurface stress in anisotropic formations: Theory and laboratory verification," *Geophysics*, vol. 69, pp. 415–425, March-April 2004.

[32] Duquennoy, M., Ouaftouh, M., Devos, D., Jenot, F., and Ourak, M., "Effective elastic constants in acoustoelasticity," *Applied Physics Letters*, vol. 92, no. 24, p. 244105, 2008.

[33] Stobbe, D. M., "Acoustoelasticity in 7075-T651 Aluminum and Dependence of Third Order Elastic Constants on Fatigue Damage," Master's thesis, Georgia Institute of Technology, 2005.

[34] Lematre, M., Feuillard, G., Delaunay, T., and Lethiecq, M., "Modeling of ultrasonic wave propagation in integrated piezoelectric structures under residual stress," *IEEE Transactions on Ultrasonics, Ferroelectrics, and Frequency Control*, vol. 53, pp. 685–696, April 2006.

[35] Lee, S. J. and Michaels, J. E., "Comparison of the effects of applied loads and temperature variations on guided wave propagation," in *Review of Progress in Quantitative Nondestructive Evaluation*, vol. 30, 2011, in press.